Stretto di Messina

Concessionaria per la progettazione, realizzazione e gestione del collegamento stabile tra la Sicilia e il Continente Organismo di Diritto Pubblico
(Legge n° 1158 del 17 dicembre 1971, modificata dal D.Lgs. n°114 del 24 aprile 2003)

EurolinK

PONTE SULLO STRETTO DI MESSINA

PROGETTO DEFINITIVO

EUROLINK S.C.p.A.

IMPREGILO S.p.A. (MANDATARIA)
SOCIETÀ ITALIANA PER CONDOTTE D'ACQUA S.p.A. (MANDANTE)
COOPERATIVA MURATORI E CEMENTISTI - C.M.C. DI RAVENNA SOC. COOP. A.R.L. (MANDANTE)
SACYR S.A.U. (MANDANTE)
ISHIKAWAJIMA - HARIMA HEAVY INDUSTRIES CO. LTD (MANDANTE)
A.C.I. S.C.P.A. - CONSORZIO STABILE (MANDANTE)

IL PROGETTISTA	IL CONTRAENTE GENERALE	STRETTO DI MESSINA	STRETTO DI MESSINA
COWI Ing. E.M. Veje Dott. Ing. E. Pagani Ordine Ingegneri Milano n° 15408 EurolinK	Project Manager (Ing. P.P. Marcheselli)	Direttore Generale e RUP Validazione (Ing. G. Fiammenghi)	Amministratore Delegato (Dott. P. Ciucci)

Unità Funzionale	OPERA DI ATTRAVERSAMENTO	PF0065_F0
Tipo di sistema	SOTTOSTRUTTURE	
Raggruppamento di opere/attività	BLOCCHI DI ANCORAGGIO	
Opera - tratto d'opera - parte d'opera	Geotechnical Design Reports	
Titolo del documento	Sicily Anchor Block – evaluation of block behaviour via 3D FE analyses and of bearing capacity, Annex	

CODICE: C G 1 0 0 0 P C L D P S T B 4 B S 0 0 0 0 0 0 0 3 F0

REV	DATA	DESCRIZIONE	REDATTO	VERIFICATO	APPROVATO
F0	20/06/2011	EMISSIONE FINALE	FB	GV	SR

NOME DEL FILE: PF0065_F0_ANX

INDEX

1 EXECUTIVE SUMMARY

This report describes the static 3D finite element analyses performed for the Sicily Anchor Block. The calculations are based on both drawings and cable forces provided in the tender design; account is also given for the influence of the cable forces computed from the global IBDAS model version 3.3b and version 3.3f. The analyses are carried out using the commercial code *Plaxis*^{3D} *Foundation*.

Earthquake-induced block displacements and safety against sliding, rotation and bearing capacity failure are evaluated in the companion report "Sicily anchor block: earthquake-induced displacements and safety against ultimate limit states", using the displacement-based approach, and the pseudo-static approach.

Chapter 2 describes the soil profile on the Sicily shore (Figure 1).

Starting from ground level and moving downwards the following units are encountered: *Depositi Costieri* (Coastal Deposits); *Ghiaie di Messina* (Messina Gravel); *Depositi Continentali* (Continental Deposits); *Conglomerato di Pezzo* (Pezzo Conglomerate); *Cristallino* (Crystalline bedrock). A plan view at the site of the Sicily Anchor Block is shown in Figure 2. The two longitudinal sections and the cross section indicated in Figure 2 are shown in Figure 3, Figure 4 and Figure 5. For the Sicily Anchor Block, the relevant geological unit is the Messina Gravel, with a stiffer deep layer for $z < -75$ m a.s.l.. Table 1 summarises the main mechanical parameters obtained from the geotechnical characterisation for the relevant layer.

Chapter 3 details input data of the 3D FEM analyses.

Figure 12, Figure 13 and Figure 14 show a perspective, plan view and lateral view of the 3D mesh used in the analyses, extending 400 m parallel to the axis of the bridge, 450 m orthogonal to the axis of the bridge, 150 m below the highest ground level and 106.5 m below the lowest ground level. The highest ground level is at +56.0 m a.s.l. and it is horizontal for about 187 m, while the lowest ground level is at +12.5 m a.s.l. and it is horizontal for about 114 m; the remaining 99 m consist of 13 steps of soil with a height less then 4.5 m, which is the maximum compatible with the cohesive strength assigned to the soil.

The groundwater level coincides with the sea level, at 0 m a.s.l..

Figure 15 and Figure 16 show a perspective view and a plan view of the pre-excavation of a foundation area around the construction site.

The constitutive soil model adopted in the FEM analyses is an elastic-plastic rate independent model with isotropic hardening (Hardening Soil) available in the library of the code *Plaxis*^{3D} *Foundation*. In the model, the elastic behaviour is defined by isotropic elasticity through a stress-dependent Young's modulus, *E*'. For plastic loading from isotropic stress states, the model predicts a non linear stress-strain relationship with tangent initial modulus equal to *E'*. Values of *E'* were related to the shear modulus at small-strain G_0 obtained from the cross-hole test carried out in the site. In particular, values of the parameters reported in Table 2 were obtained by best fitting the cross-hole test results in Figure 19.

The Sicily Anchor Block consists of a reinforced concrete block with a trapezoidal shape in plane, 100 m long in north-south direction; in east-west direction the smaller base of the trapezium is about 80 m in length, whereas the larger base is about 120 m in length, so the block has a 100 m mean width. The top and the bottom of the block consist of two different planes respectively: in north-south direction the front of the anchor block has an inclination of about 15° on the top and of about 25° on the bottom; the rear end of the anchor block has an inclination of about 7° on the top and of about 8° on the bottom. The maximum level of the anchor block is +60 m a.s.l. and deepest end of the structure is at +1 m a.s.l.. The anchor block includes four splay chambers: two for main cables; the other two will be filled with granular material after installation of the main cables. 3D model for anchor block has the same shape in plan as the actual design, whereas in section it was necessary to introduce some simplifications because of the inability of *Plaxis*^{3D} *Foundation* to deal with inclined planes; in these simplifications the same volumes (and weights) of the actual design are maintained. Figure 20 shows a north-west top view, a south-west bottom view and a perspective view of the main cable chambers. The anchor block was modelled as a reinforced concrete element, with parameters reported in Table 3; the granular material of the ballast chamber, *filling material*, was modelled as a Mohr-Coulomb material with the properties of the in situ soil deposit; the main chamber will be filled with a stiff Linear-Elastic material without mass, *empty material*, with the only aim to create mesh nodes for the application of the design forces.

Each diaphragm wall of the excavation retaining system (in red in Figure 10) has 2.5 m width, 1 m thick and a variable overall length. The two lines of diaphragm walls in east-west direction (transversal diaphragm walls) have the same overall length, that is 23 m; also the two lines of diaphragm walls in north-south direction (longitudinal diaphragm walls) have the same overall length, but each diaphragm wall has a different length that ranges from 23 m to about 40 m in the rear part of the anchor block, and from 27 m to 23 m in the front. Figure 21 shows a perspective view of the 3D diaphragm walls model; Figure 22 shows a scheme of the longitudinal diaphragm

walls with indication of a label for each kind of wall; Table 4 summarises the level of the top and of the bottom of each diaphragm wall, its overall length and the depths of excavation; Table 5 summarises the geometrical and mechanical properties of the diaphragm walls.

Pre-stressed soil anchors are spaced 2.5 m horizontally and have a variable vertical spacing, with an average of 5 m. Anchor bars and grouted bodies have different areas and lengths. For sake of simplicity in *Plaxis*^{3D} *Foundation* soil anchors were modelled as Plaxis *spring* elements with an elastic-plastic constitutive model: pre-stress was chosen as a service force; the maximum force was associated with the elastic extension of the anchor bar, but maintaining the same stiffness of the case without pre-stress. In the 3D model, the horizontal spacing is 5 m, instead of 2.5 m as from design, and so the considered maximum force is doubled; to minimise the effect of the larger distance between two consecutive anchors in comparison with the design, a Plaxis *beam* is introduced to connect all the co-planar soil anchors. Table 6, Table 7 and Table 8 summarise the geometrical and mechanical properties of the structural elements; Table 9 summarises the levels of the different levels of springs; Figure 25 introduces of various quantities according to the beam's local system of axes; Figure 26 shows a perspective view of the levels of springs and connecting beams.

The soil in the middle and in the front of the construction site is treated using secant jet-grouted columns down to a maximum depth of 30 m, with a thickness of 18.5 m, and to a maximum depth of 20 m, with a thickness 7 m, respectively; the jet-grouted columns will be confined by the diaphragm walls. The 3D model of jet-grouting has practically the same size in plan than the actual design, whereas in section it was necessary to do same simplifications because of the inability of *Plaxis*^{3D} Foundation to deal with inclined planes, however the same volumes (and weights) of the grouted areas as from design are maintained. Figure 27 shows a perspective view of the jet-grouting model; Table 10 summarises the mechanical properties of the jet-grouted columns.

The main aim of the analyses is to evaluate the displacements of the anchor block due to the application of the design forces. To this purpose the whole construction sequence was reproduced in the analysis, with the intent to obtain a stress state in the soil, before application of the design loads, as near as possible to the actual stress state. The analyses were carried out in terms of effective stresses, assuming drained conditions for all soil deposits. The calculation steps defined in the analyses are: generation of the initial stress state and of the ground level configuration; pre-excavation; activation of diaphragm walls and jet grouting; excavation to foundation level with simultaneous activation of springs; construction of anchor block; filling of the pre-excavation and of

the ballast chambers with granular material; application of the design loads. An incremental analysis of the design loads was carried out to obtain the maximum force.

Chapter 4 details the output data of the 3D FEM analyses.

Based on the results obtained two kinematic mechanisms for the block were reconstructed: one is of pure translation and the other one is of roto-translation around the centre of gravity. Figure 33 and Figure 34 show the un-deformed (in black) and the deformed (in red, scaled up 200 times) configuration of the block for the two mechanism, for the ULS load case. Ten points were selected for output along a longitudinal section through the centre of gravity; all points are located at different elevation of the rear end and of the front end of the block; one point, *F*, is located approximately at the centre of the block. The location of the ten points is detailed in Figure 35. Table 17 summarises the displacements of the centre of gravity, its direction on the horizontal and the rotation around the barycentre of the Sicily Anchor Block for the two kinematic mechanisms and for the three loading conditions considered. Under SILS loading condition the average displacement is about 27 mm and the average direction is about 14° on the horizontal; it is possible to say that this inclination is the inclination of the most likely sliding surface for this load case; for SLS2 load case the average displacement is about 28 mm and the average direction is again about 14° on the horizontal; for ULS loading condition the average displacement is about 33 mm and the average direction is about 15.5° on the horizontal.

Load-settlement curves obtained for the ten points in the incremental analysis of the design loads are plotted from Figure 36 to Figure 40.

To estimate the maximum force that can be applied to the anchor block, and therefore the "distance" from the collapse of soil around the Sicily Anchor Block, load-settlements curves were interpolated with an hyperbolic function (Figure 41); this procedure yielded a value of F_{max} between 15100 MN and 16500 MN, that is a safety factor against increasing design forces of about 3.75 – 4.15 for ULS loading condition and of about 5 – 5.5 for SILS loading condition.

Figure 42 to Figure 60 shown *Plaxis*^{3D} *Foundation* output in terms of relative shear stress contours, horizontal and vertical displacement in a longitudinal and in a cross section, total displacement contours in the 3D FE mesh, effective normal stresses on the interface element of the transversal diaphragm walls, for the main calculation phases: initial phase, complete excavation inside the diaphragm walls, end of anchor block construction, application of the forces corresponding to the SILS loading condition and to the ULS loading conditions.

Appendix A and appendix B. Updated cable forces obtained from global IBDAS model version 3.3b and version 3.3f

The forces transmitted by the main cables to the Sicilia Anchor Block have been re-evaluated using the global IBDAS model version 3.3b and version 3.3f. The worst load combinations were selected for each limit state (SILS, SLS2 and ULS) for both static and seismic conditions, using 6 different criteria (Table A.1 – Table A.2 for IBDAS 3.3b and Table B.1 – Table B.2 for IBDAS 3.3f). For both IBDAS model versions a low difference is observed between the tender design and the updated (IBDAS) cable forces, the ratio being in the range of 1.06 to 0.90 for IBDAS 3.3b (Table A.3) and in the range of 1.08 to 0.93 for IBDAS 3.3f (Table B.3); the higher value refers to the ULS load combination, while the lower is obtained for the SILS load combination. For the Ultimate Limit State (ULS) cable forces provided by the tender design, referred to in the 3D FE analyses, are 5.8% higher than the corresponding IBDAS 3.3b values and are 8% higher than the corresponding IBDAS 3.3f values, this resulting in a conservative estimate of the behaviour of the Sicilia Anchor Block. Performance of the anchor block under SILS and SLS2 load cases are also discussed in § 4.

2 SOIL PROFILE AND GEOTECHNICAL CHARACTERISATION

Figure 1 shows the soil profile on the Sicily shore of the strait. The present level of the ground at the location of the anchor block is in between +22 m a.s.l. and +59 a.s.l. with a descending angle of about 25° towards the North. The groundwater level coincides with the sea level, at 0 m a.s.l..
Starting from ground level and moving downwards the following units are encountered:

1. *Depositi Costieri* (Coastal Deposits). Sand and gravel with very little or no fine content; occasionally, silty peaty layers appear in the lower part of the formation. The thickness of this formation is difficult to evaluate as it rests on the very similar formation of the *Ghiaie di Messina.*
2. *Ghiaie di Messina* (Messina Gravel/Terrace Deposits). Gravel and sand, with very occasional silty layers. The thickness of this formation can reach more than 170 m.
3. *Depositi Continentali* (Continental Deposits)/*Calcarenite di Vinco* (Vinco Calcarenite). Clayey-sandy deposit, consisting of layers of silt or silt and sand, with significant gravel content/Bio-calcarenite and fossiliferous calcarenite, with thin silty layers.
4. *Conglomerato di Pezzo* (Pezzo Conglomerate). Soft rock, consisting of clasts of different dimensions in a silty-sandy matrix and sandstone. The thickness of this formation is larger than 200 m.
5. *Cristallino* (Crystalline bedrock). Tectonised granite.

Figure 2 shows a plan view at the location of the Sicily Anchor Block, together with the available site investigation. The three longitudinal sections and the cross section indicated in Figure 2 are shown in Figure 3, Figure 4, Figure 5 and Figure 6. The Messina Gravel/Terrace Deposits unit extends from the ground level over a thickness of about 200m, but at about -75 m a.s.l. an increase in stiffness is observed.
The permeability of the deposits was evaluated by pumping tests carried out from a well located in the area of the Sicily Tower and extending 40 m b.g.l., and by Lefranc permeability tests carried out in a borehole at depths of 10 m b.g.l. to 38 m b.g.l..
Due to the small distance of the source line (sea) from the well, the high permeability and the small compressibility of the deposits, the pumping tests were interpreted assuming steady state

conditions (Mansur and Kauffman, 1962). The resulting value of the horizontal permeability is $k_h = 5\times10^{-3}$ m/s.

Lefranc permeability tests have a more local character than well pumping tests and are affected by the disturbance created during borehole formation; in addition, their interpretation depends on the assumed ratio k_h/k_v. Their results must therefore be considered reliable within one order of magnitude. The values of k_v assuming $k_h/k_v = 10$ range from 2×10^{-3} to 5×10^{-2} (m/s); for $k_h/k_v = 1$, k_v is not substantially different from that obtained by the well pumping test, being in the range of 2.6×10^{-4} to 5.8×10^{-3} (m/s).

Since no *in-situ* evaluation of permeability was carried out at the location of the Sicily Anchor Block, data obtained from the *in-situ* test carried out at the location of Sicily Tower were adopted.

In the area of the Sicily Anchor Block erosion phenomena of the Messina Gravel are less important than on the site of Sicily Tower, so that deviation of K_0 from its normally consolidated value is mainly due to ageing effects:

$$\frac{K_0}{K_0(NC)} = \left(\frac{t}{t_p}\right)^{C_{\alpha e}/C_c} \qquad (1)$$

in which *t* is the time elapsed from the deposition of the Messina Gravel, between 4×10^5 and 6×10^5 years, t_p is the end of primary consolidation time, about 10^{-2} year, $C_{\alpha e}$ is the secondary compression coefficient, and C_c is the compression index. For granular soils, typical values of the ratio $C_{\alpha e}/C_c$ are about 0.02 (Mesri, 1989) and therefore the maximum estimated increase of K_0 due to ageing effects is of the order of 42%. It follows:

$$K_0 = 1.42 \times K_0(NC) = 1.42 \times (1-\sin\varphi'_p) = 0.47 \qquad (2)$$

in which $\varphi'_p = 42°$ as described ahead.

The relative density of the Messina Gravel was estimated from the SPT and LPT results using the procedure proposed by Cubrinovski and Ishihara (1999): values of $D_R = 40$ % to 60 % were obtained as shown in Figure 7. The angle of shearing resistance at peak $\varphi'_P = 41° – 44°$ was then evaluated through the relationship proposed by Schmertmann (1975) (Figure 7).

The constant-volume friction angle was evaluated following Bolton (1986):

$$\varphi'_{cv} = \varphi'_p - 3\,D_R(10 - \ln p') + 3° \qquad (3)$$

That, for $\varphi'_P = 40°$, $D_R = 50\%$ and $p' = 200$ kPa, provides $\varphi'_{cv} = 36°$.

The stiffness profile of Messina gravel was obtained from two cross-hole tests carried out in the vicinity of the Sicily Anchor Block, down to a depth of 100 m b.g.l. The results of the cross-hole

tests in terms of shear wave velocity, V_s, versus depth are given in Figure 8. The same results are shown in the figure as profiles of small strain shear modulus, G_0:

$$G_0 = \rho V_S^2 \qquad (4)$$

G_0 increases from about 100 MPa at the ground level to about 400 MPa at a depth of 80 m b.g.l.; below this depth the data are more dispersed with an average value of 450 MPa.

Table 1 summarizes the main mechanical parameters obtained from the geotechnical characterisation above.

Table 1. Properties of soil

	depth (m b.g.l.)	K_0	φ'_p (°)	φ'_{cv} (°)	K_h (m/s)	G_0 (MPa)
Messina Gravel	0÷20	0.43	44	35	5×10^{-3}	50÷150
Messina Gravel	20÷80	0.47	42	37	5×10^{-3}	150÷400
Messina Gravel	> 80	0.47	42	37	5×10^{-3}	450

3 3D NUMERICAL ANALYSIS OF THE SICILY ANCHOR BLOCK

Figure 9 shows a plan view and a longitudinal section of the anchor block as defined in the tender design; in Figure 10 the red lines indicate the outline of the diaphragm wall needed to support the excavation. Two views of the anchor block as provided in the tender design are shown in Figure 11.

The Sicily Anchor Block consists of a reinforced concrete block with a trapezoidal shape in plane. It is 100 m long in the North-South direction while in the East-West direction the smaller side is about 80 m in length, whereas the larger one is about 120 m long, this resulting in a mean width of 100 m. The top and the bottom of the block consist of two different planes, respectively: the front of the anchor block has an inclination of about 15° at the top and of about 25° at the bottom; the rear end of the anchor block has an inclination of about 7° at the top and of about 8° at the bottom. The maximum elevation of the anchor block is +60 m a.s.l. and the deepest end of the structure is at +1 m a.s.l.. The anchor block includes four splay chambers: two of them are for the main cables, the other two are to be filled with granular material after installation of the main cables.

The inability of *Plaxis*^{3D} *Foundation* to model inclined planes did not permit to reproduce the exact geometry of the block, as well as the slope of the ground level around the block. In any case, a close estimate of the shape of the block and of the ground surface was achieved describing inclined planes as stepwise surfaces.

3.1 Soil model

3.1.1 Geometrical soil model

From Figure 12 to Figure 14 it is shown a perspective view, a plan view and a lateral view of the 3D mesh used in the analyses. The mesh is 400 m long in the direction parallel to the axis of the bridge, 450 m wide in the direction orthogonal to the bridge axis, and is 150 m high from the maximum elevation of ground surface.

The maximum ground level, at +56.0 m a.s.l, extends horizontally for about 187 m, while the lower ground level, at +12.5 m a.s.l., is horizontal for about 114 m; the remaining 99 m consist of 13 steps of soil less then 4.5 m high.

The soil profile consists of two horizontal layers, both of Messina Gravel: the upper layer extends from ground level to about -75 m a.s.l., the one below extends to the mesh bottom and is characterised by a higher stiffness.
The groundwater level coincides with the sea level, at 0 m a.s.l..
The design assumptions for the construction of the anchor block involve a pre-excavation of the foundation area around the construction site (Figure 15 and Figure 16). The construction site is bounded by diaphragm walls while the foundation area is the area required for all construction operations.
In the 3D model pre-excavation involves the area in front of the anchor block, that is excavated from the ground level to +51 m a.s.l., the area at the rear end of the block, excavated from the ground level to +17 m a.s.l., and the area in between, excavated between the two levels mentioned above through 13 steps of soil less then 4.5 m high.
The pre-excavation level is connected with the ground level also in the transversal direction through steps of soil less then 4.5 m high, in number sufficient to ensure an inclination equal to about 2/3.

3.1.2 Constitutive soil model

The behaviour of the anchor block was analysed through three-dimensional FE analyses performed using the code *Plaxis*^{3D} *Foundation 2.2*. The mechanical behaviour of the soil was described using the constitutive model Hardening Soil available in the model library of the code. The model is capable of reproducing soil non-linearity due to the occurrence of plastic strains from the beginning of the loading process. The computed non linear stress-strain relationship has tangent initial modulus equal to E'_0; upon unloading, the model assumes elastic behaviour with Young's modulus E'_0, thus reproducing a significant change in stiffness. In the model, soil stiffness depends on the effective stress state.
The calibration of the constitutive model was carried out using the results from the cross hole test carried out at the site and from published results of compression triaxial tests carried out on large-diameter reconstituted samples of gravelly soils (Tanaka et al., 1987). The cross-hole test was used to evaluate the shear modulus at small strains G_0 and to describe its variation with effective stress. The remaining soil parameters were selected to obtain a satisfactory description of the soil non-linearity observed in the triaxial tests published in the literature.
Hardening soil model is an elastic-plastic rate independent model with isotropic hardening. The elastic behaviour is defined by isotropic elasticity through a stress-dependent Young's modulus:

$$E' = E^{ref}\left(\frac{c'\cdot\cot\varphi' + \sigma_3'}{c'\cdot\cot\varphi' + p^{ref}}\right)^m \qquad (5)$$

where σ'_3 is the minimum principal effective stress, c' is the cohesion, φ' is the angle of shearing resistance, p^{ref} = 100 kPa is a reference pressure; E^{ref} and m are model parameters.
The model has two yield surfaces f_s and f_v with independent isotropic hardening depending on distortional plastic strain $\gamma_p = (2\cdot\varepsilon^p_1 - \varepsilon^p_v)$ and on volumetric plastic strains ε^p_v, respectively; the two surfaces have the following equations:

$$f_s = \frac{1}{E'_{50}}\frac{q}{(1-0.9\cdot q/q_f)} - \frac{2q}{E'} - \gamma^p = 0 \qquad (6)$$

$$f_v = \frac{\tilde{q}^2}{\alpha^2} + p'^2 - p'^2_c = 0 \qquad (7)$$

In eqn. (6), E'_{50} is given by an expression similar to eqn.(5), but, in contrast to E', it is not used within a concept of elasticity. Hardening of the f_s surface is isotropic and depends on the plastic distortional strain $\gamma_p = (2\cdot\varepsilon^p_1 - \varepsilon^p_v)$.
In eqn. (7), p' is the mean effective stress; $\tilde{q}$ is a generalised deviator stress, that accounts for the dependence of strength on the intermediate principal effective stress σ'_2; α controls the shape of the f_v surface in the $\tilde{q}$ -p' plane and can be related to the coefficient of earth pressure at rest K_0 for normally consolidated states. The hardening parameter p'_c is the size of the current f_v surface and is related to the plastic volumetric strains ε_v^p through the hardening law, written in the incremental form as:

$$d\varepsilon^p_v = \frac{\beta}{p^{ref}}\left(\frac{p'_c}{p^{ref}}\right)^m \cdot dp'_c \qquad (8)$$

where β is a parameter that controls the variation of p'_c with the plastic volumetric strains. In the model formulation implemented in *Plaxis*, the parameter E'^{oed}, which is related to β, has to be specified. This is the constrained modulus for one-dimensional plastic loading, and depends on the maximum principal effective stress σ'_3 through the relationship:

$$E'_{oed} = E'^{ref}_{oed}\cdot\left(\frac{c'\cdot\cot\varphi' + \sigma_3'}{c'\cdot\cot\varphi' + p^{ref}}\right)^m \qquad (9)$$

where σ'_3 is the minimum principal effective stress.
The initial value of the hardening parameter p'_c is related to the one-dimensional vertical yield stress, and can therefore be specified by assigning a value for the overconsolidation ratio OCR. It

is worth mentioning that OCR has to be regarded as a yield stress ratio (YSR) defined in the framework of strain hardening plasticity, so that values of OCR > 1 can be specified also for geologically normally consolidated soil deposits exhibiting a yield stress larger than the in situ stress.

The flow rule is associated for states lying on the surface f_v, while a non associated flow rule is used for states on the surface f_s. The latter is derived from the theory of stress dilatancy by Rowe (1962): the mobilised dilatancy angle ψ_m depends on the current stress state through the angle of mobilised friction $\varphi'm$ and the angle of friction at constant volume φ'_{cv}:

$$\sin\psi_m = \frac{\sin\varphi'_m - \sin\varphi'_{cv}}{1-\sin\varphi'_m \sin\varphi'_{cv}} \qquad (10)$$

In turn, φ'_{cv} can be obtained from the angle of shearing resistance φ' and the angle of dilatancy ψ at failure:

$$\sin\varphi'_{cv} = \frac{\sin\varphi' - \sin\psi}{1-\sin\varphi'\sin\psi} \qquad (11)$$

Figure 17 shows the shape of the yield surfaces f_v and f_s and schematically indicates their evolution.

For plastic loading from isotropic stress states, the model predicts a non linear stress-strain relationship with tangent initial modulus equal to E'. Therefore, values of E' were related to the shear modulus at small-strain G_0 obtained from the cross-hole tests carried out at the site. In particular, values of E'^{ref} and m were obtained by best fitting the cross-hole test results using eqn. (5) and assuming $\nu' = 0.2$.

The remaining model parameters $E'_{50}{}^{ref}$ and $E'_{oed}{}^{ref}$ were calibrated on the results of triaxial compression tests carried out on large-diameter reconstituted samples of gravelly soils (Tanaka et al., 1987). Figure 18 shows the comparison between model simulations and the experimental results mentioned above.

3.1.3 Soil parameters

Figure 19 shows the profile of G_0 against the depth b.g.l.. The continuous line in the figure represents the prediction of G_0 obtained using eqn. (5) with the values of c', φ', E'^{ref} and m reported in Table 2. Specifically, the values of σ'_3 were obtained using the values of K_0 given in Table 2. Values of E'^{ref} and m were obtained by best fitting the cross-hole test results and assuming $\nu' = 0.2$. For the Messina Gravel, a non zero value of cohesion was introduced to simulate non

zero values of stiffness at shallow depths (see Figure 19); this low value of cohesion does not significantly affect the behaviour of the layer in terms of strength.

Stiffness decay with shear strain was assumed using ratios of $E'^{ref} / E'_{50}{}^{ref} = 20$ and of $E'_{50}{}^{ref} / E'_{oed}{}^{ref} = 1.0$; a value for the angle of dilatancy at failure $\psi = 0$ was adopted.

Values of YSR > 1 was used for the Messina Gravel to reproduce a yield stress larger than the in situ stress.

Table 2. Hardening soil parameters for the foundation soil

Soil	γ (kN/m^3)	c' (kPa)	φ' (°)	K_0	YSR	ν	E'^{ref} (kPa)	m	$E'_{50}{}^{ref}$ (kPa)	$E'_{oed}{}^{ref}$ (kPa)
Messina gravel (z<-75 m a.s.l.)	20.0	20.0	42	0.47	2.0	0.2	$4.08 \cdot 10^5$	0.6	$2.04 \cdot 10^4$	$2.04 \cdot 10^4$
Messina gravel (z>-75 m a.s.l.)	20.0	20.0	42	0.47	2.0	0.2	$1.08 \cdot 10^6$	0.1	$5.40 \cdot 10^4$	$5.00 \cdot 10^4$

Soil permeability was evaluated from the in situ measurements reported in the Geotechnical Report of the tender design (PP/2R/A24); a constant value of $k = 10^{-3}$ m/s was adopted in the analyses.

3.2 Structural elements

3.2.1 Anchor block

As already mentioned, the Sicily Anchor Block (Figure 9 to Figure 11) consists of a reinforced concrete block with a trapezoidal shape in plane. It is 100 m long in the North-South direction while in the East-West direction the smaller side is 80 m in length, whereas the larger one is 120 m long, this resulting in a mean width of 100 m. In the East-West direction, at elevations higher than the top of the longitudinal diaphragm walls, the block is about 5 m wider.

The top and the bottom of the block consist of two different planes, respectively: the front of the anchor block has an inclination of about 15° at the top and of about 25° at the bottom; the rear end of the anchor block has an inclination of about 7° at the top and of about 8° at the bottom. The maximum elevation of the anchor block is +60 m a.s.l. and the deepest end of the structure is at +1 m a.s.l..

The anchor block includes four splay chambers: two of them are for the main cables, the other two are to be filled with granular material after installation of the main cables.

The inability of *Plaxis*^{3D} *Foundation* to model inclined planes did not permitted to reproduce the exact geometry of the block, as well as the slope of the ground level around the block. In any case, a close estimate of the shape of the block and of ground surface was achieved describing inclined planes as stepwise surfaces. Anyway, the model of the anchor block has the same shape in plane as specified in the tender design.

Figure 20 shows a North-West top view of the block model, a South-West bottom view of the block model and a perspective view of the chambers of the main cables.

The top of the block was limited by two horizontal planes at elevation of +48.5 m a.s.l. and +56 m a.s.l.; the base of the block was described, in the longitudinal direction, through a stepwise surface reproducing the inclination of the bottom portions of the block mentioned above. The front of the block was modelled with three steps about 4.5 m high (+35.2; +29.2; +25.0 and +21.0 m a.s.l) and the rear end of the block with four steps about 2 m high (+8.5; +6.2; +4.0; +1.5 and 0.0 m a.s.l).

Along the longitudinal section, the splay chambers were modelled using a number of steps (1 – 3) sufficient to reproduce the actual distribution of the weights: for sake of simplicity the main cable chambers have a slightly different shape in plane, but the same volume was maintained.

The anchor block was modelled as reinforced concrete using the parameters reported in Table 3. The granular material of the ballast chambers, denoted as *filling material*, was modelled as a Mohr-Coulomb material with properties similar to those of Messina Gravel at 2.5 m b.g.l.; specifically, an operative shear modulus equal to 40% of G_0 of Messina Gravel was adopted together with the values of effective cohesion and angle of shearing resistance listed in Table 3. The chambers of the main cables were filled with a stiff, weightless Linear-Elastic material, denoted as *empty material*, with the only aim to create mesh nodes for the application of the design forces.

Table 3. Soil parameters for the anchor block

Soil	Constitutive model	γ (kN/m^3)	E'^{ref} (kPa)	G'^{ref} (kPa)	ν	c' (kN/m^2)	ϕ (°)
anchor block	Linear elastic	25.0	3.0E+07	1.3E+07	0.15	---	---
filling material	Mohr Coulomb	19.0	9.0E+04	3.9E+04	0.20	25	40
empty material	Linear elastic	0.0	3.0E+07	1.3E+07	0.15	---	---

3.2.2 Diaphragm walls

Figure 10 shows the diaphragm walls needed to support the excavation (red lines in the figure): each diaphragm wall is 2.5 m wide, 1 m thick and is characterised by a variable length. Diaphragm walls to be installed in the East-West direction (transversal diaphragm walls) have a constant length of 23 m; those installed along the North-South direction (longitudinal diaphragm walls) have a length that ranges from 23 m to about 40 m in the rear part of the anchor block, and from 27 m to 23 m in the front of the block. Before installing the diaphragm walls, an excavation from the ground surface is to be carried out, that is about 12 m deep at the front of the block, and about 27 m deep in the middle of the rear part of the block (Figure 16).

Figure 21 shows a perspective view of the 3D model of the diaphragm walls. For sake of simplicity, not all the longitudinal diaphragm walls were modelled with their actual length, but 12 different heights of diaphragm walls were considered, that best reproduce the actual elevation of the bottom of the diaphragms; Figure 22 shows a scheme of the longitudinal diaphragm walls together with the indication of the excavation bottom.

The top of the diaphragm walls coincides with the pre-excavation level that, in the model, has a slightly lower elevation than the actual level, this resulting in a slightly lower length of the diaphragm walls.

Table 4 summarizes the elevation of the top and bottom of each diaphragm wall, the diaphragm length and the pre-excavation depth.

Table 4. Geometry of diaphragm walls

diaphragm wall	top (m a.sl.)	bottom (m a.sl.)	length (m)	pre-excav depth (m)
A - 1	+17.0	+6.0	11.0	17.0-15.5
B	+21.0	+6.0	15.0	19.5
C	+25.0	+3.0	22.0	21.0
D	+28.0	+3.0	25.0	21.8
E	+32.0	0.0	32.0	25.8
F	+35.2	0.0	35.2	26.7
G	+39.0	+6.5	32.5	18.0
H	+42.5	+17.0	25.5	17.5
I	+46.0	+21.0	25.0	16.8
J	+48.5	+25.0	23.5	13.3
K - 2	+51.0	+28.0	23.0	15.8

The diaphragm walls were modelled as Plaxis *wall* elements. These are shell elements with thickness d =1 m and weight per unit volume γ. In order to define their behaviour, the code requires 6 stiffness values, namely E_1, E_2, G_{12}, G_{13}, G_{23}, ν_{12}. The required values of stiffness moduli were obtained using the procedure outlined below (see Figure 23); the stiffness along direction 1 was obtained as:

$$E_1 = E_{cls} = 3 \times 10^7 \text{ kPa} \quad (12)$$

To take into account the lack of structural continuity between contiguous diaphragm walls, the elastic modulus E_2 was decreased by an order of magnitude: the stiffness along direction 2 was obtained as:

$$E_2 = \frac{E_{cls}}{10} = 3 \times 10^6 \text{ kPa} \quad (13)$$

Following the same criteria the shear stiffness G_{12} and G_{13} were calculated based on the reinforced concrete elastic modulus, whereas the shear stiffness G_{23} was decreased by an order of magnitude:

$$G_{12} = G_{13} = \frac{E_{cls}}{2 \cdot (1+\nu)} = 1.30 \times 10^7 \text{ kPa} \quad (14)$$

$$G_{23} = \frac{E_{cls}/10}{2 \cdot (1+\nu)} = 1.30 \times 10^6 \text{ kPa} \quad (15)$$

Table 5 summarizes the geometrical and mechanical properties of the diaphragm walls.

Table 5. Properties of diaphragm walls

	γ (kN/m^3)	d (m)	E_1 (GPa)	E_2 (GPa)	$G_{12} = G_{13}$ (GPa)	G_{23} (GPa)	ν
diaphragm walls	5.0	1.0	3.00×10^7	3.00×10^6	1.30×10^7	1.30×10^6	0.15

The contact between diaphragm walls and soil is modelled using the Plaxis *interface* elements that consists of eight pairs of nodes, compatible with the 8-noded quadrilateral side of a soil elements. In the FE formulation the coordinates of each pair of nodes are identical, which means that the element has zero thickness. However, each interface is assigned a "virtual thickness" which is an imaginary dimension used to calculate the stiffness properties of the interface. The roughness of the interaction is modelled choosing a suitable value for the strength reduction factor in the interface, R_{inter}; this factor relates the interface strength (wall friction and adhesion) with the soil strength (friction angle and cohesion) using an elastic-plastic model (Coulomb criterion):

$$c_i = R_{inter} c_{soil}$$
$$\tan(\varphi_i) = R_{inter} \tan(\varphi_{soil}) \qquad (16)$$

In the analyses it was assumed $R_{inter} = 0.67$.

3.2.3 Retaining anchors

Some levels of retaining anchors, varying in number along the different sides of the pit according to the depth of the excavation, have been designed to cooperate with the diaphragm walls to support the excavation. Generally, for each support level, one or two retaining anchors are planned for each diaphragm wall, resulting in an horizontal spacing of 2.5 m. The retaining anchors are 15 degrees inclined on the horizontal and will be pre-stressed.

Anchor bars as well as grouted bodies have different areas and lengths. The area of the anchor bars ranges from 6 strands with a 0.6" nominal diameter, to 8 strands with a 0.6" nominal diameter; their length is in between 20 m and 29 m, while the length of the grouted bodies ranges from 10 m to 12 m.

In the FE analyses the retaining anchors were modelled as Plaxis SPRINGS elements. These elements simulate anchors in a simplified way, without taking into account anchor – soil interaction. A bi-linear stiffness is assigned to each spring through a force-displacement (T-u) diagram (*Figure* 24 left side).

The maximum force of the retaining anchor was evaluated using the method proposed by Bustamante and Doix (1985) for micro-piles performed with repeated and selective injections:

$$T_{lim} = \pi \cdot d_g \cdot L_g \cdot \tau \qquad (17)$$

where d_g and L_g are the diameter and the length of the grout body and τ is shear stress at the soil – grout body interface. The actual diameter of the grouted body is $d_g = \alpha\, d$, α being a parameter depending on grouting technology and mechanical characteristics of the grouted soil, and d being the nominal diameter of the grouted body; in the following it was assumed $\alpha = 1.5$ and d = 15 cm.

Pre-tension values T_{pret} of the anchors were defined dividing the limit skin resistance T_{lim} by a factor of 2.5.

The elastic extension u_{lim} of the anchor bar induced by the maximum force T_{lim}, depends on the area A_{bar} and the free length L_{bar} of the anchor bar, through equation:

$$u_{lim} = \frac{T_{lim} \cdot L_{bar}}{E_{steel} \cdot A_{bar}} \qquad (18)$$

with E_{steel} = 210 GPa. The mean area was referred to 7 strands with a 0.6" nominal diameter, whereas u_{lim} was evaluated for each value of L_{bar}. Based on the values of T_{lim} and u_{lim} listed in Table 6, which were computed for the different values of L_{bar}, the mean values of T_{lim} and u_{lim} were adopted in the analyses.

Table 6. Properties of retaining anchors

E_{strand} (kPa)	A_{bar} (m^2)	T_{lim} (kN)	L_{bar} (m)	u_{lim} (m)
2.10E+08	1.28E-03	1413.7	20	1.05E-01
			25	1.32E-01
			29	1.53E-01
		1555.1	20	1.16E-01
			22	1.28E-01
		1696.5	20	1.27E-01
average		1555.0	---	1.3E-01

Vertical spacing of retaining anchors was of 5 to 8 m, depending on the geometry of the retaining system in the 3D model. For computational reasons, the longitudinal spacing was of 5.0 m, rather than 2.5 m as in the tender design, each spring thus representing a pair of retaining anchors. This was considered in the properties definition by doubling the limit skin resistance and the pre-tension force of each anchor: $T_{lim,mod} = 2T_{lim}$, $T_{pret,mod} = 2T_{pret}$. In addition, a connecting beam was placed at

the elevation of each level of retaining anchors to simulate an homogeneous distribution of the forces on the retaining walls. The geometrical dimensions of the beam were selected to reduce of about 10 times the free horizontal displacement of a point placed between two anchors.

Figure 24 (right) shows the force-displacement (T-u) relationship adopted for the pre-tensioned springs.

Table 7 summarizes the stiffness properties assigned to the springs in the numerical model; the u_{mod} values were assigned using the equation:

$$u_{\text{mod}} = \left(1 - \frac{T_{\text{pret}}}{T_{\text{lim}}}\right) \cdot u_{\text{lim}} \qquad (19)$$

Table 8 summarises the geometrical and mechanical properties of the beam. Figure 25 shows the definitions of various quantities according to the beam's local system of axes. Figure 26 shows a perspective view of the springs levels with the connecting beams. Table 9 summarises the elevation of the levels of the retaining anchors.

Table 7. Properties of springs

	horizontal slope (°)	$T_{lim,model}$ (kN)	$T_{pret,model}$ (KN)	u_{mod} (m)
springs	15	3110	1245	7.80E-02

Table 8. Properties of beams

	γ (kN/m^3)	b (m)	h (m)	E (GPa)	I_2 (m^4)	I_3 (m^4)	I_{23} (m^4)
beams	0.0	2.3	0.5	3.0E+07	5.07E-01	2.40E-02	0

Table 9. Vertical spacing of springs

	Elev. (m a.s.l.)	inter-axis (m)
top of wall	+51.0	---
1st level	+46.0	5.0
2nd level	+39.0	7.0
3rd level	+32.0	7.0
4th level	+28.0	4.0
5th level	+21.0	7.0
6th level	+12.5	8.5
7th level	+6.2	6.3
8th level	+1.5	4.7

3.2.4 Jet-grouted columns

In the excavation area of the anchor block a limited portion of soil is to be treated with jet-grouting. Treatment, located in the front and in the middle of the excavation site consists of secant jet-grouted columns down to a maximum depth of 30 m (from +25.5 m a.s.l. to +7.0 m a.s.l.), with a width in plane of 18.5 m, and to a maximum depth of 20 m (from +35 m a.s.l. to +28 m a.s.l.), with a width of 7 m; the jet-grouted columns will be confined by the diaphragm walls.

The 3D model of the jet-grouted area has nearly the same size in plane as in the tender design, while along the longitudinal section a stepwise surface was described, characterised by the same volumes of the actual design. The jet-grouted zone planned in the middle of the construction area ranges from +25.0 m a.s.l. to +8.5 m a.s.l., while in the front of the construction area it is located from +35.2 m a.s.l. to +28.0 m a.s.l. (Figure 27).

The mechanical properties of the jet-grouted columns were selected using published results (Croce *et al.*, 2004). Table 10 summarizes the adopted quantities; specifically, an unconfined strength $\sigma_c = 10$ MPa was assumed for the columns, with a ratio $E'/\sigma_c = 500$ and a stiffness decay described by $E'^{ref}/E'_{50}{}^{ref} = 2$ and $E'_{50}{}^{ref}/E'_{oed}{}^{ref} = 1$.

Table 10. Hardening soil parameters for the jet-grouted soil

Soil	γ (kN/m^3)	c' (kPa)	φ'_{cv} (°)	E'^{ref} (kPa)	m	$E'_{50}{}^{ref}$ (kPa)	$E'_{oed}{}^{ref}$ (kPa)
jet-grouting	22.0	2600	35	$5 \cdot 10^6$	0.2	$2.5 \cdot 10^6$	$2.5 \cdot 10^6$

A constant value for the permeability k = 10^{-7} m/s was assumed for the jet-grouted soil.

3.3 Calculation steps of analysis

The 3D FE analysis is mainly focused on the evaluation of the block displacements induced by the cable forces. To this purpose the whole construction sequence was reproduced in order to reproduce the soil stress state existing before the application of the cable forces.

The analyses were carried out in terms of effective stresses, assuming drained conditions for the Messina gravel.

The calculation steps defined in the analysis are summarized below:

1. Computation of initial stress state.
2. Pre-excavation stages.
3. Activation of diaphragm walls and jet grouting.
4. Progressive excavation inside the diaphragm walls to the base of the anchor block with simultaneous activation of springs.
5. Progressive activation of the anchor block.
6. Filling of the pre-excavation area and of the ballast chambers with granular material.
7. Reset of displacements to zero and application of the cable forces.
8. Incremental analysis by increasing the cable forces (8a) or by reducing the soil strength parameters (8b).

The initial stress state is generated through the K_0 procedure available in *Plaxis*^{3D} *Foundation*, in which the initial effective vertical stress σ'_{v0} is related to the initial effective horizontal stress σ'_{h0} using the coefficient of earth pressure at rest K_0 ($\sigma'_{h0} = K_0\, \sigma'_{v0}$).

To reproduce the inclined ground surface, an horizontal ground level was first defined in the *Input Program* of *Plaxis*^{3D} *Foundation*, at the elevation of +56 m a.s.l., and excavation stages were then defined in the *Calculation Program* of *Plaxis*^{3D} *Foundation*, to attain the final stepwise configuration of ground surface, as shown in Figure 12. A nil phase was finally added to obtain a balanced configuration.

The pre-excavation configuration, showed in Figure 15, was reached by subsequent excavations stages of height lower than 4.5 m.

The diaphragm walls and the jet-grouted areas were activated using a wished-in-place technique, *i.e.* changing the properties of the corresponding clusters of elements.

The base of the block was reached through subsequent excavations and simultaneous installation of the retaining anchors. Figure 28 shows two perspective views of the deepest configuration of the excavated area.
Each diaphragm wall had different length and number of levels of springs, as summarised in Table 11.

Table 11. Digging heights for each kind of diaphragm wall

diaphragm wall	max wall length (m)	number of level of springs
A - 1	17.0 – 15.5	3
B	19.5	2
C	21.0	3
D	21.8	2
E	25.8	3
F	26.7	4
G	18.0	2
H	17.5	3
I	16.8	2
J	13.3	2
K - 2	15.8	2

Construction of the anchor block occurred progressively, using a number of construction stages. Specifically, a layer of fluid concrete, about 3 m high, is activated first; then setting of concrete is simulated changing the cluster properties to those of solid concrete; finally a new layer of fluid concrete is added. This procedure continues until the end of block construction. The levels of retaining anchors and the corresponding connecting beams were progressively deactivated before activating the cluster of fluid concrete. Figure 29 shows an intermediate step of the block construction in which the solid and the fluid concrete are installed.
Installation of fluid concrete was simulated to reproduce the lateral pressure acting on the diaphragm wall when pouring the concrete. The fluid concrete was assimilated to a linear-elastic material with a small shear stiffness and a Poisson's ratio close to 0.5 (Table 12).

Table 12. Linear-elastic soil parameters for the anchor block

Soil	γ (kN/m^3)	E'^{ref} (kPa)	G'^{ref} (kPa)	ν
solid concrete	25.0	3.0E+07	1.3E+07	0.150
fluid concrete	25.0	3.0E+02	1.0E+02	0.495

At the end of block construction, the pre-excavation area was refilled with granular material to restore the original ground surface. The filling material was assimilated to an elastic-perfectly plastic material with Mohr-Coulomb failure criterion; its properties are those listed in Table 3.

The loads to be applied to the Sicily Anchor Block were those obtained by the structural analyses of the tender design. Table 13 reports the three loading conditions corresponding to the limit states SILS, SLS2 and ULS; the values of the cable forces listed in Table 13 are inclusive of the partial load factors. The forces are directed upwards, with an inclination of 15 degrees to the horizontal. In § 4 the influence of the cable forces computed using the global IBDAS model version 3.3b (Table A.1 – Table A.2) and version 3.3f (Table B.1 – Table B.2) are also discussed.

Table 13. Cable forces in the Sicilia Anchor Block (tender design)

Load case	Forces in main cable
SILS	3146 MN
SLS2	3250 MN
ULS	3964 MN

In the 3D model, for each loading condition the forces were divided between the two main cables; each force is applied in one point (see point *T.S.* in Figure 10). Figure 30 and Figure 31 show a perspective view and a front view of the anchor block and of the applied forces.

The cable forces were applied in steps to minimise the out-of-balance force of the calculation procedure. To reach the force corresponding the SILS limit state, 11 increments were adopted; the following increment reaches the SLS2 load case, and with two further increments the ULS limit state condition is obtained.

In these FE analyses a numerical solution was always found. According to the current Italian Code (Norme Tecniche per le Costruzioni - DM 14.01.2008), which introduces partial safety factors for limit state design, the designer should evaluate and compare Design Actions with Design Resistances. If the actions are lower or equal to the resistances, anchor block performance is satisfactory against the ultimate limit state. In FE analyses, similar to those described in the

previous sections, this comparison is meaningless, as either the numerical analysis converges towards a solution or it doesn't, i.e. convergence is not obtained. This two options are strongly dependent on the algorithms built in the software (a calculation may not converge because a small and not significant portion of the model undergoes high shear strain).

Therefore, to evaluate the safety of the anchor block against the occurrence of a limit state, a series of incremental analyses were carried out to evaluate the "distance" from a general failure condition. Specifically, starting from the SILS, SLS2 and ULS loading conditions, analyses were carried out in which the loads were increased, until substantial displacements developed, indicating that a failure mechanism was being attained.

Another possible way to evaluate safety against ultimate limit states is to perform φ' – c' reduction analyses in which the strength properties of the soils are gradually reduced until a failure mechanism is approached. For the case of the Sicily Anchor Block, this procedure was not applicable because local instability of the stepwise, non horizontal, ground surface occurred when reducing φ' and c'.

4 RESULTS OF THE 3D ANALYSES

4.1 Application of the design forces

Figure 32 shows the deformed FE mesh for the ULS load condition, scaled up 300 times.

The response of the anchor block to the application of the external loads mainly consists in a translation towards the Sicily tower, associated with a downward rotational. Specifically, based on the computed displacements, two deformation mechanisms were evaluated: one is of pure translation and the other one is of roto-translation around the centre of gravity.

The first mechanism is characterized by the average displacement and the average inclination α, as obtained by the quantities computed at the centre of gravity and at the selected nodes of the block; the other one is characterized by the displacement of the centre of gravity and by the rotation around it.

Figure 33 shows the un-deformed (in black) and the deformed (in red, scaled up 200 times) configuration of the block as obtained for the first mechanism, for the ULS load condition. Figure 34 shows the translation of the centre of gravity (scaled up 200 times), with its direction, and the rotation of the whole block around it, for the ULS load condition.

Ten points were selected for the output and are shown in Figure 35. Because of the symmetry of the problem, all points are located along the longitudinal section through the centre of gravity, at different elevations of the rear end and of the front of the block; point *F* is located within the block. Points *A* and *B* are located at the top of the block, at +56.0 m a.s.l.; points *C* and *D* are at +48.4 m a.s.l.; points *E*, *F* and *G* at +21.0 m a.s.l.; points *H* and *I* at +8.5 m a.s.l. and point *J* is at 0.0 m a.s.l.

Table 14 – Table 16 report the computed displacements, their inclination α to the horizontal and the rotation around the centre of gravity for the three loading conditions listed in Table 13, together with their average values. The maximum horizontal (*X* direction) and vertical (*Y* direction) displacements are bolded.

Table 17 summarizes the displacement of the centre of gravity, its inclination to the horizontal and the rotation around the barycentre of the Sicily Anchor Block, for the two kinematic mechanisms and for the three loading conditions considered in the tender design..

Under SILS loading condition, the average displacement is of about 27 mm and the average inclination α is of about 14° to the horizontal; under SLS2 loading conditions the average displacement is of about 28 mm and the average inclination α is again of about 14° to the

horizontal; under ULS loading condition the average displacement is of about 35 mm and the average inclination is again α =14° to the horizontal.

It is worth noting that the inclination α computed in the 3D analyses is in very good agreement with that obtained in the plane-strain analyses (α = 14.2) carried out to evaluate the earthquake-induced block displacements, discussed in the companion report "Sicily anchor block: earthquake-induced displacements and safety against ultimate limit states".

Table 14. Displacements of the selected points at the end of SILS load case (F=3146 MN)

point	X (m)	Y (m)	U_X (mm)	U_Y (mm)	|U| (mm)	α (°)	β_{CG} (°)
A	240.0	56.0	**34.70**	-7.85	35.58	-12.74	0.04
B	212.6	56.0	34.26	2.91	34.38	4.86	0.04
C	240.0	48.5	31.53	-7.82	32.49	-13.93	0.04
D	170.0	48.5	27.70	11.29	29.91	22.17	0.02
E	212.6	21.0	21.83	2.17	21.94	5.69	0.07
F	155.0	0.0	21.86	7.51	23.11	18.96	0.02
G	155.0	21.0	21.68	**14.25**	25.94	33.31	0.02
H	212.6	8.5	18.59	2.05	18.70	6.31	0.05
I	155.0	8.5	19.02	14.16	23.71	36.66	0.01
J	155.0	0.0	17.04	13.97	22.04	39.35	0.01
CG	193.0	28.0	23.54	6.75	24.49	15.99	---
average	---	---	---	---	26.57	14.24	0.031

Table 15. Displacements of the selected points at the end of SLS2 load case (F=3250 MN)

point	X (m)	Y (m)	U_X (mm)	U_Y (mm)	|U| (mm)	α (°)	β_{CG} (°)
A	240.0	56.0	**36.04**	-8.18	36.96	-12.79	0.04
B	212.6	56.0	35.58	3.00	35.70	4.83	0.04
C	240.0	48.5	32.75	-8.16	33.75	-13.99	0.04
D	170.0	48.5	28.78	11.73	31.08	22.18	0.02
E	212.6	21.0	22.66	2.24	22.77	5.64	0.07
F	155.0	0.0	22.69	7.80	23.99	18.96	0.02
G	155.0	21.0	22.51	**14.82**	26.95	33.36	0.02
H	212.6	8.5	19.29	2.11	19.40	6.25	0.04
I	155.0	8.5	19.74	14.73	24.63	36.73	0.01
J	155.0	0.0	17.67	14.54	22.88	39.43	0.01
CG	193.0	28.0	24.44	7.00	25.42	15.98	---
average	---	---	---	---	27.59	14.23	0.031

Table 16. Displacements of the selected points at the end of ULS load case (F=3964 MN)

point	X (m)	Y (m)	U_X (mm)	U_Y (mm)	|U| (mm)	α (°)	β_{CG} (°)
A	240.0	56.0	**45.29**	-10.51	46.49	-13.06	0.05
B	212.6	56.0	44.70	3.61	44.85	4.62	0.06
C	240.0	48.5	41.13	-10.47	42.44	-14.29	0.05
D	170.0	48.5	36.24	14.81	39.15	22.23	0.01
E	212.6	21.0	28.40	2.66	28.52	5.35	0.07
F	155.0	0.0	28.45	9.76	30.07	18.93	0.02
G	155.0	21.0	28.24	**18.77**	33.91	33.61	0.02
H	212.6	8.5	24.11	2.51	24.24	5.93	0.04
I	155.0	8.5	24.69	18.66	30.95	37.08	0.01
J	155.0	0.0	22.06	18.42	28.74	39.87	0.01
CG	193.0	28.0	30.68	8.73	31.90	15.89	---
average	---	---	---	---	34.66	14.20	0.030

Table 17. Summary of displacements and rotations for the two kinematic mechanism and for the three load cases

	Translation		Roto-translation		
load cases	$\|U\|_{av}$ (mm)	α_{av} (°)	$\|U\|_{CG}$ (mm)	α_{CG} (°)	β_{CG} (°)
SILS	26.6	14.2	24.49	15.99	0.031
SLS2	27.6	14.2	25.42	15.98	0.031
ULS	34.7	14.2	31.90	15.89	0.030

4.2 Load – displacement curves: incremental analysis

The comments above on the meaning of a ULS calculation carried out using numerical analyses, justify the use of load-displacement curves as a tool for evaluating the safety of the anchor block against ultimate limit states. In the following, the load-settlement curves of selected points will be reported and commented.

Before starting the incremental analyses, the displacements calculated in the preliminary stages of excavation and block construction were reset to zero, so that the load-displacement curves discussed in the following refer to the application of the external loads only. The excavation and construction stages were in fact only simulated to reproduce the stress state at the beginning of the loading process.

The load-displacement curves computed with the incremental analyses for the ten selected points are plotted from Figure 36 to Figure 38. Figure 39 and Figure 40 show the increase of rotation of horizontal and vertical alignments, respectively, with increasing loading. In each figure, three continuous lines identify the SILS, SLS2 and ULS loading conditions as obtained in the tender design; the dashed lines are for the SILS, SLS2 and ULS loading cases as obtained from the global IBDAS model version 3.3b and version 3.3f. The low differences between the cable forces obtained from the tender design and those provided by the global IBDAS models result in negligible differences in the displacement field of the anchor block. In the following comments are referred to tender design cable forces that provided the higher values for the ULS load conditions.

From data in Table 14 – Table 16 and from Figure 36 – Figure 40 it is possible to observe that:

- from loading conditions SILS to loading condition ULS, that is with an increase of the design force of about 26%, the maximum horizontal (*X*) and vertical (*Y*) displacements increase of about 30.5% and 32% respectively;

- the settlements of points belonging to the same vertical and horizontal alignments are not the same because of a small deformation of the anchor block;
- differences in the load-rotation curves for all the alignments, with the exception of alignments E – G and H – I, can be attributed again to a small deformation of the anchor block;
- points A and C have a negative displacement, that is move downwards, because of the clockwise rotation of the block.

To evaluate the ultimate failure load, and thus the "distance" from the development of a collapse mechanism in the soil around the anchor block, a hyperbolic best fitting of the load-displacement curves can be carried out. Figure 41 shows the load – displacement curves in a diagram in which |u| is on x-axis and |u|/|F| is on the y-axis; in this way the curves, with the exception of their initial portion, plot along a line with an inclination to the horizontal denoted *n*. The maximum force is the limiting value of the load as the displacement approaches infinity, that is F_{max}=1/n; conservatively this is generally taken as F_{max}=0.9/n.

The range of values of *n* and F_{max} are shown in the figure: F_{max} was evaluated to be in between 15100 MN and 16500 MN that, for the ULS loading condition, results in a global safety factor of 3.75 to 4.15.

4.3 Plaxis^{3D} Foundation output

In the following a selection of the output will be presented for relevant steps. According to *Plaxis*^{3D} *Foundation* sign conventions, compressive stresses and deformations are negative.

The soil stress state during the main stages of the analyses is shown using contours of relative shear stress ratio τ_{rel}, that gives an indication of the proximity of the stress state to the available shear strength. Relative shear stress ratio is defined as:

$$\tau_{rel} = \frac{\tau_{mob}}{\tau_{max}} \qquad (20)$$

where τ_{mob} is the mobilised shear strength (i.e. the radius of the Mohr stress circle) and τ_{max} is the maximum value of shear stress, for the case where the Mohr's circle is expanded to touch the Coulomb failure envelope, while keeping the centre of Mohr's circle constant.

In the following, the figures will be referred to two sections: a longitudinal section through the centre of gravity of the block, in the North-South direction, at *Z* = 225 m, and a transversal section, in the East-West direction, at *X* = 172 m.

4.3.1 Soil stress state

Figure 42 and Figure 43 show the contours of relative shear stress computed in the longitudinal and transversal sections at the initial stage and at the end of excavation, respectively. At the end of excavation, a high degree of shear strength mobilisation in observed in the soil close to the diaphragm walls.

At the end of block construction, the contours of τ_{rel} shown in Figure 44 show a decrease of the mobilised shear strength due to the increase of the normal effective stress induced by the weight of the anchor block.

Figure 45 shows the contours of τ_{rel} computed for the SILS loading condition (minimum design force), while Figure 47 refers to the ULS loading condition (maximum design force).

Application of cable forces induce an increase of mobilised shear strength in the rear end of the block, and a decrease at its base, though the values of τ_{rel} induced by ULS loading conditions are higher than those obtained for the SILS load case.

Figure 46 and Figure 48 show the effective normal stresses acting on the soil-wall interface elements of the transversal diaphragm walls (East-West direction) for the SILS and the ULS loading conditions, respectively. For both the examined loading conditions, SILS and ULS, compressive normal stress act on the front and rear diaphragm walls with maximum values of -280 ÷ -300 kPa for the SILS loading condition, and of -300 ÷ -360 kPa for the ULS loading conditions.

For the ULS loading condition, Figure 49 shows the contours of vertical effective stress σ_{YY} and horizontal effective stress σ_{XX} acting in the horizontal plane at Y = 42.5 m s.l.m., while Figure 50 shows the contours of horizontal effective stress σ_{XX} acting in the longitudinal section and of horizontal effective stress σ_{ZZ} acting in the transversal section.

Finally, again for the ULS loading condition, Figure 51 shows the contours of vertical effective stress σ_{YY} computed in the longitudinal and transversal sections of the anchor block.

4.3.2 Displacements

Figure 52 shows the contours of vertical displacements induced in the foundation soil by the block construction: maximum settlements of about 50 mm are computed, the contours showing that settlements approach zero at about -65 m a.s.l., that is at a depth of about 60 m below the base of the block.

Figure 53 – Figure 56 show displacement contours computed for the SILS loading condition (minimum design force), while Figure 57 – Figure 60 refer to the ULS loading condition (maximum

design force). The displacement fields discussed in the following refer to application of cable force only, since displacements induced by the previous stages of excavation and block construction were reset to zero before their application.

The displacements plotted in Figure 53 for the SILS loading conditions show that maximum values are attained at the point of application of the cable forces; the maximum displacement at the top of the anchor block is in between 32 and 36 mm; the displacements in the soil, at the ground surface, approach zero at a distance of about 100 m from the front of the block (X = 350 m). In the transversal direction, soil displacements become negligible at a distance of about 90 m from the block sides. Figure 54 shows two perspective views of the contours of displacements of the anchor block.

Figure 55 and Figure 56 show the contours of horizontal (X direction) and vertical (Y direction) displacements computed in the longitudinal and transversal central sections.

The displacements plotted in Figure 57 for the ULS loading condition, show that the maximum values are attained at the point of application of the cable forces; the maximum total displacement at the top of the block is between 44 and 48 mm; the displacements in the soil, at ground level, approach zero at a distance of about 110 m from the front of the block (X = 360 m). Again, in the transversal direction, soil displacements become negligible at a distance of about 90 m from the block sides, as for the SILS loading condition. Figure 58 shows two perspective views of the contours of displacements of the anchor block.

Figure 59 and Figure 60 show the contours of horizontal (X direction) and vertical (Y direction) displacements computed in the longitudinal and transversal central sections.

5 CONCLUSIONS

In this report, the behaviour of Sicily Anchor Block under the application of SILS, SLS2 and ULS loading conditions was studied through static 3D FE analysis using the code *Plaxis*^{3D} *Foundation*. The calculations are based on both drawings and cable forces provided in the tender design; account is also given for the influence of the cable forces computed from the global IBDAS model version 3.3b and version 3.3f. Evaluation of earthquake-induced block displacements and of safety against ultimate limit states are discussed in the companion report "Sicily anchor block: earthquake-induced displacements and safety against ultimate limit states".

The Sicily Anchor Block consists of a massive, reinforced concrete block with a trapezoidal shape in plane. It is 100 m long in the North-South direction while in the East-West direction the smaller side is 80 m in length, whereas the larger one is 120 m long, this resulting in a mean width of 100 m. In the East-West direction, at elevations higher than the top of the longitudinal diaphragm walls, the block is about 5 m wider.

The top and the bottom of the block consist of two different planes, respectively: the front of the anchor block has an inclination of about 15° at the top and of about 25° at the bottom; the rear end of the anchor block has an inclination of about 7° at the top and of about 8° at the bottom. The maximum elevation of the anchor block is +60 m a.s.l. and the deepest end of the structure is at +1 m a.s.l..

The anchor block includes four splay chambers: two of them are for the main cables, the other two are to be filled with granular material after installation of the main cables.

The excavation needed for block construction is supported by diaphragm walls, with a thickness of 1.0 m and a width of 2.5 m, whose length varies according to the shape of the block. The earth retaining system include levels of retaining anchors, varying in number along the different sides of the pit. In the middle and in the front of the construction site jet-grouted columns are planned down to a maximum depth of 30 m with a thickness of 18.5 m and to a maximum depth of 20 m with a thickness of 7 m respectively; the jet-grouted columns are confined by the diaphragm walls.

On the Sicily shore, starting from ground level and moving downwards the following units are encountered: *Depositi Costieri* (Coastal Deposits); *Ghiaie di Messina* (Messina Gravel); *Depositi Continentali* (Continental Deposits); *Conglomerato di Pezzo* (Pezzo Conglomerate); *Cristallino* (Crystalline bedrock). For the Sicily Anchor Block, the relevant geological unit is the Messina Gravel that is characterised by an increase in small strain shear stiffness at an elevation of about -75 m a.s.l..

The 3D FE mesh used in the analyses is 400 m long in the direction parallel to the bridge axis, 450 m wide in the direction orthogonal to the bridge axis and 150 m high, considering the highest elevation of ground surface, at +56.0 m a.s.l.. The groundwater level coincides with the sea level, at 0 m a.s.l..

In the FE analyses, the mechanical behaviour of the soil was described using the Hardening Soil model; this is an elastic-plastic rate independent model with isotropic hardening, capable of reproducing soil non-linearity due to the occurrence of plastic strains from the beginning of the loading process. The anchor block concrete and the ballast material were described as linear elastic materials. The diaphragm walls were modelled as WALL shell elements, while the retaining anchors as SPRINGS elements. Jet-grouted soil was assimilated to an elastic-plastic material with Mohr-Coulomb failure criterion.

The FE analyses were mainly carried out to evaluate the displacement field and the stress state induced in the foundation soil by the cable forces. To this purpose, the whole construction sequence was simulated in the analyses that were carried out in terms of effective stresses, assuming drained conditions for the soil. The following sequence of steps was considered: computation of the initial stress state; pre-excavation of the construction area; activation of diaphragm walls and jet grouting; progressive excavation to reach the base of the anchor block with simultaneous activation of the levels of the retaining anchor; progressive activation of the anchor block; filling of the pre-excavated area and of the ballast chambers with granular material; application of the design loads (SILS, SLS2 and ULS loading conditions); incremental analysis with increasing external forces.

Forces in the main cables at Sicily anchor block were provided by the structural analyses for three different load combinations of the tender design (SILS, SLS2 and ULS). The direction of the force is inclined of 15 degrees to the horizontal and directed upwards, towards the Sicily tower. The influence of the cable forces computed using the global IBDAS model version 3.3b and version 3.3f are also discussed.

Starting from the computed displacements, two kinematic mechanisms for the block were reconstructed: one is of pure translation and the other one is of roto-translation around the centre of gravity. Under SILS, SLS2 and ULS loading conditions the average displacement is of about 27 mm, 28 mm and 35 mm, respectively; the average inclination is of about 14° to the horizontal for all the above loading conditions (SILS, SLS2 and ULS). The anchor block behaviour to the application of the external loads mainly consists in a translational movement, directed towards the tower, associated with a downwards rotation.

An evaluation of the ultimate failure load for the anchor block, carried out using a hyperbolic best-fitting of the load-displacement data, provided an ultimate load equal of 15100 to 16500 MN. This results in a safety factor against external increasing forces of 3.75 to 4.15 for ULS loading condition.

6 FIGURES

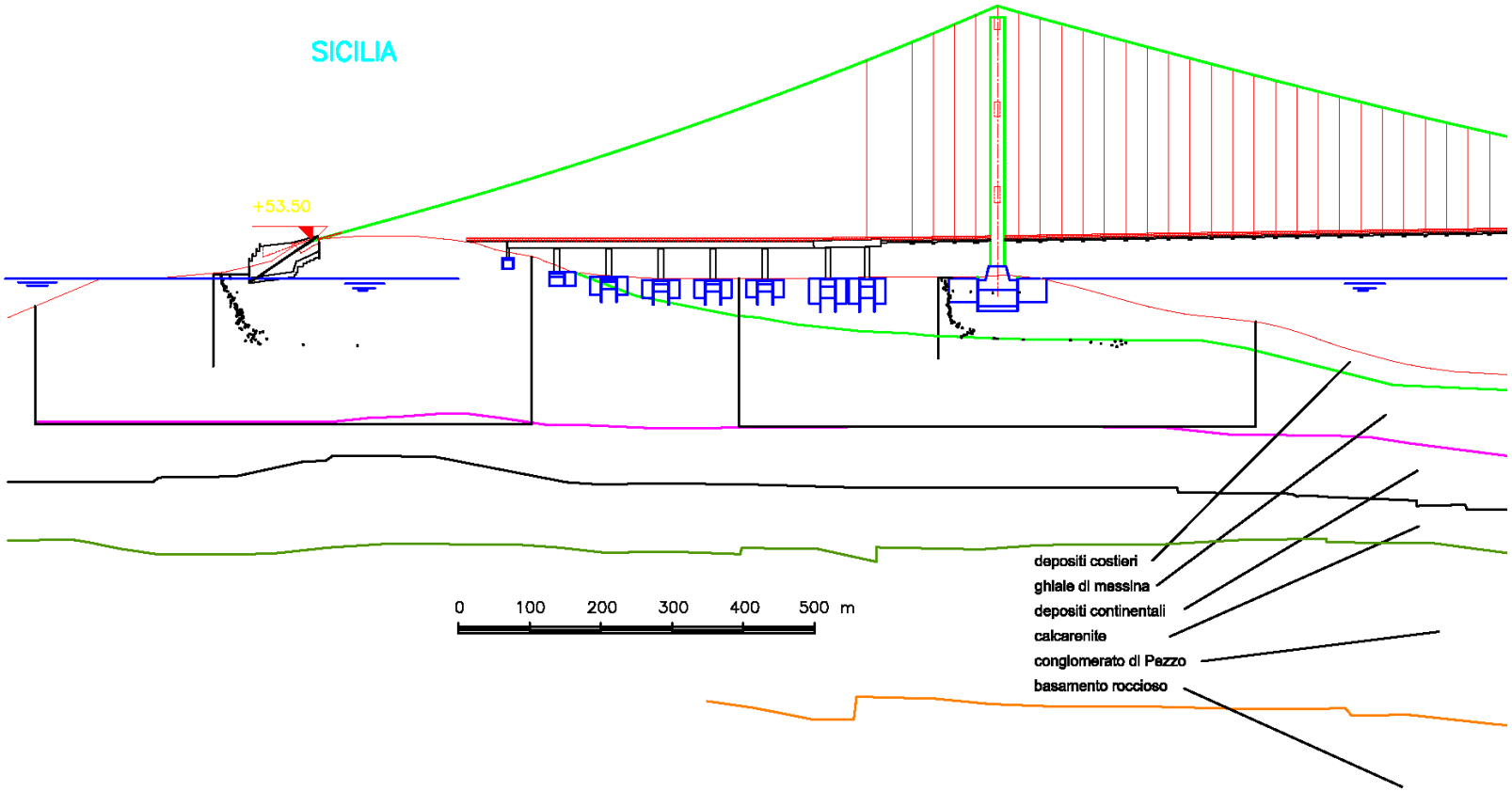

Figure 1. Soil profile on Sicily shore of Messina Strait

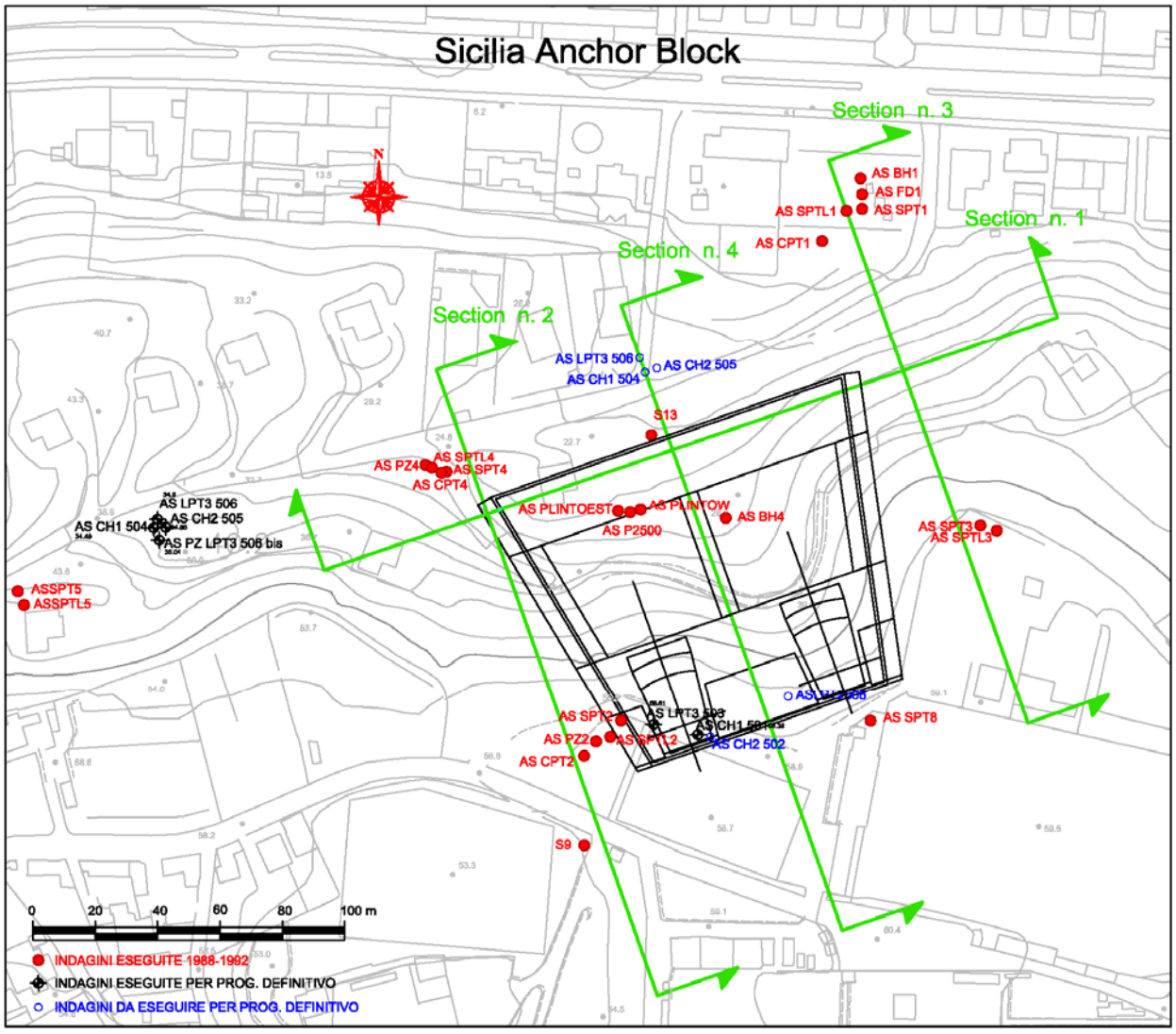

Figure 2. Plan view of Sicily anchor block

SECTION N. 1

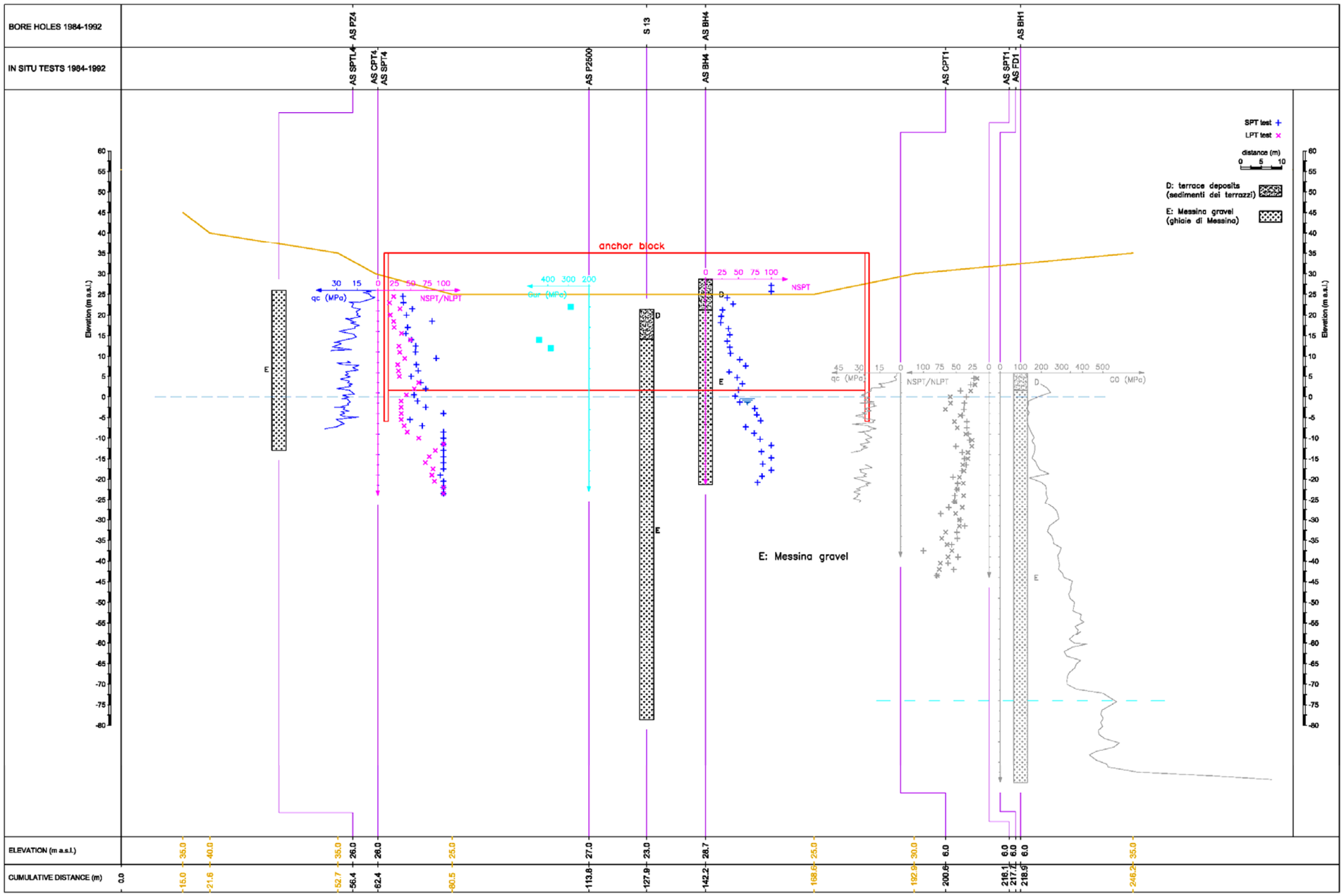

Figure 3. Cross section (section No. 1)

SECTION N. 2

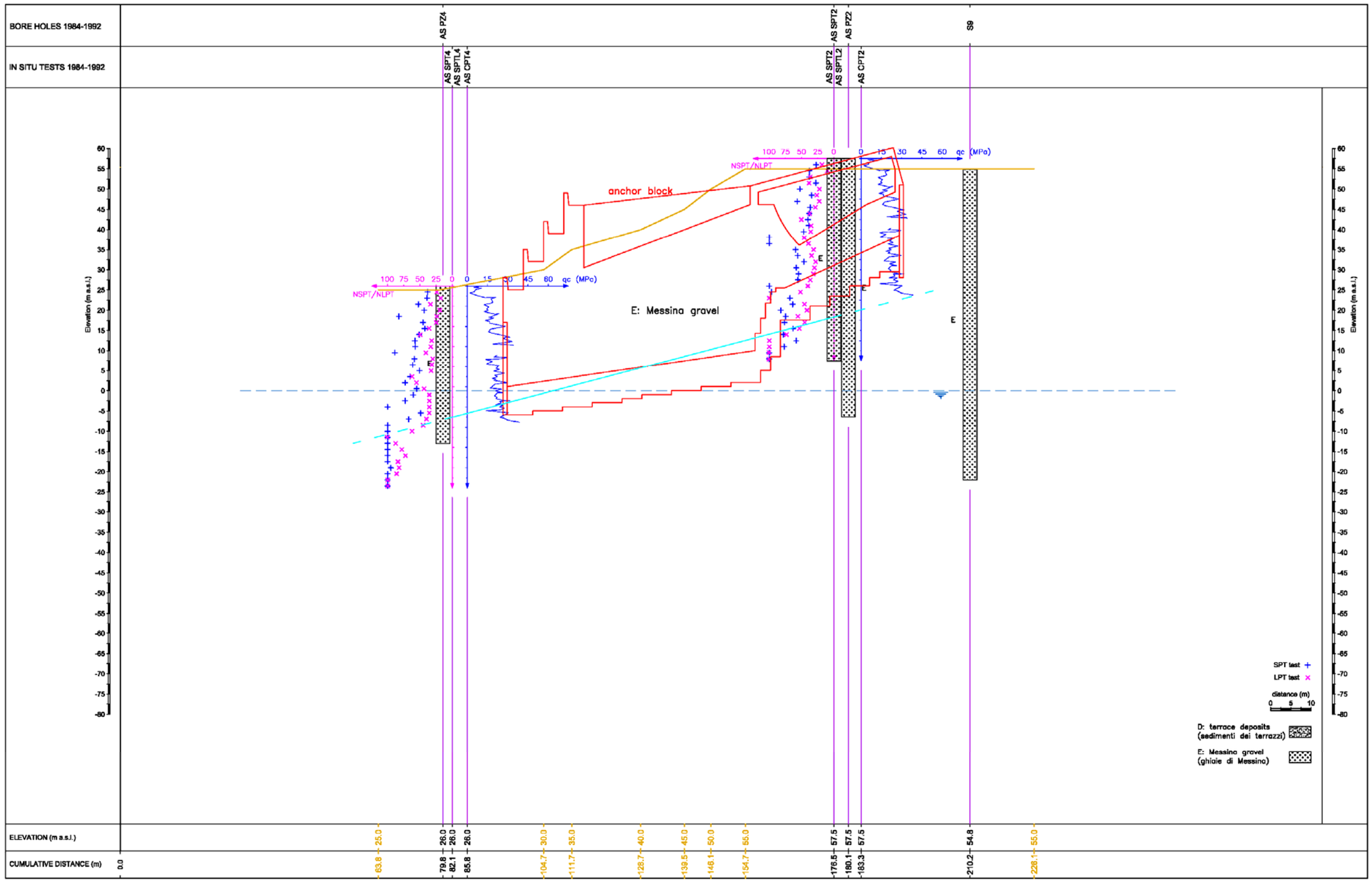

Figure 4. Longitudinal section (section No. 2)

SECTION N. 3

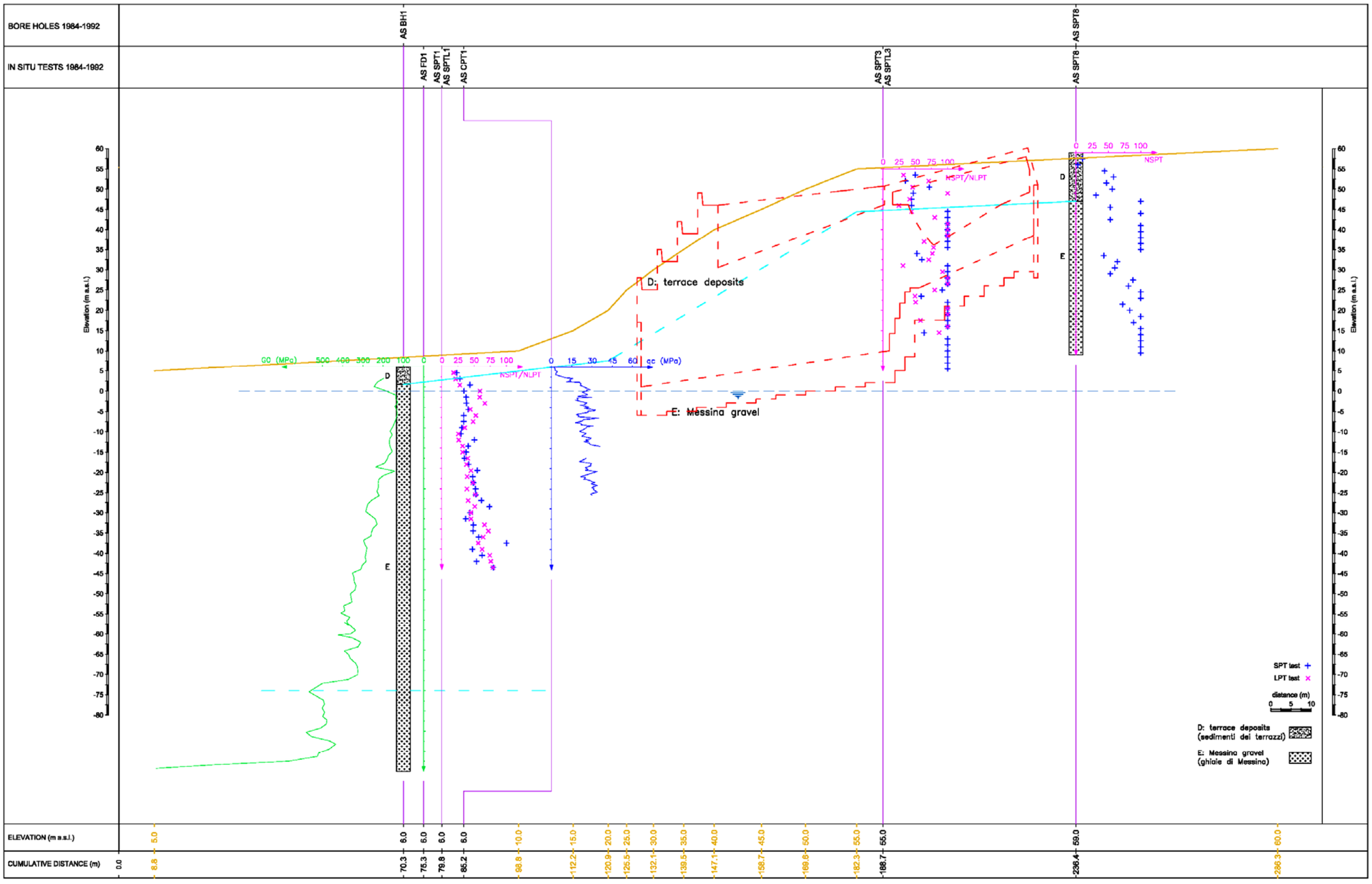

Figure 5. Longitudinal section (section No. 3)

SECTION N. 4

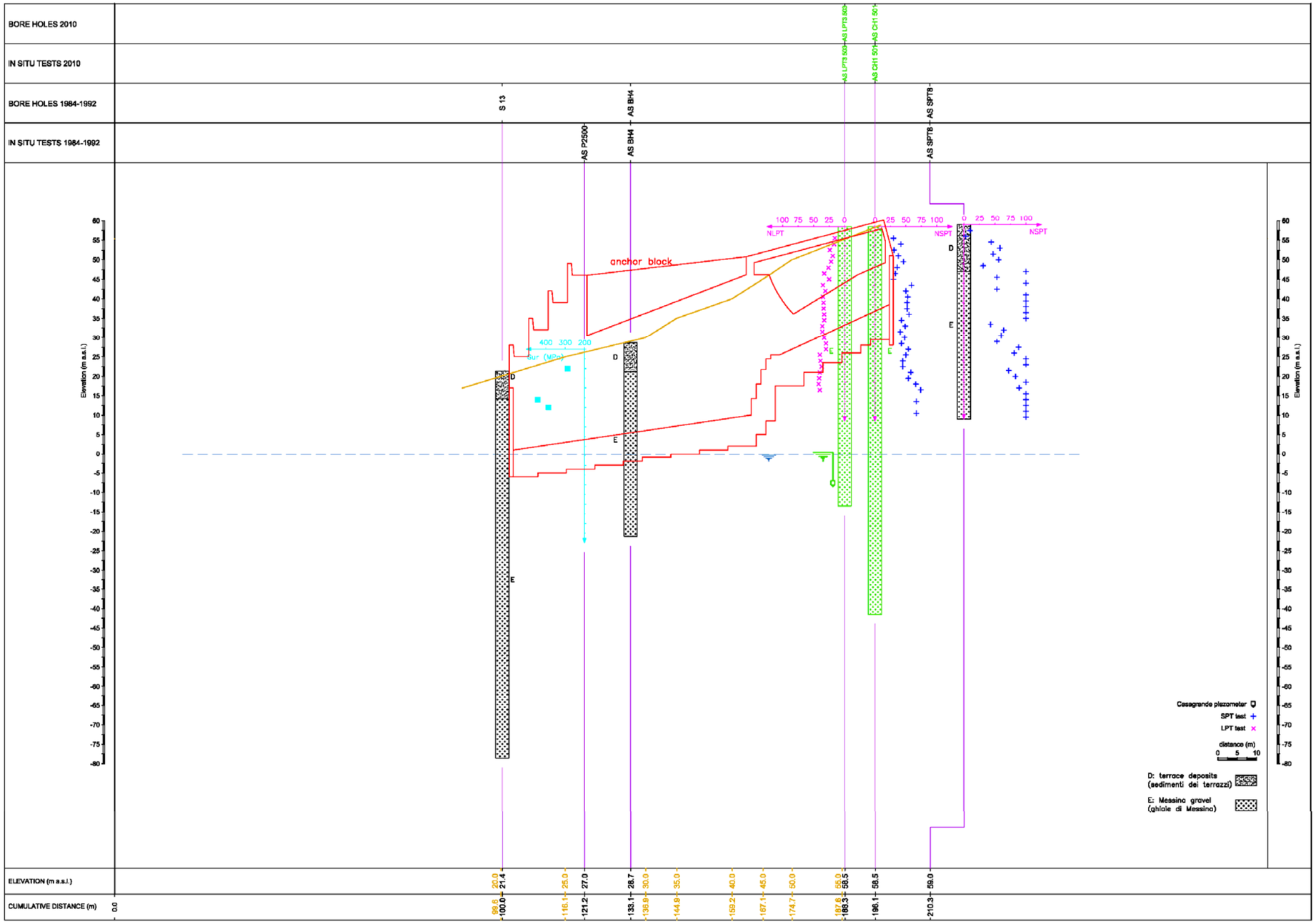

Figure 6. Longitudinal section (section No. 4)

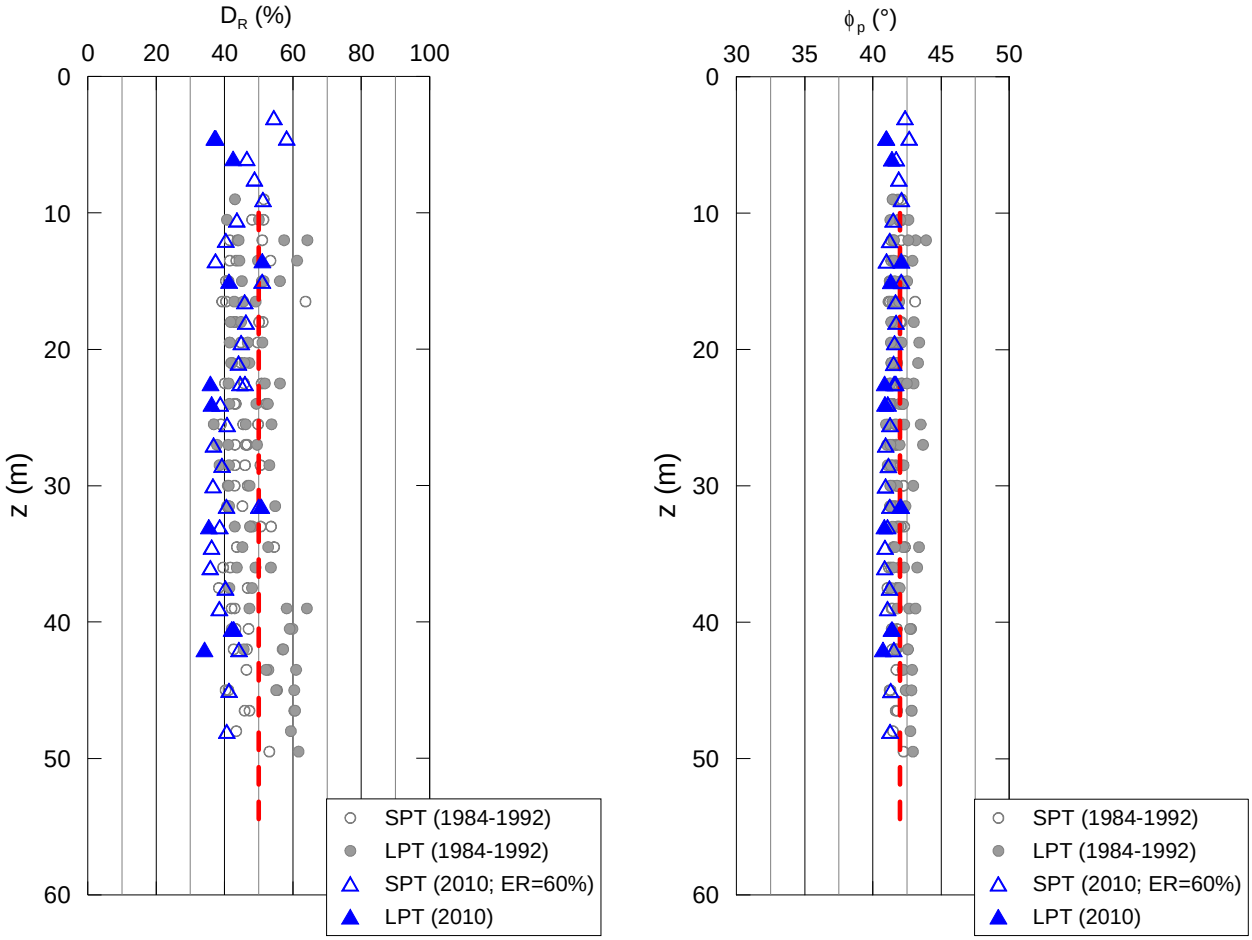

Figure 7. Sicily Anchor Block: relative density and angle of shearing resistance from SPT and LPT test results

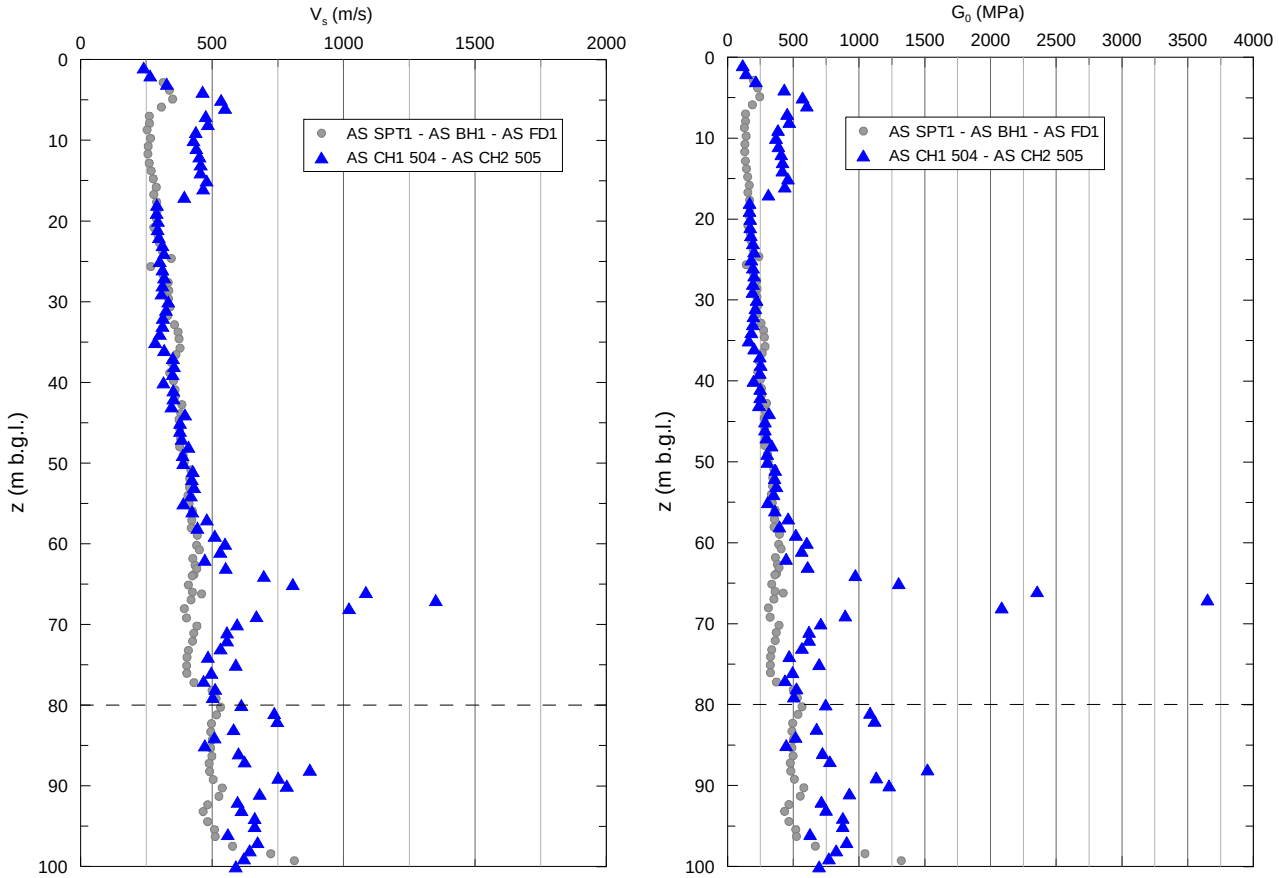

Figure 8. Sicily Anchor Block, V_s and G_0 profiles from cross-hole tests

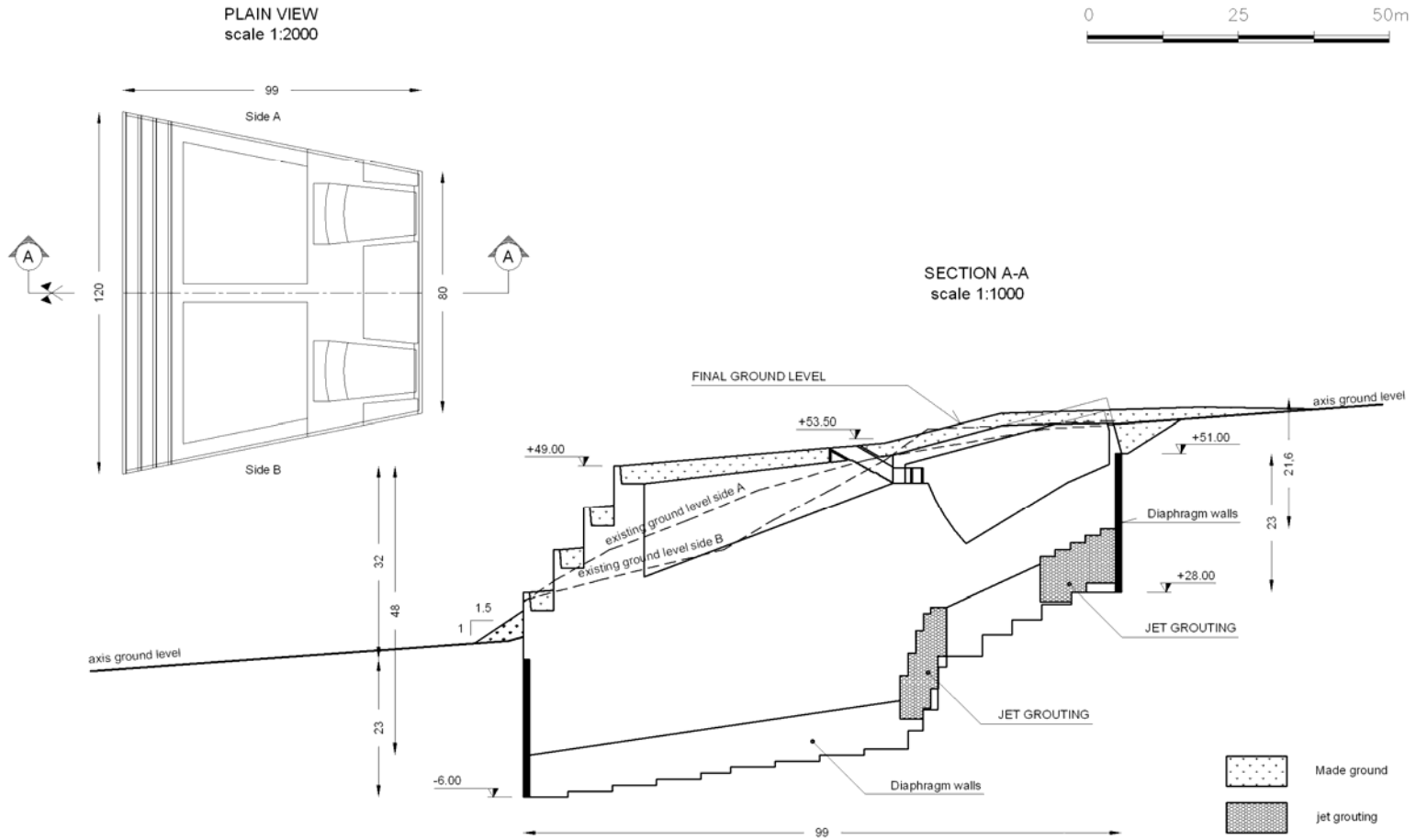

Figure 9. Plan view and longitudinal section of Sicily anchor block

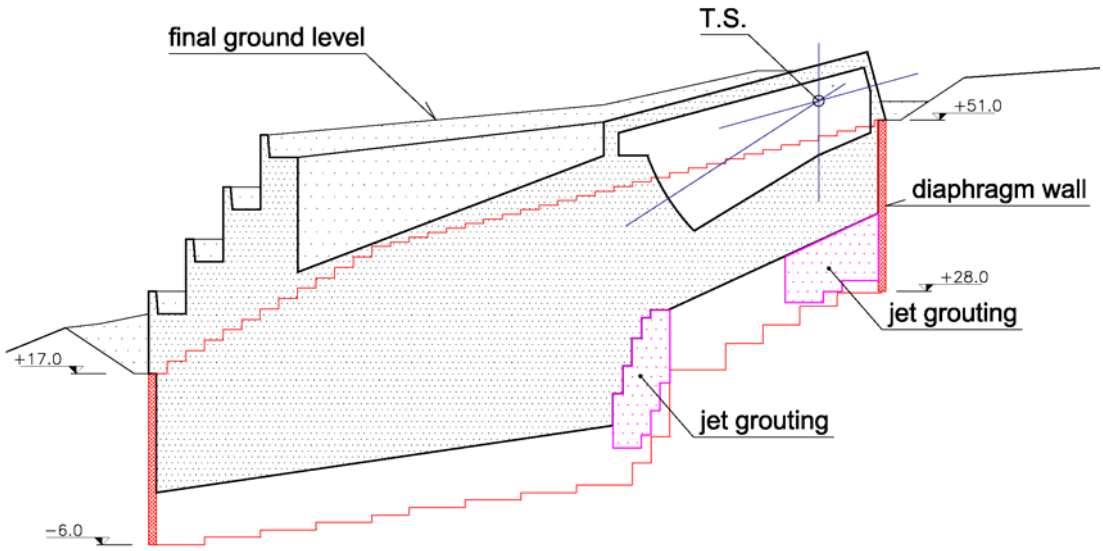

Figure 10. Longitudinal section of the Sicily Anchor Block

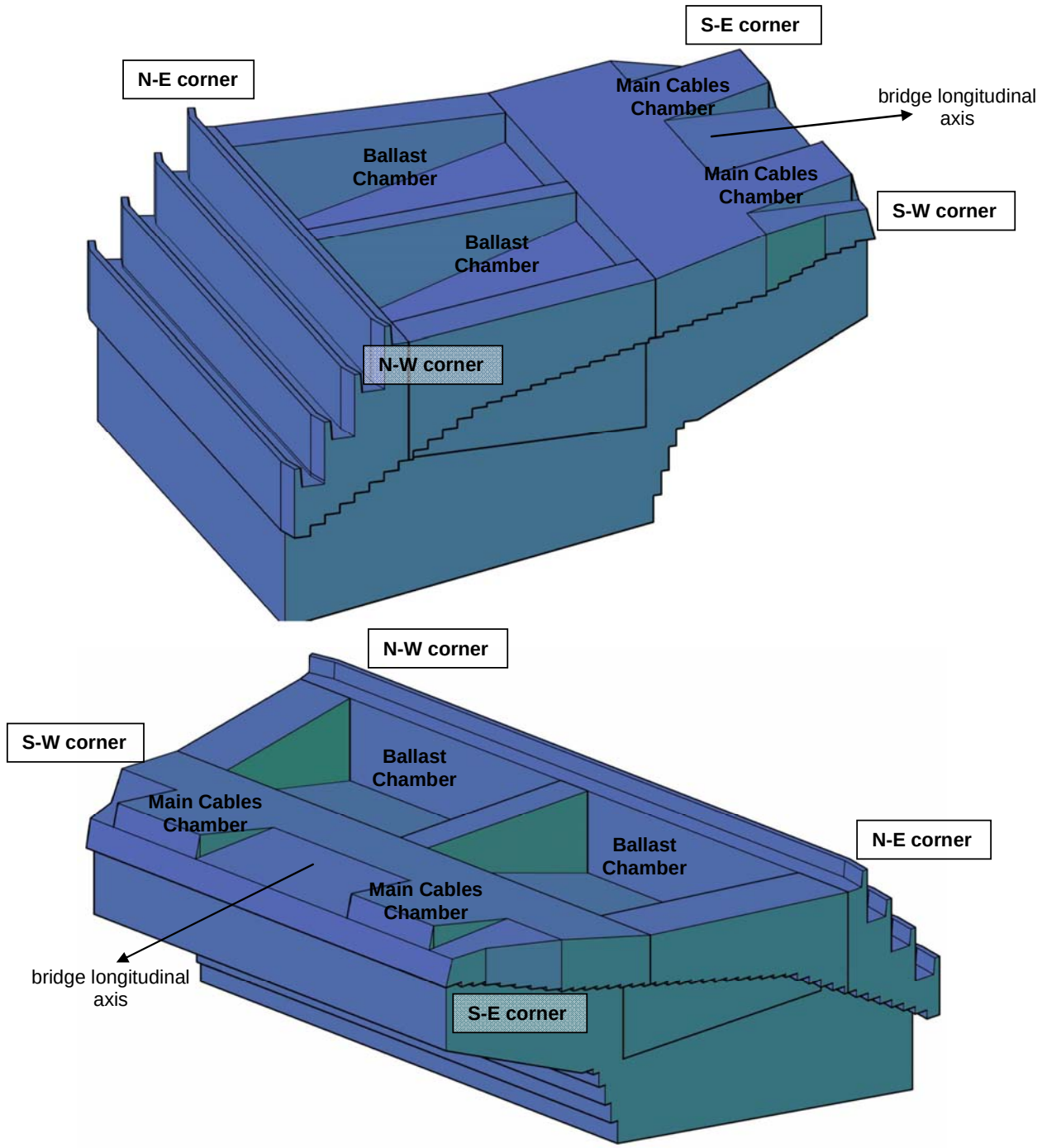

Figure 11. Perspective view of the anchor block design

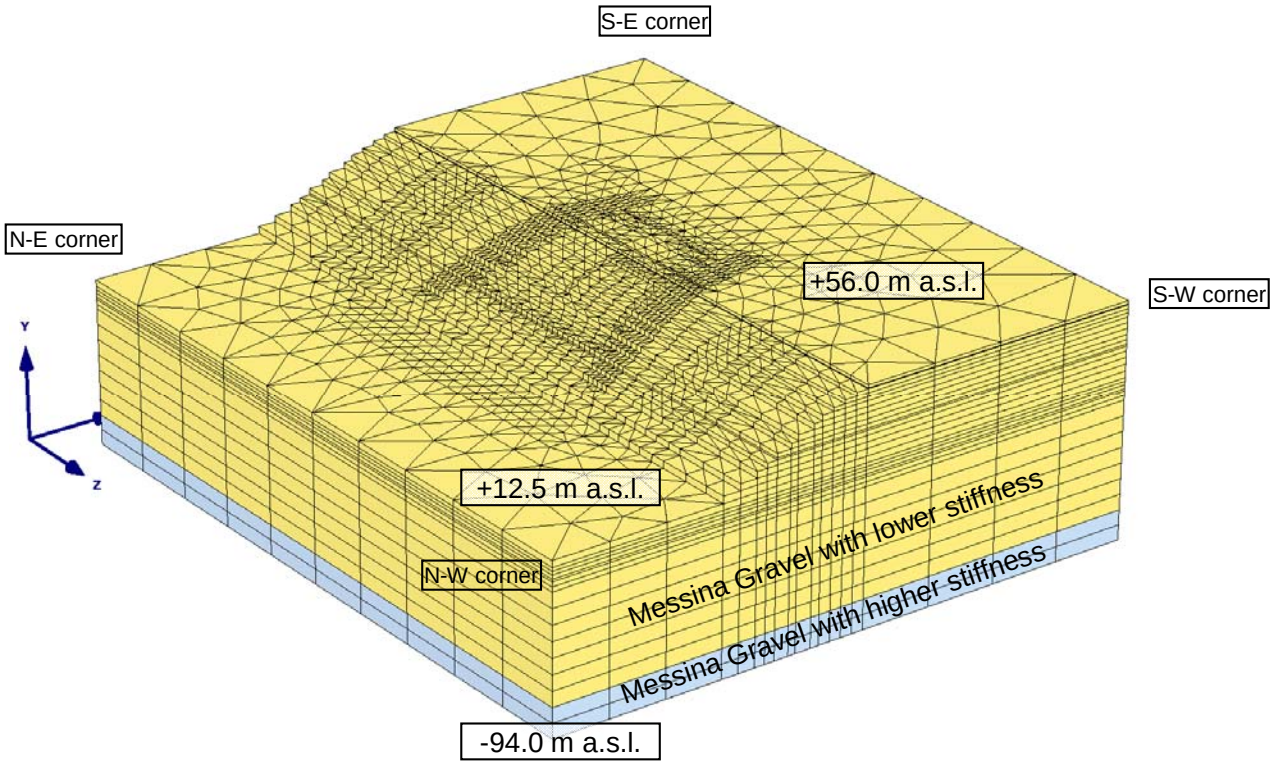

Figure 12. Perspective view of FE mesh in the initial phase

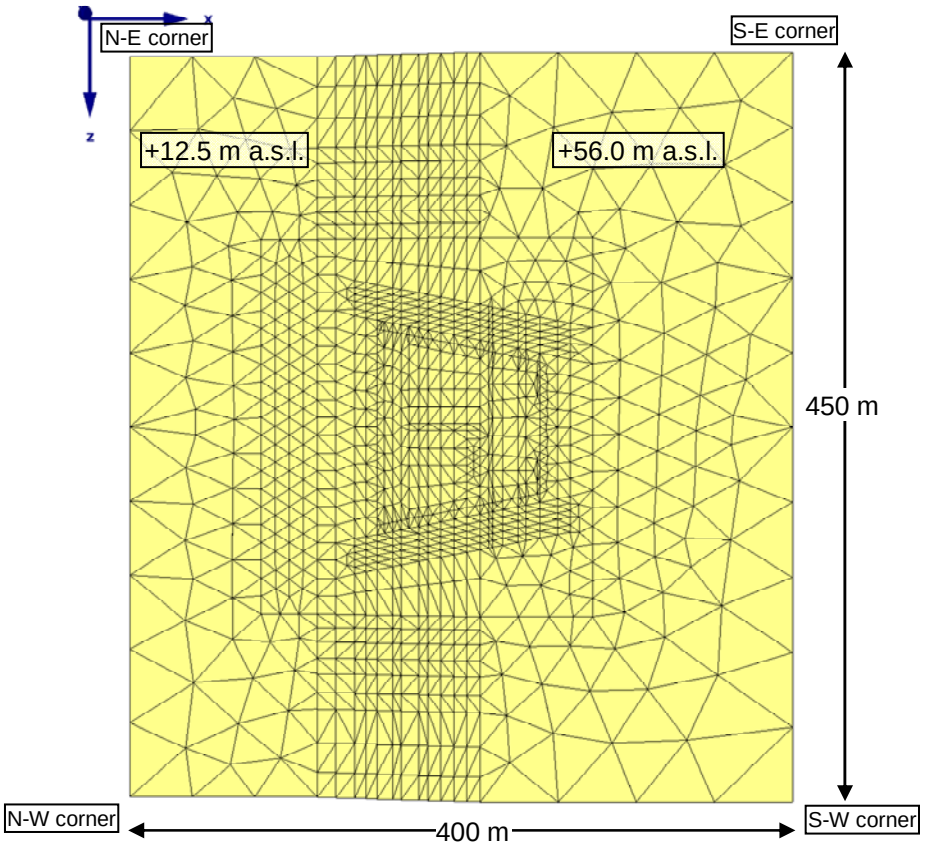

Figure 13. Plan view of FE mesh in the initial phase.

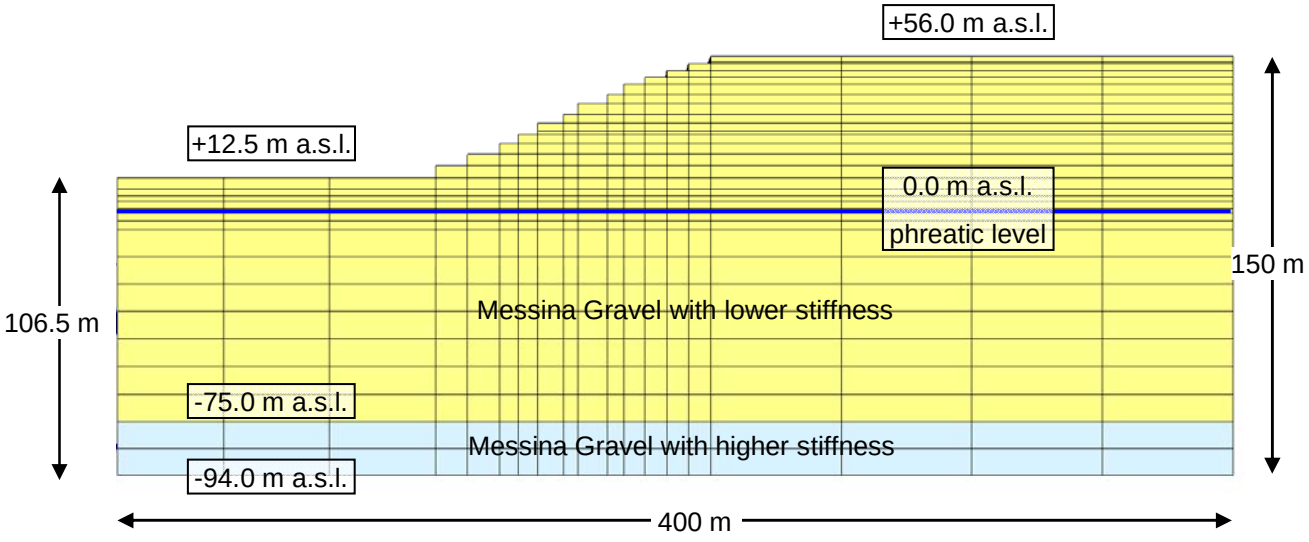

Figure 14. Front view of FE mesh in the initial phase

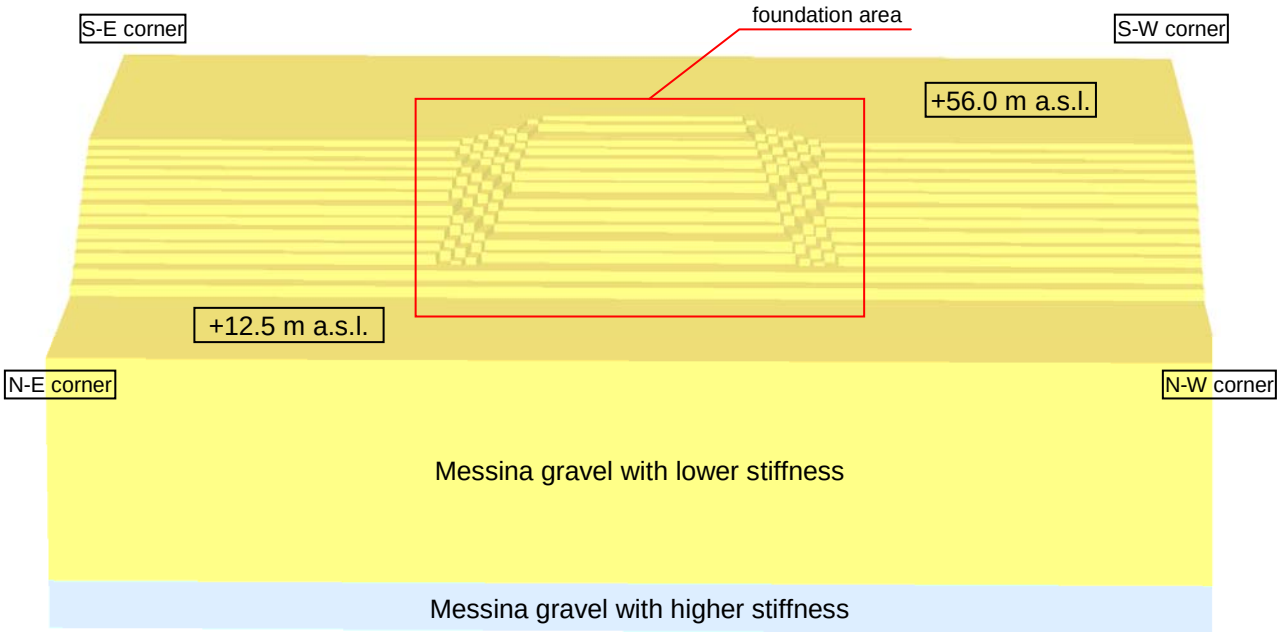

Figure 15. Perspective view of the pre-excavation stage

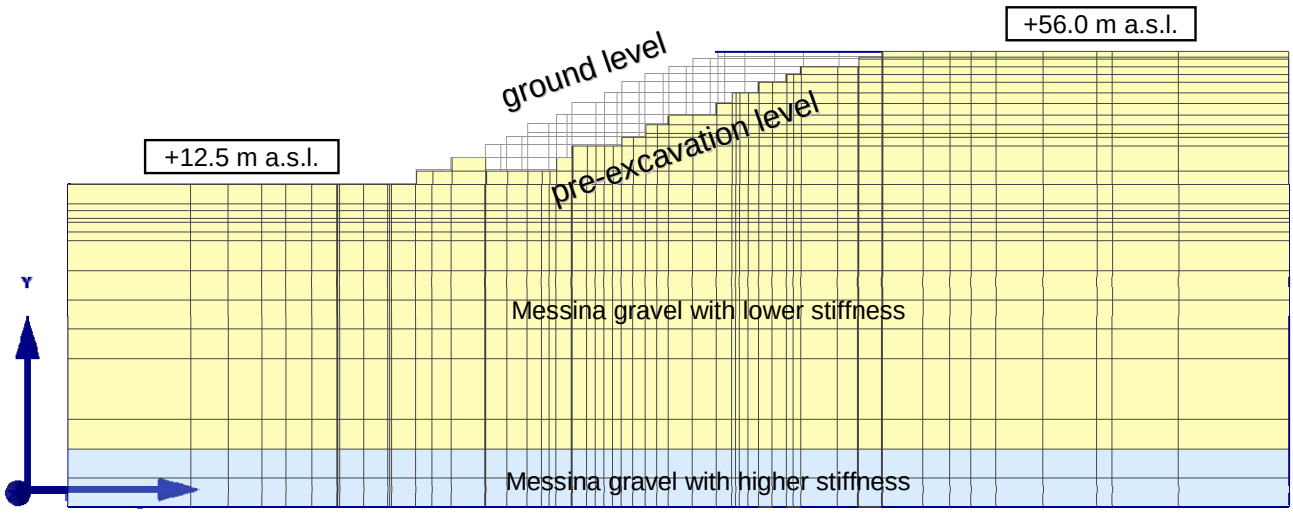

Figure 16. Longitudinal section of FE model at the pre-excavation stage

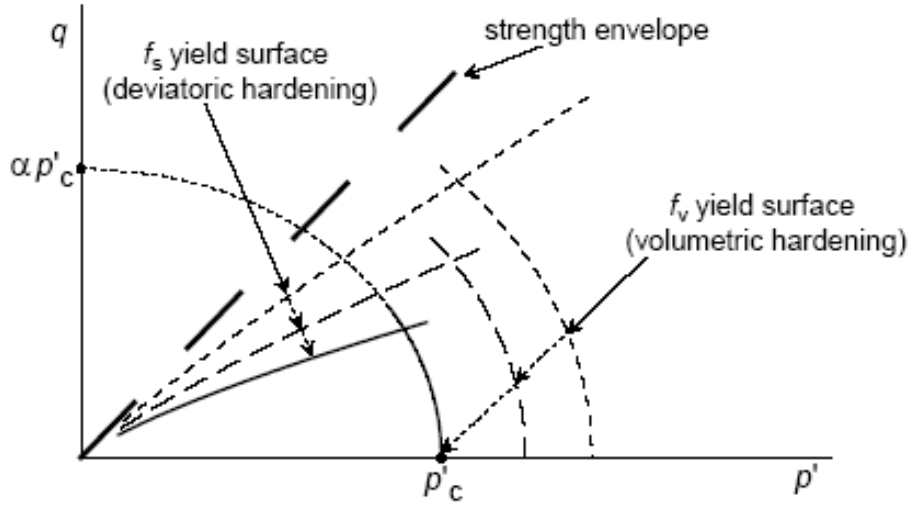

Figure 17. Yield surfaces of the Hardening Soil model and their evolution

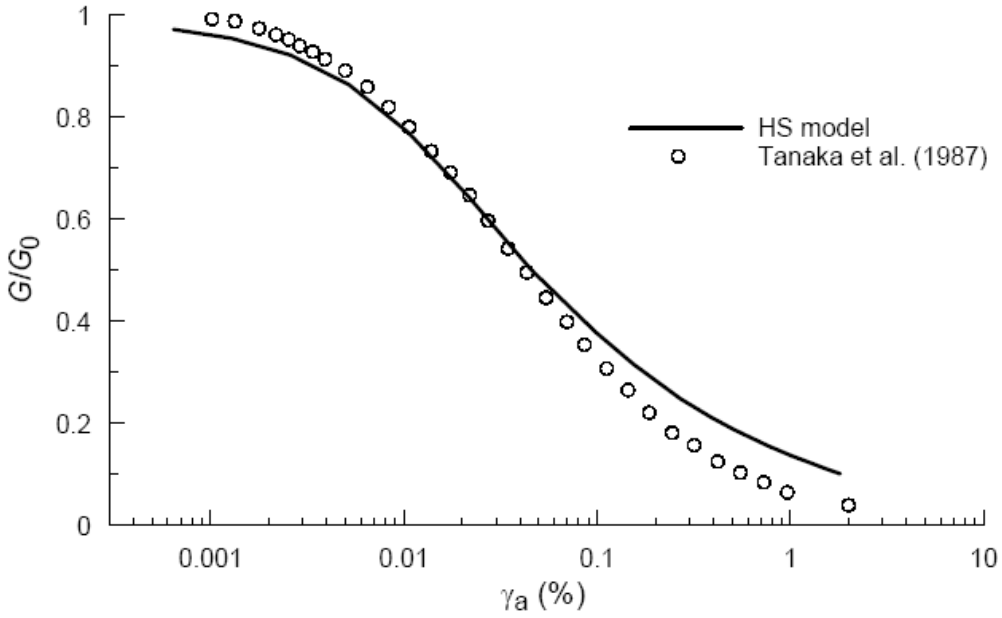

Figure 18 . Comparison between the modulus decay curve predicted by the HS model and that obtained by Tanaka et al (1987)

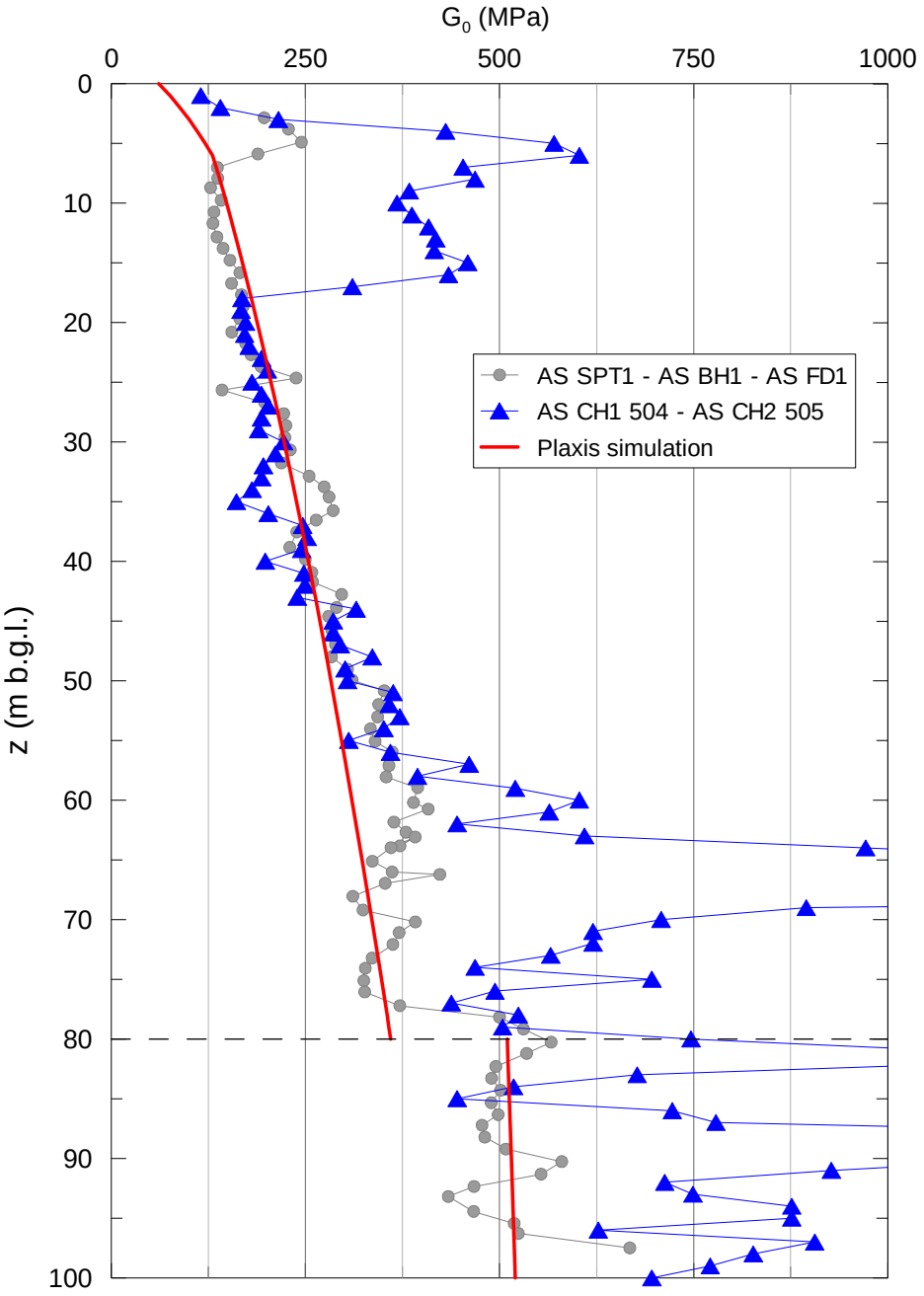

Figure 19. G_0 profile from cross-hole test and HS model prediction

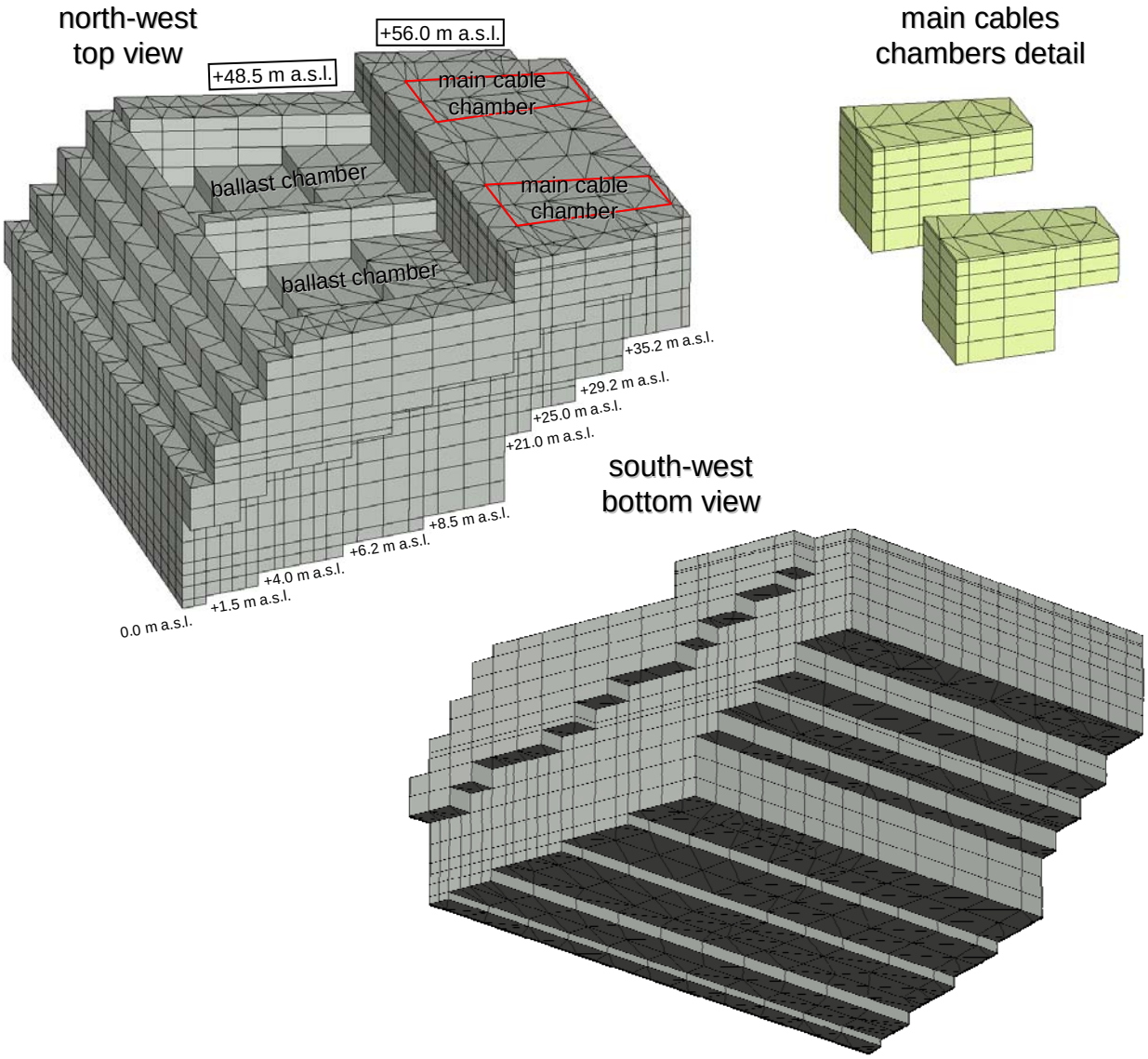

Figure 20. Perspective view of the anchor block model without filling material

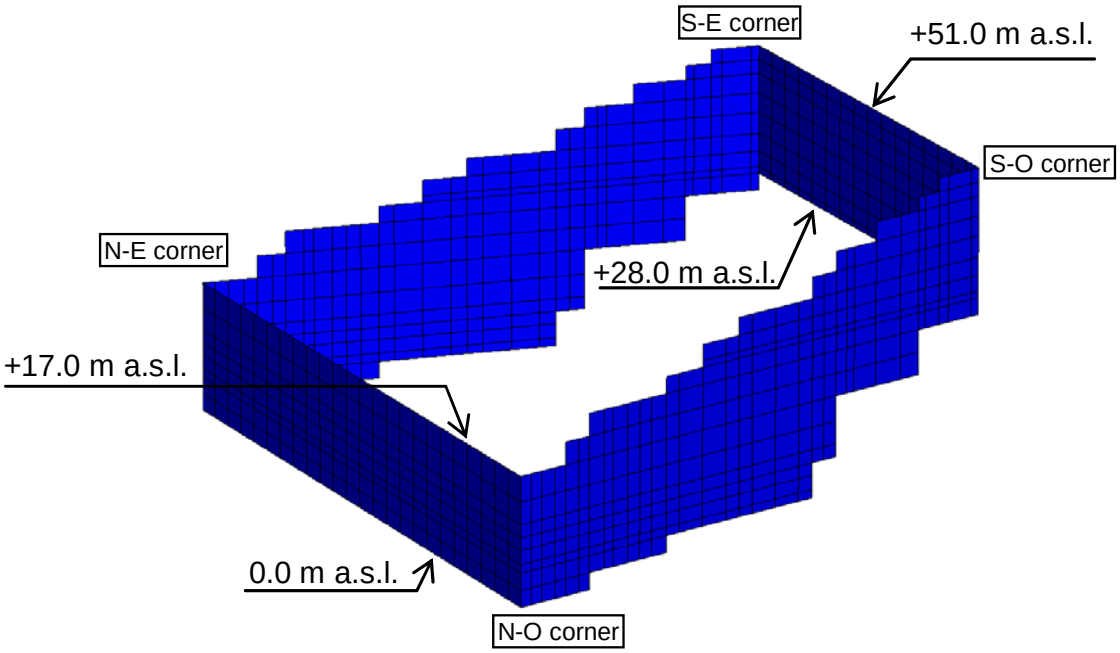

Figure 21. Perspective view of the diaphragm walls

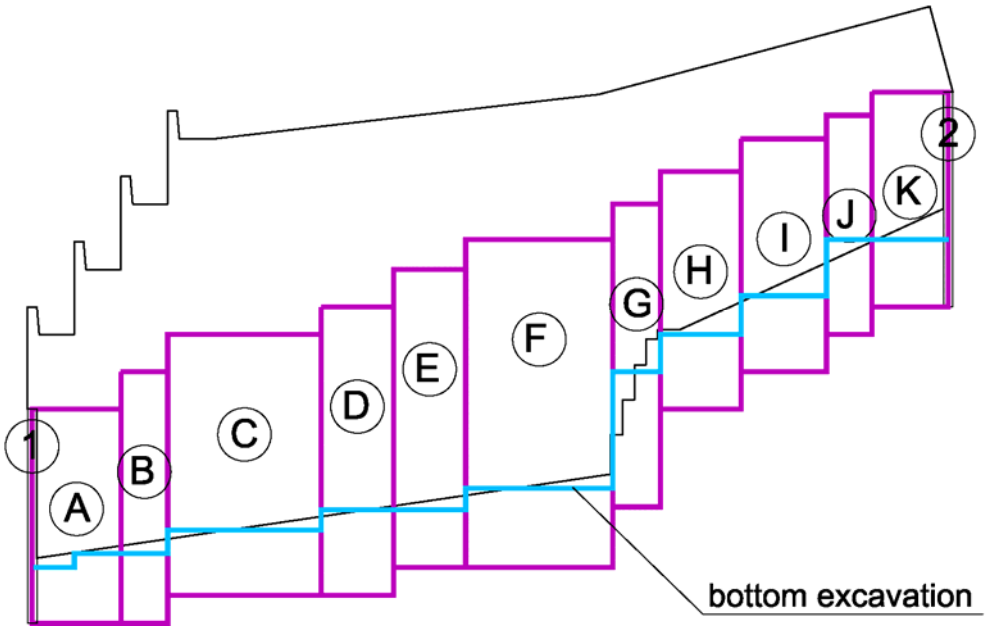

Figure 22. Scheme of the longitudinal diaphragm walls

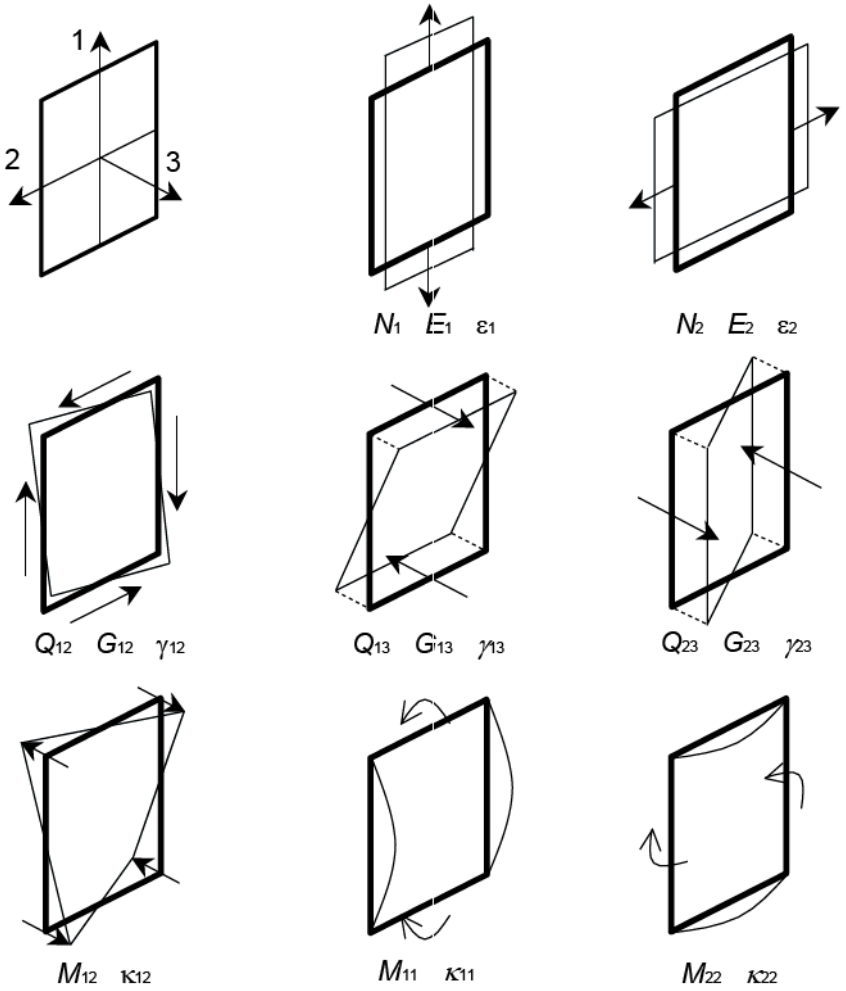

Figure 23. Wall elements in PLAXIS

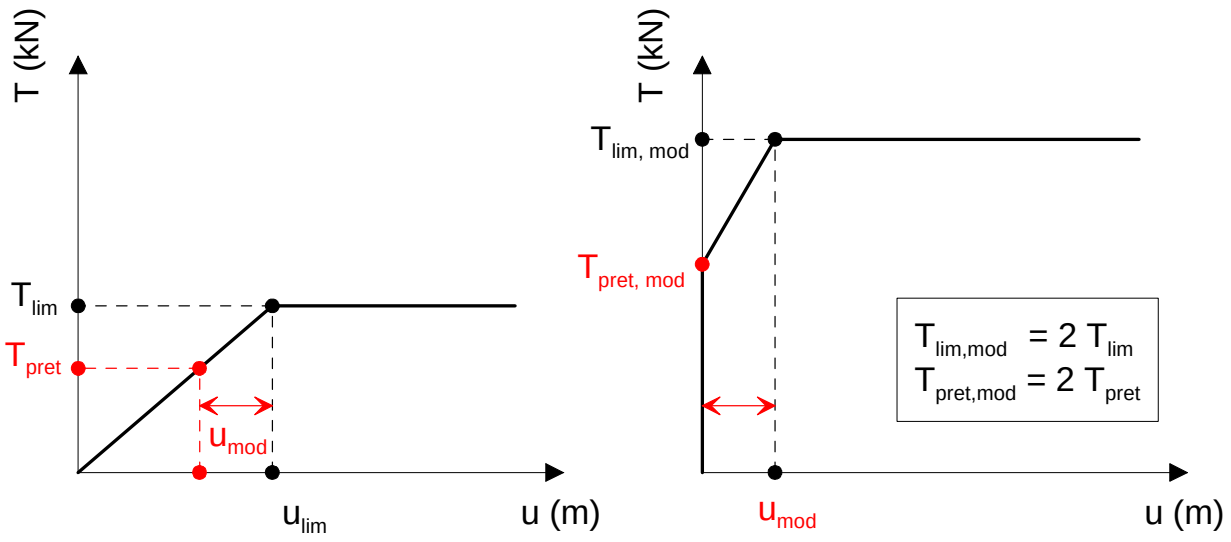

Figure 24. SPRINGS elements: non linear stiffness and (T-u) relation for the pre-tensioned springs in the model

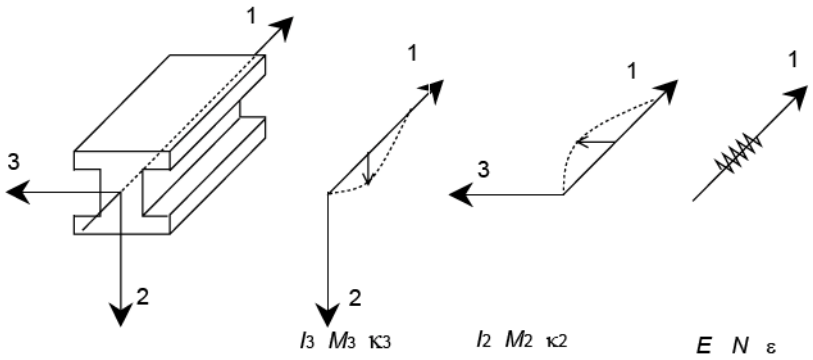

Figure 25 Beam elements in PLAXIS

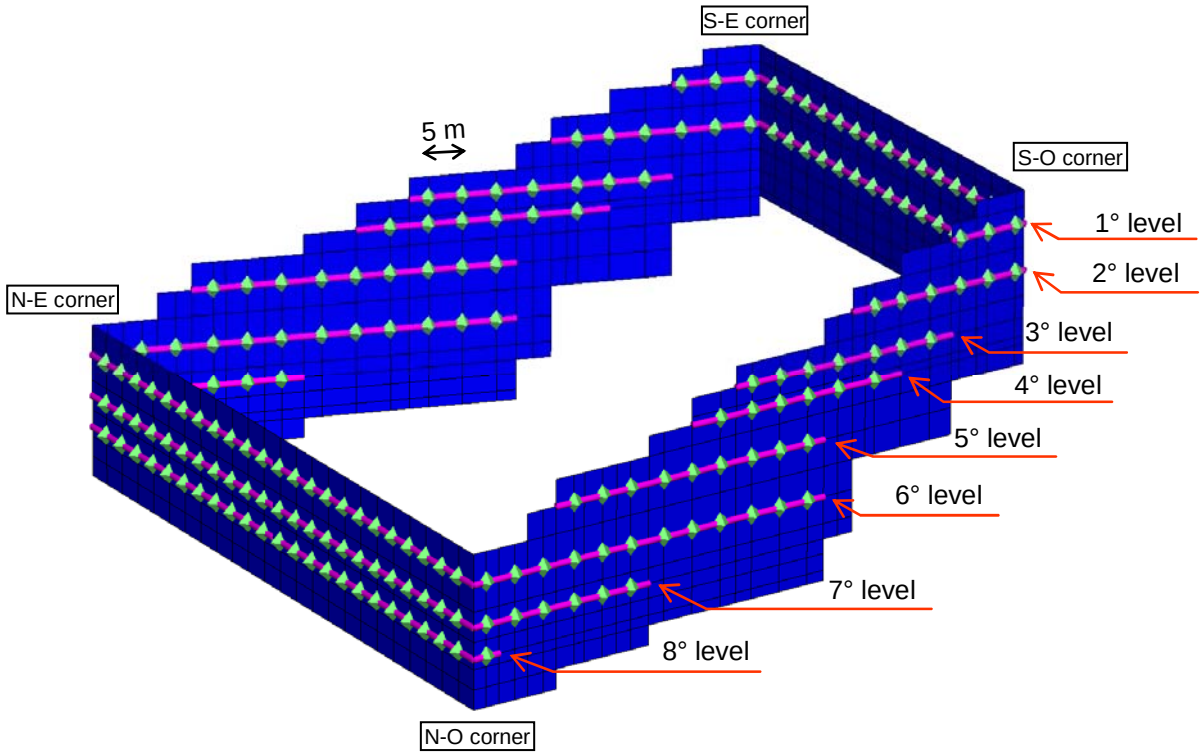

Figure 26. Perspective view of the springs and of their connecting beams

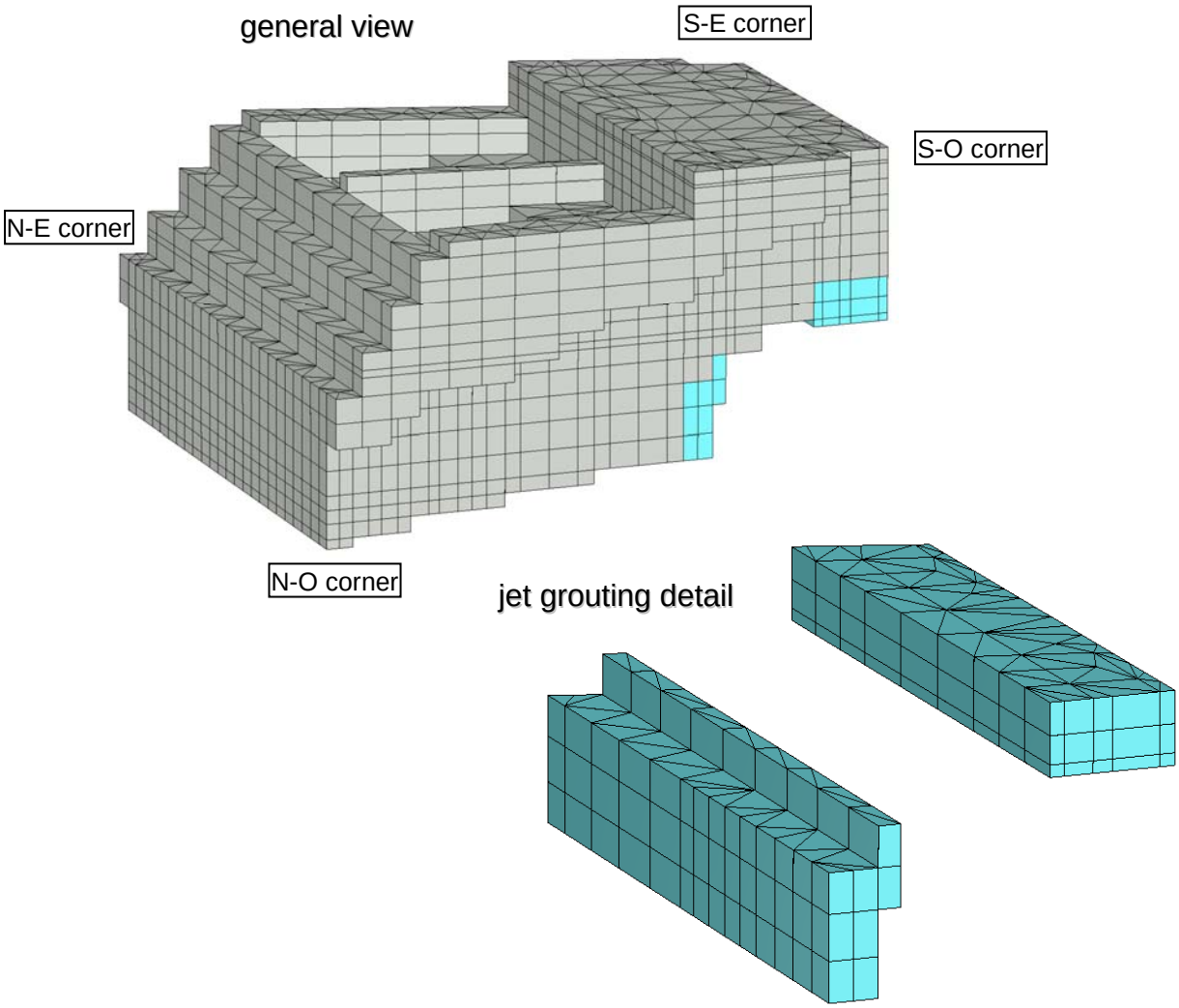

Figure 27. Perspective view of the jet-grouted soil

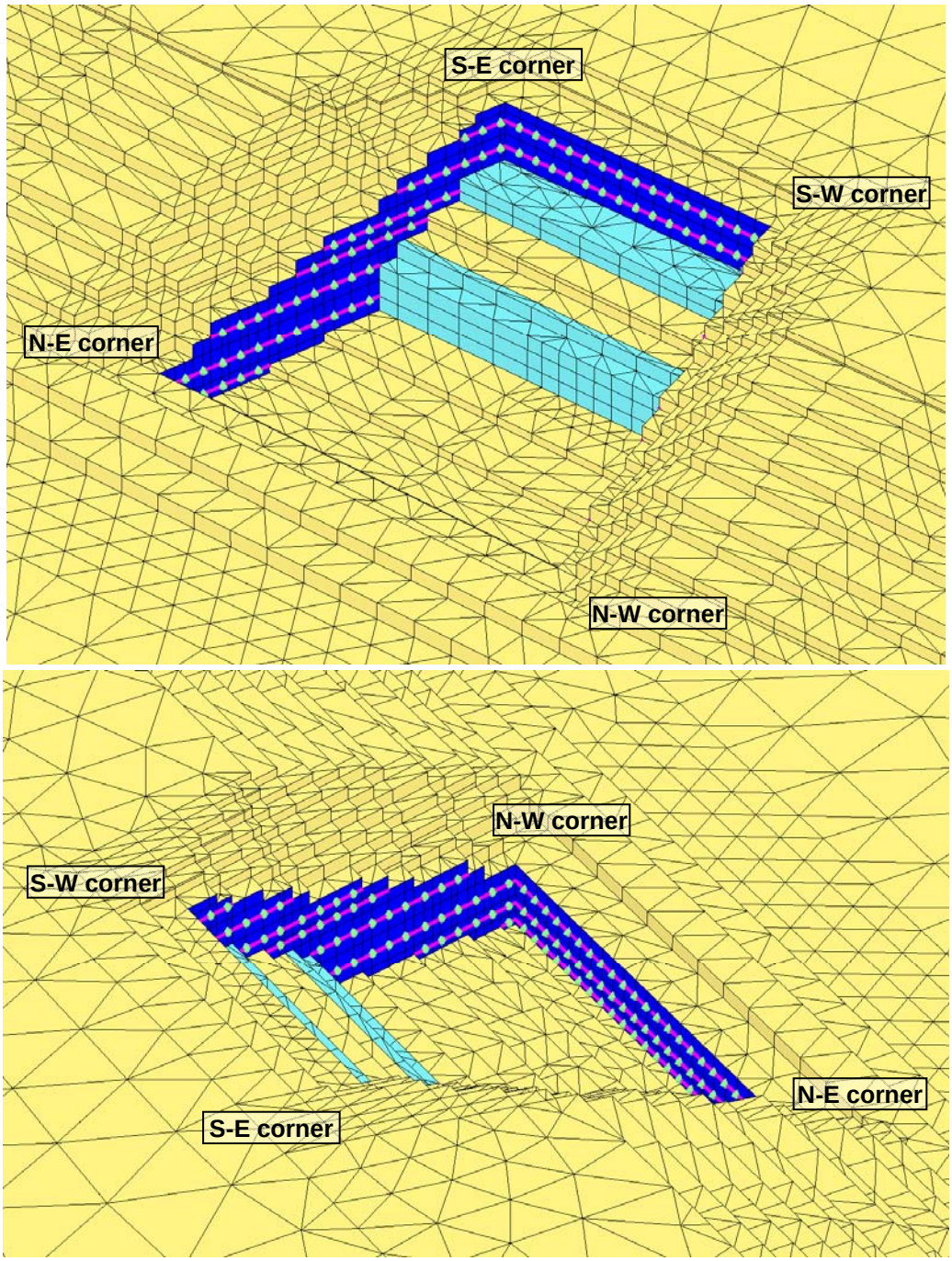

Figure 28. Perspective view of the deepest excavation level: (a) North-West top view and (b) South-East top view

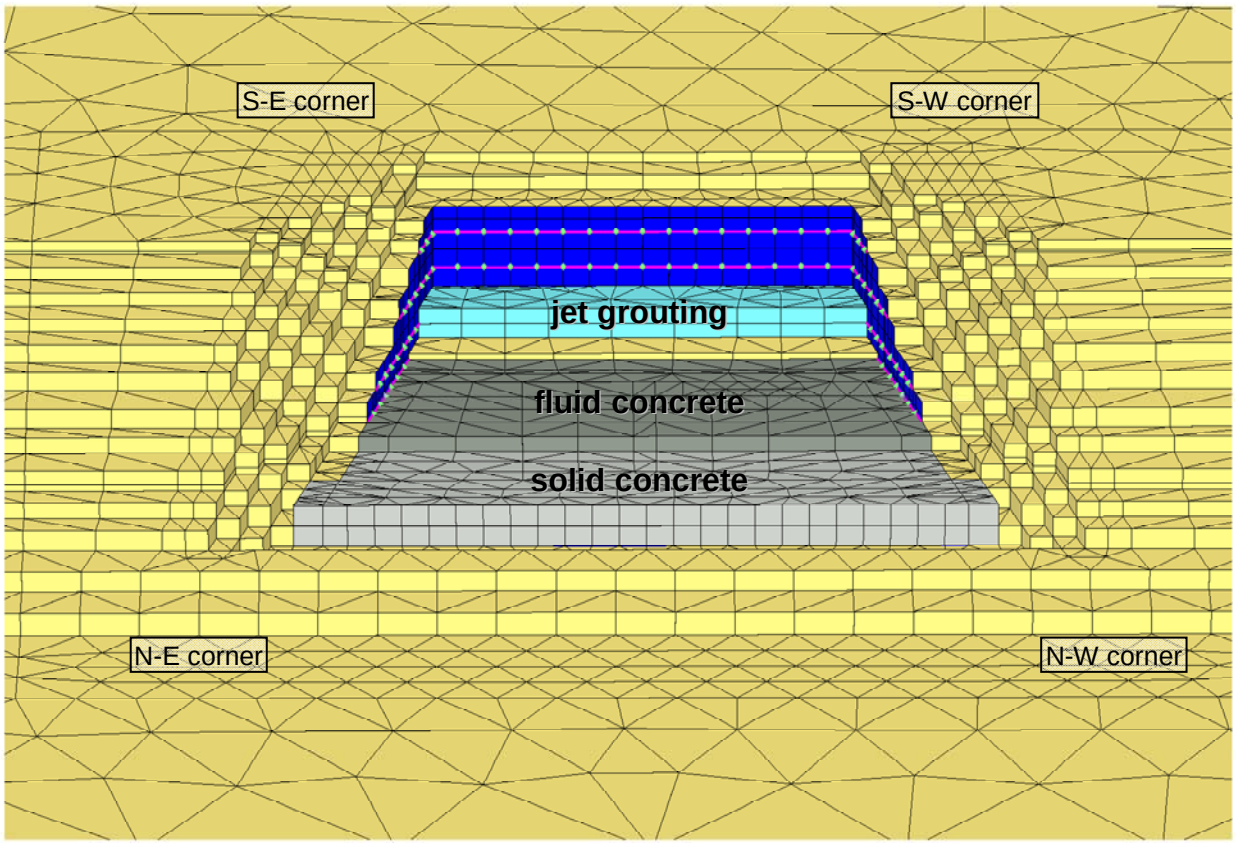

Figure 29. Perspective view of an intermediate step of block construction

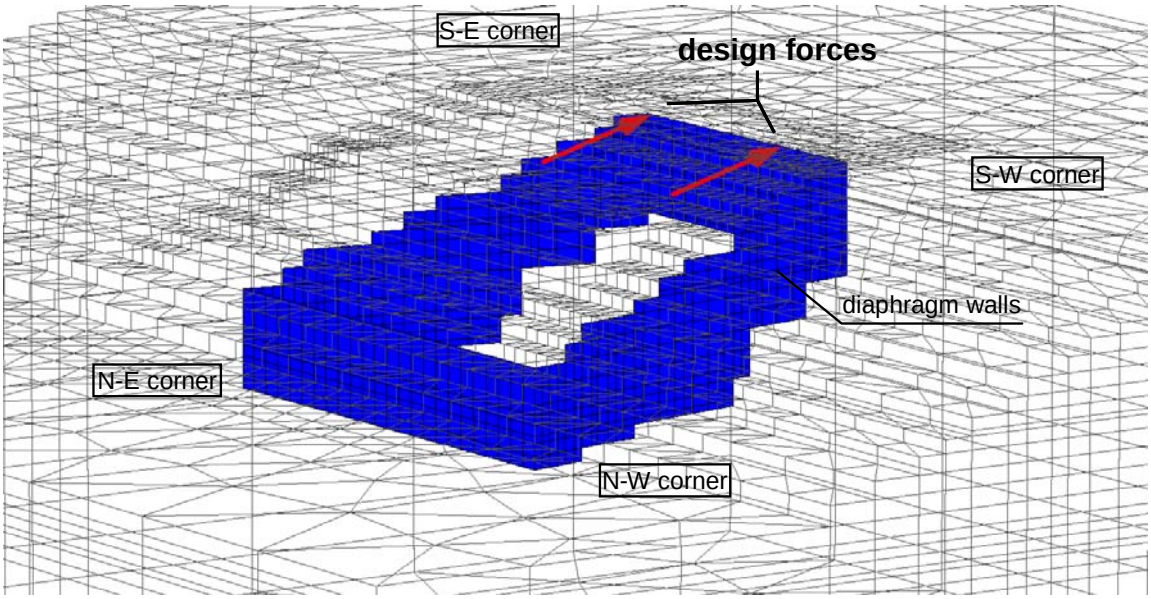

Figure 30. Perspective view of the anchor block with indication of the design forces

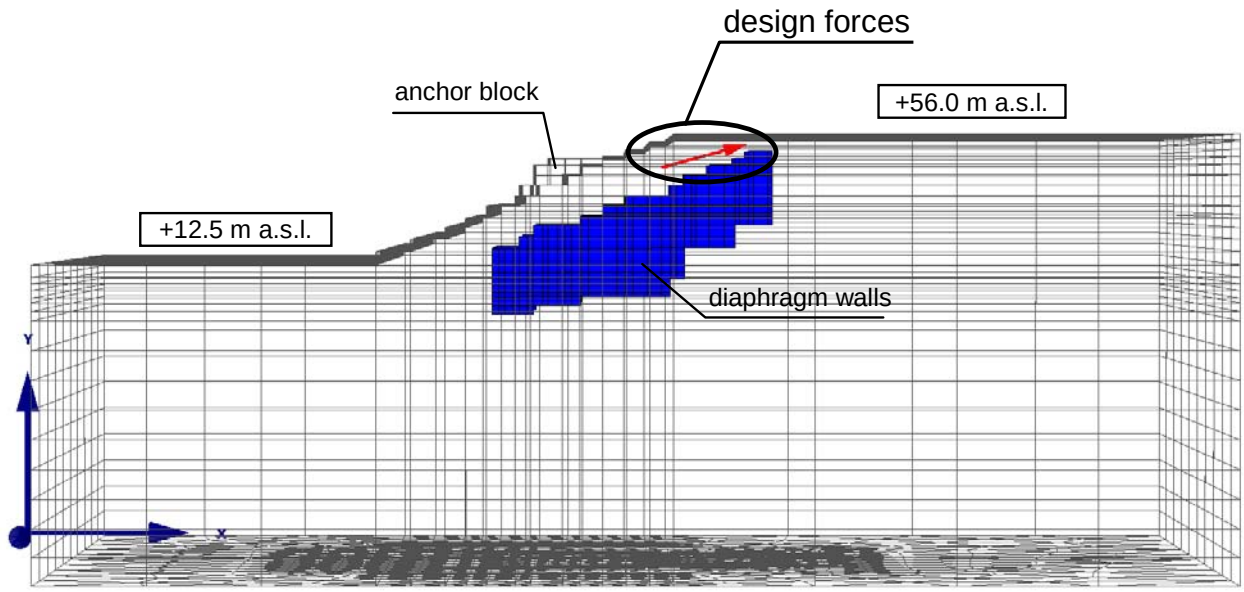

Figure 31. Front view of the anchor block with indication of the design forces

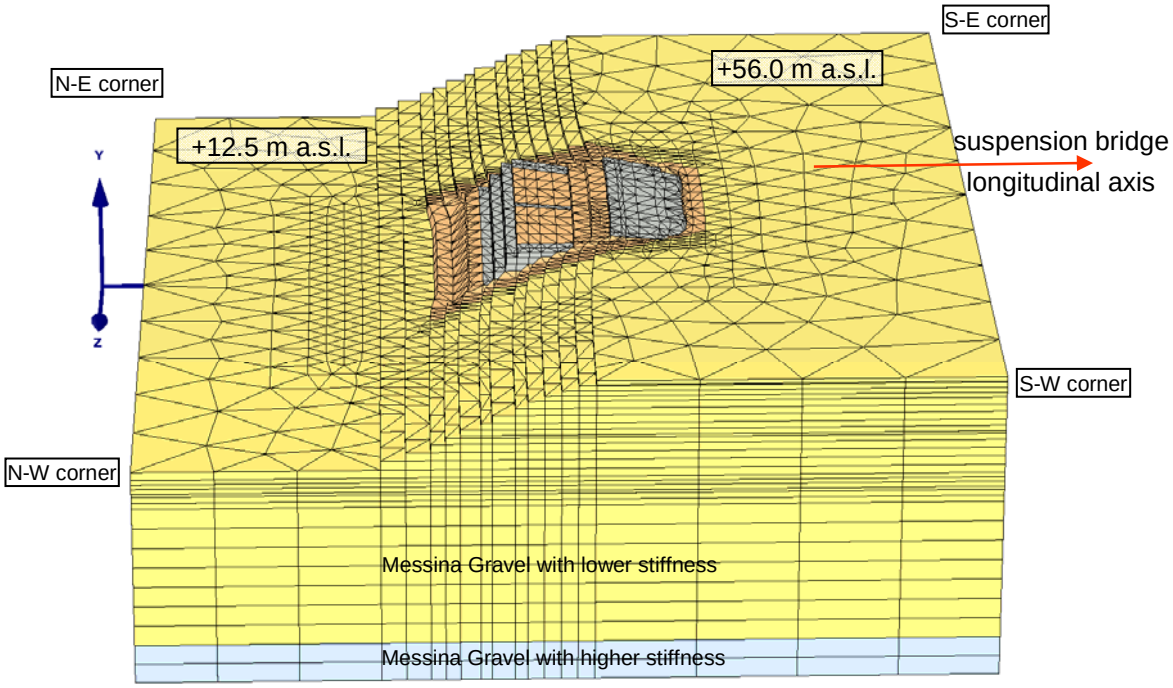

Figure 32. Deformed FE mesh for ULS loading conditions (scaled up 300 times)

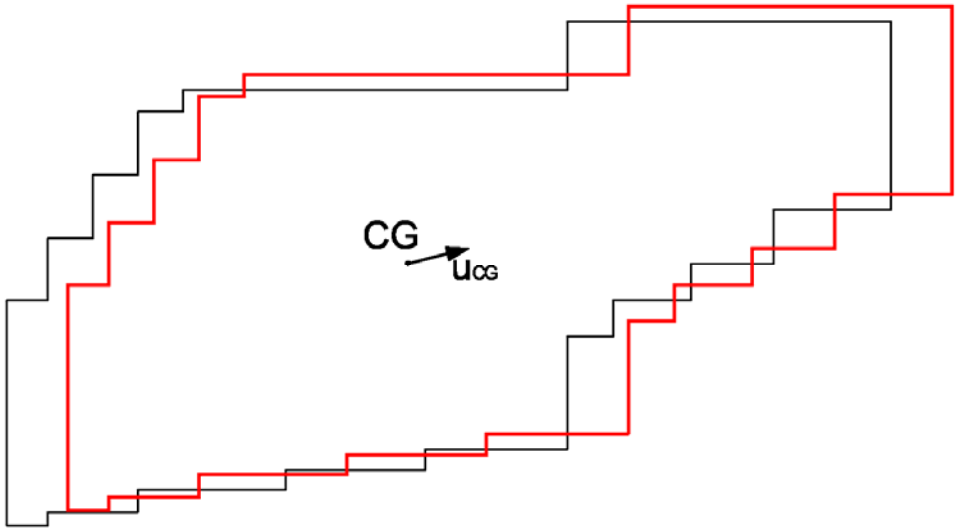

Figure 33. Translation of the block for ULS loading condition (displacement scaled up 200 times)

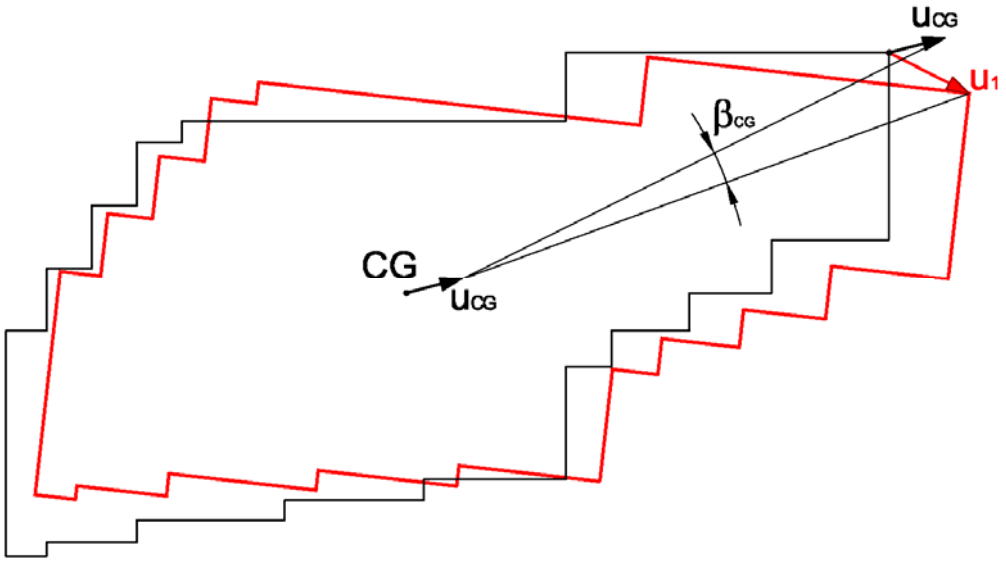

Figure 34. Rotation and translation of the block for ULS loading condition (displacement scaled up 200 times)

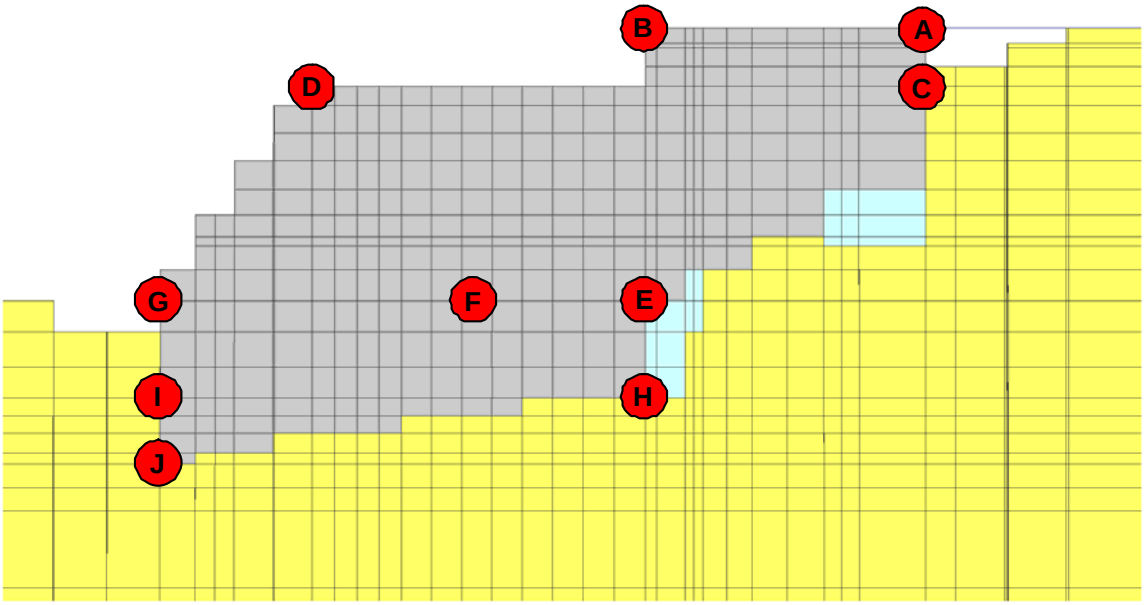

Figure 35. Location of points – longitudinal section through the centre of gravity

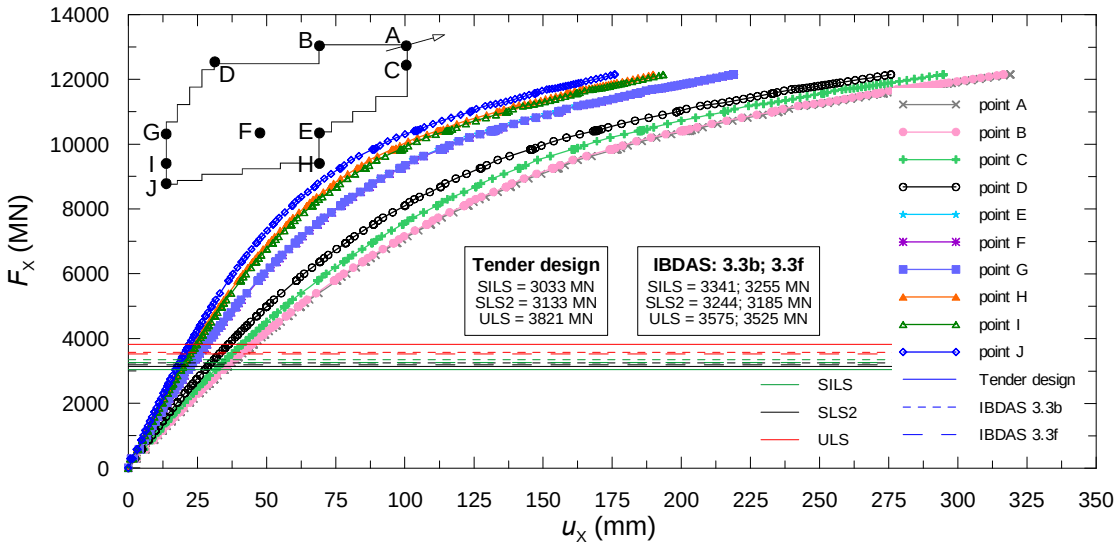

Figure 36. Load – displacement curves for the selected points; horizontal direction

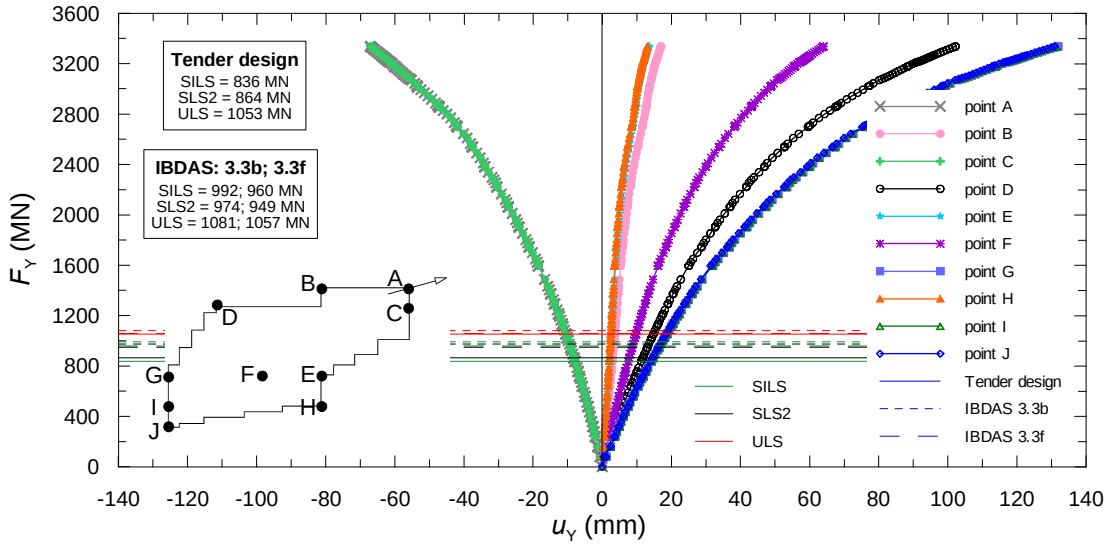

Figure 37. Load – displacement curves for all ten points; vertical direction

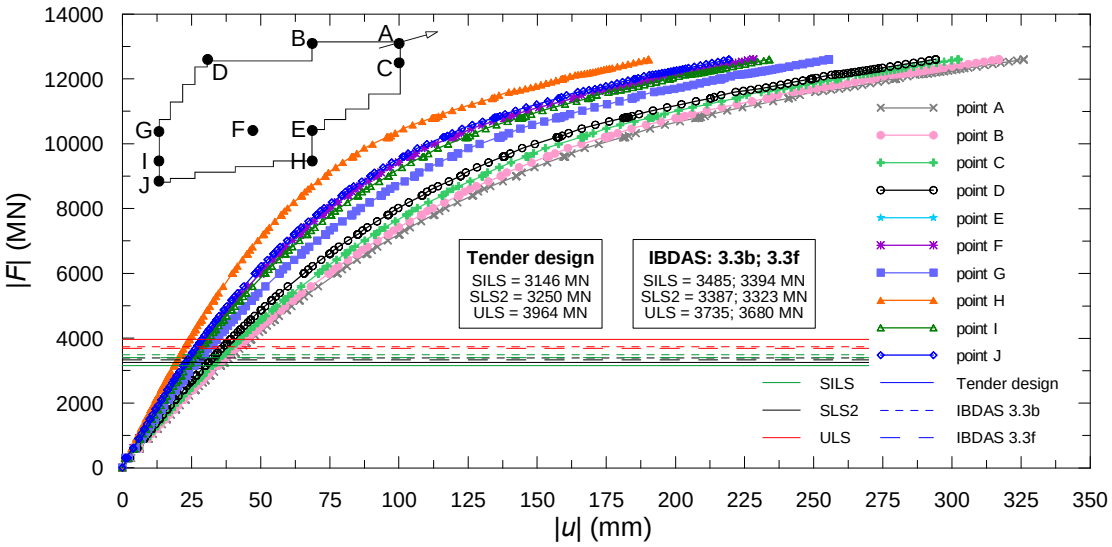

Figure 38. Load – displacement curves for the selected points

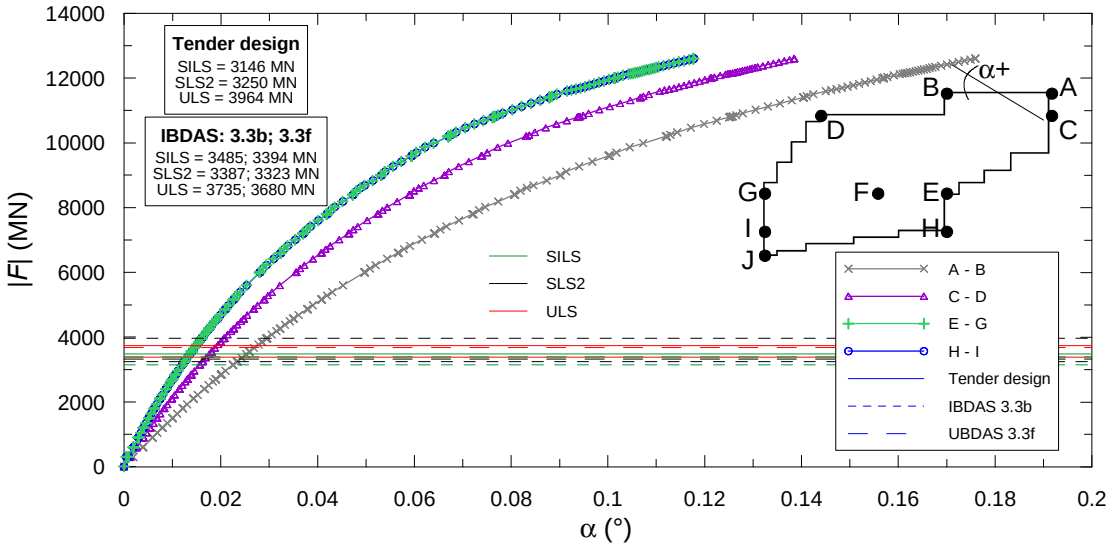

Figure 39. Load – rotation curves for horizontal alignment

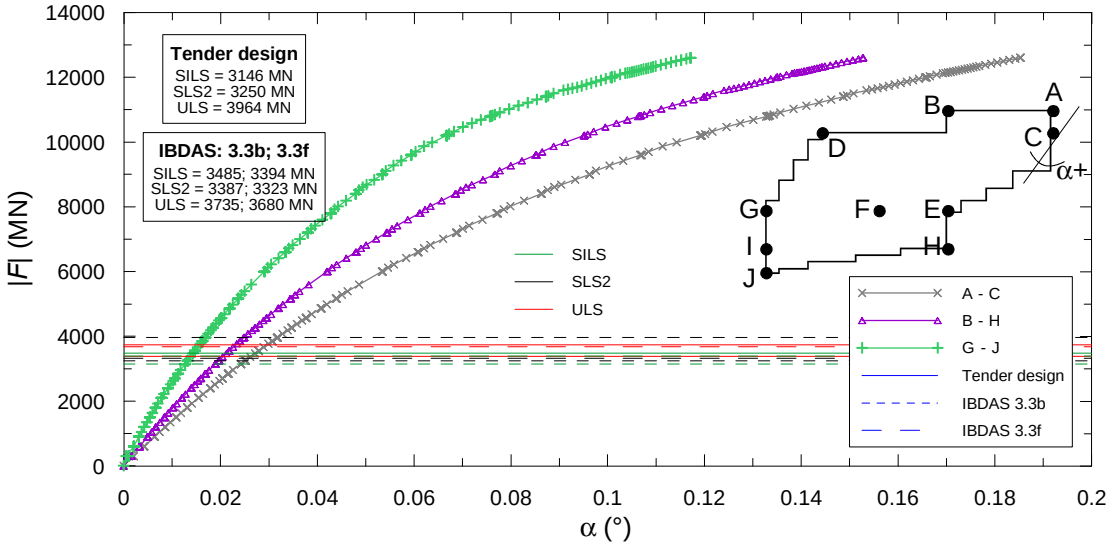

Figure 40. Load – rotation curves for vertical alignment

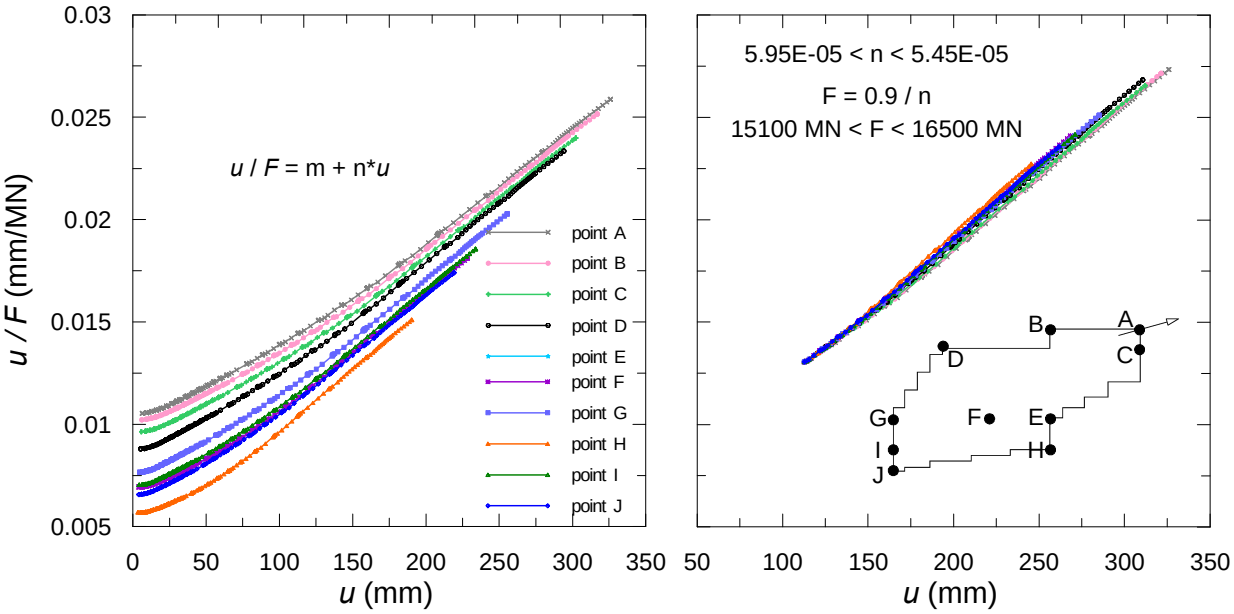

Figure 41. Load – displacement curves – hyperbolic best fitting

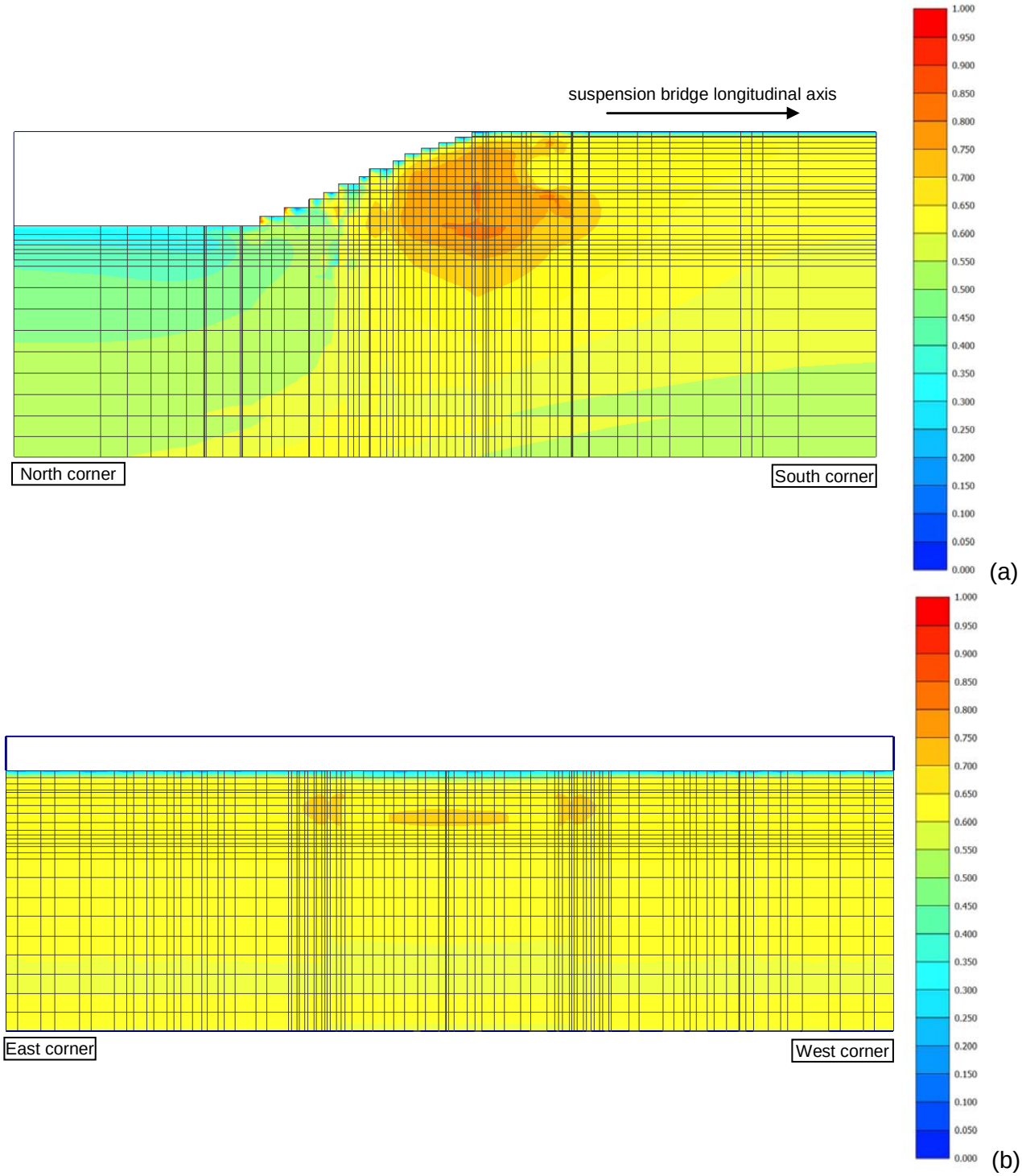

Figure 42. Initial phase: contours of τ_{rel} (a) in a longitudinal section through the centre of gravity (Z = 225 m) and (b) in a transversal section (X = 172 m)

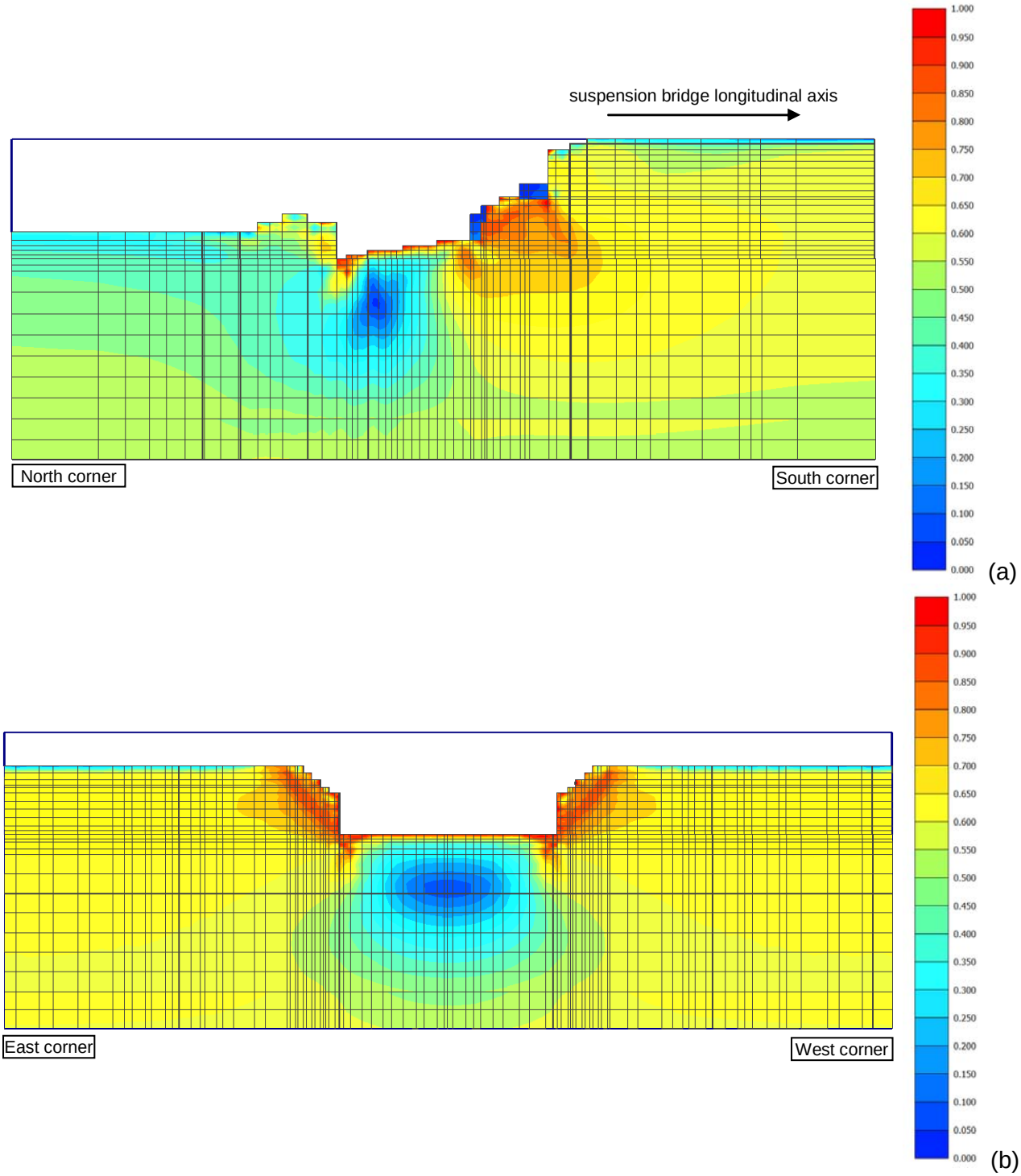

Figure 43. Complete excavation: contours of τ_{rel} (a) in a longitudinal section through the centre of gravity (Z = 225 m) and (b) in a transversal section (X = 172 m)

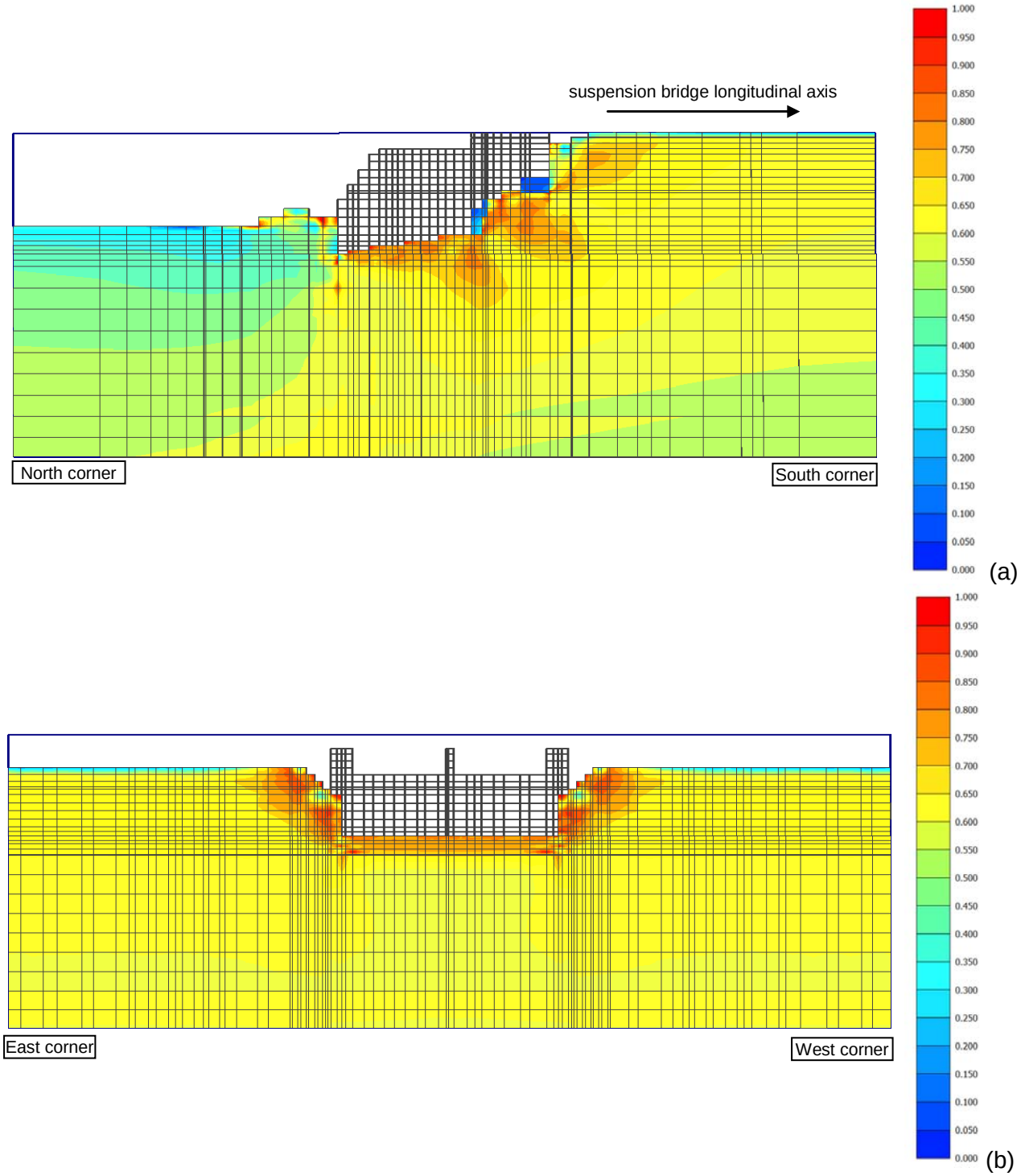

Figure 44. Complete construction of the block: contours of τ_{rel} (a) in a longitudinal section through the centre of gravity (Z = 225 m) and (b) in a transversal section (X = 172 m)

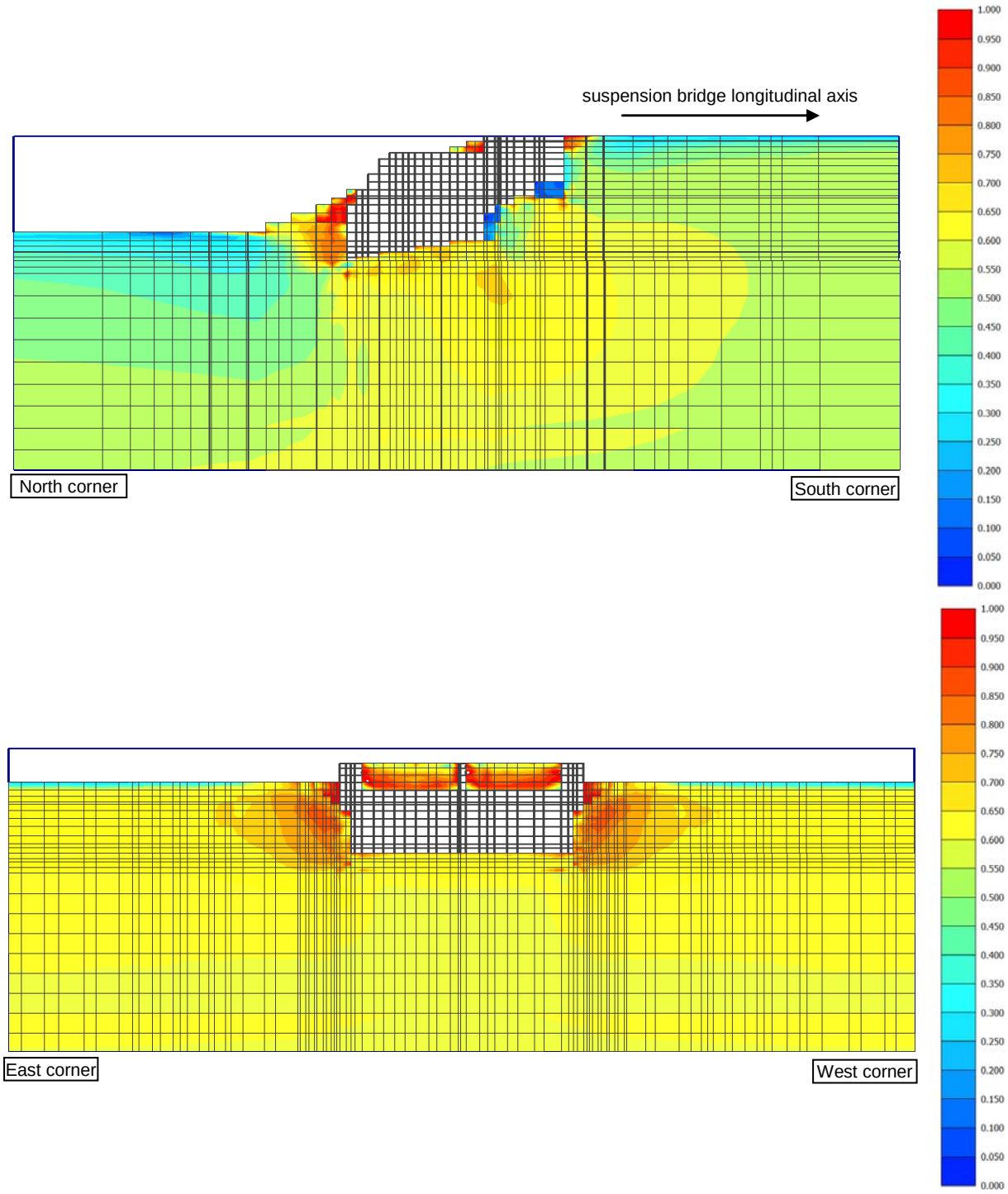

Figure 45. SILS loading condition: contousr of τ_{rel} (a) in a longitudinal section through the centre of gravity (Z = 225 m) and (b) in a transversal section (X = 172 m)

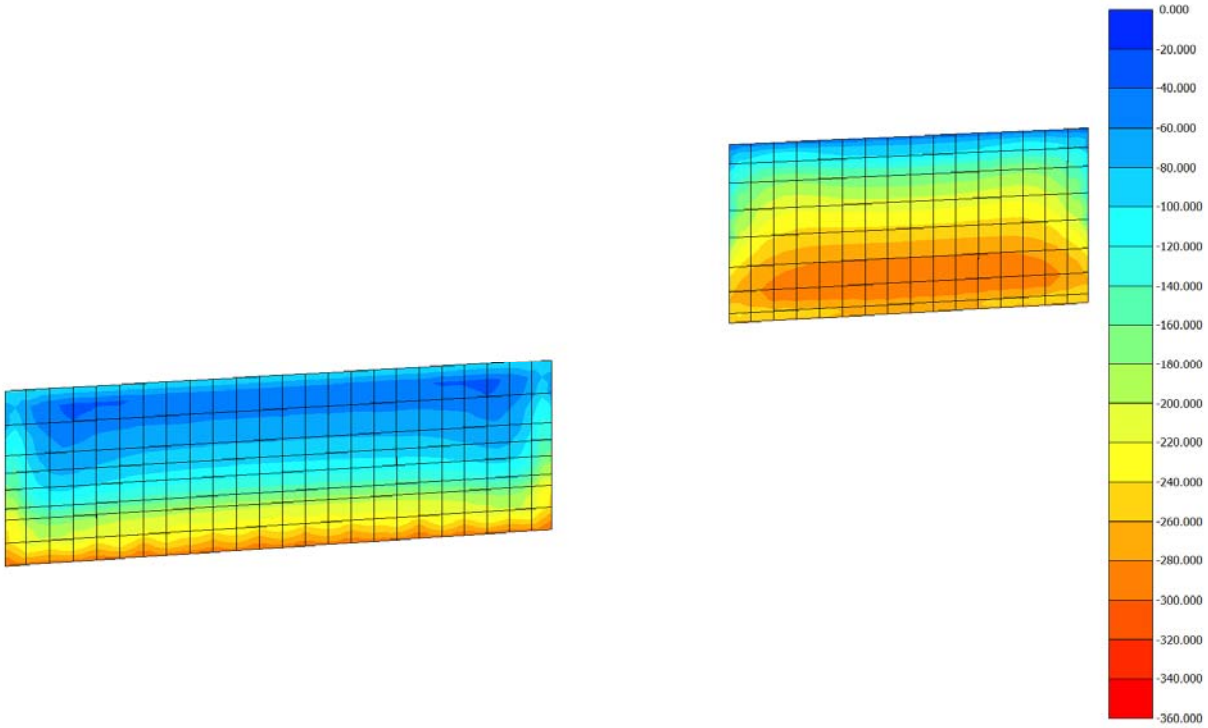

Figure 46. SILS loading condition: contours of σ_N (in kPa) acting on the soil-wall interfaces element of the transversal diaphragm walls

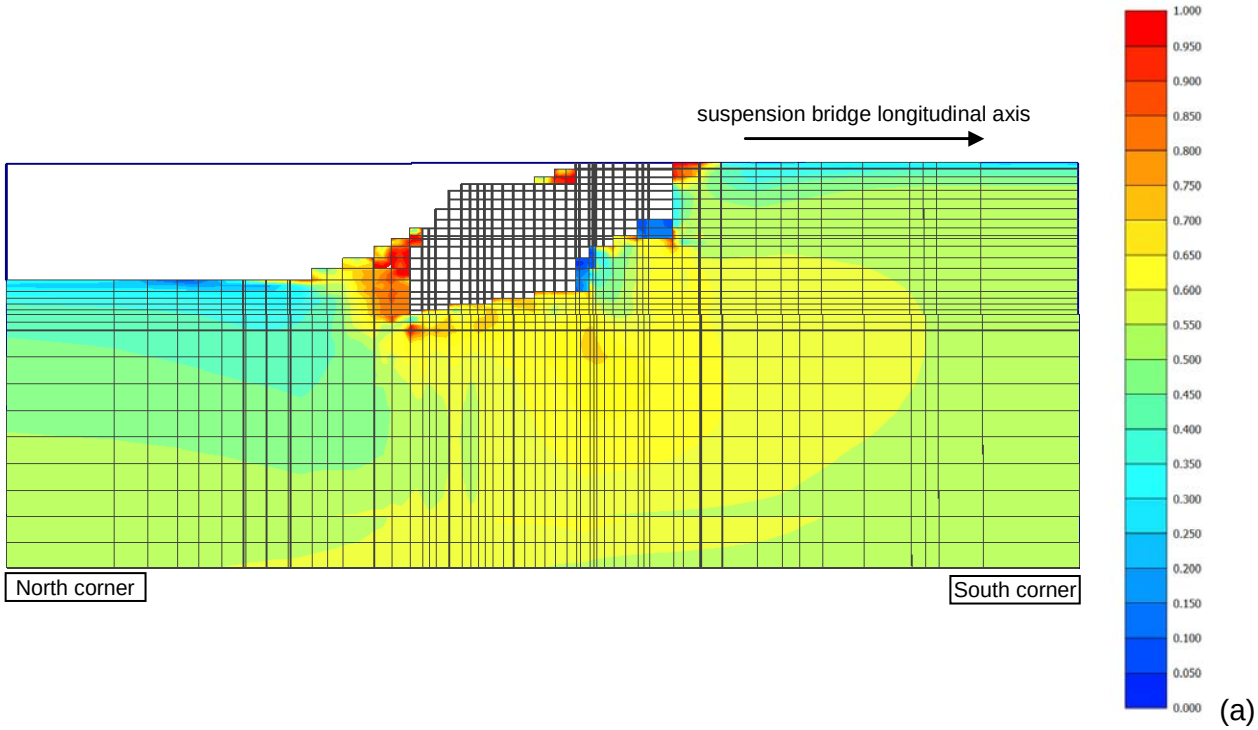

(a)

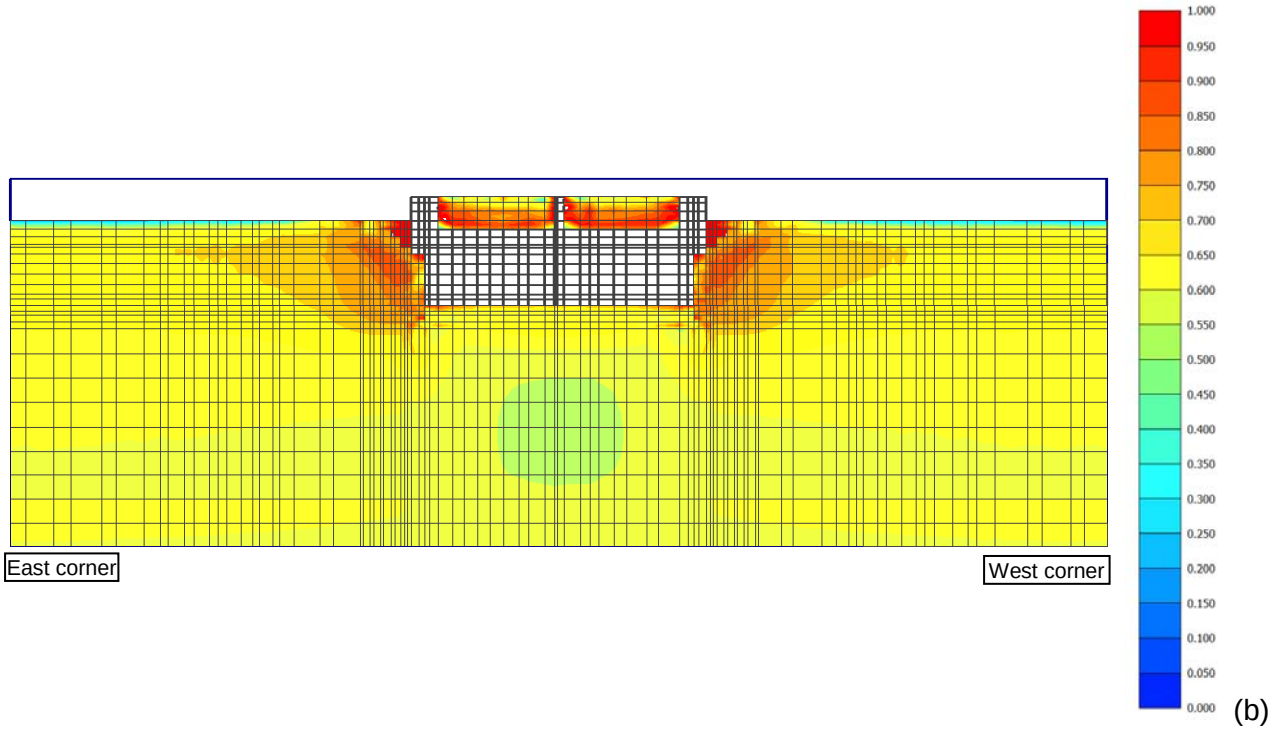

Figure 47. ULS loading condition: contours of τ_{rel} (a) in a longitudinal section through the centre of gravity (Z = 225 m) and (b) in a transversal section (X = 172 m)

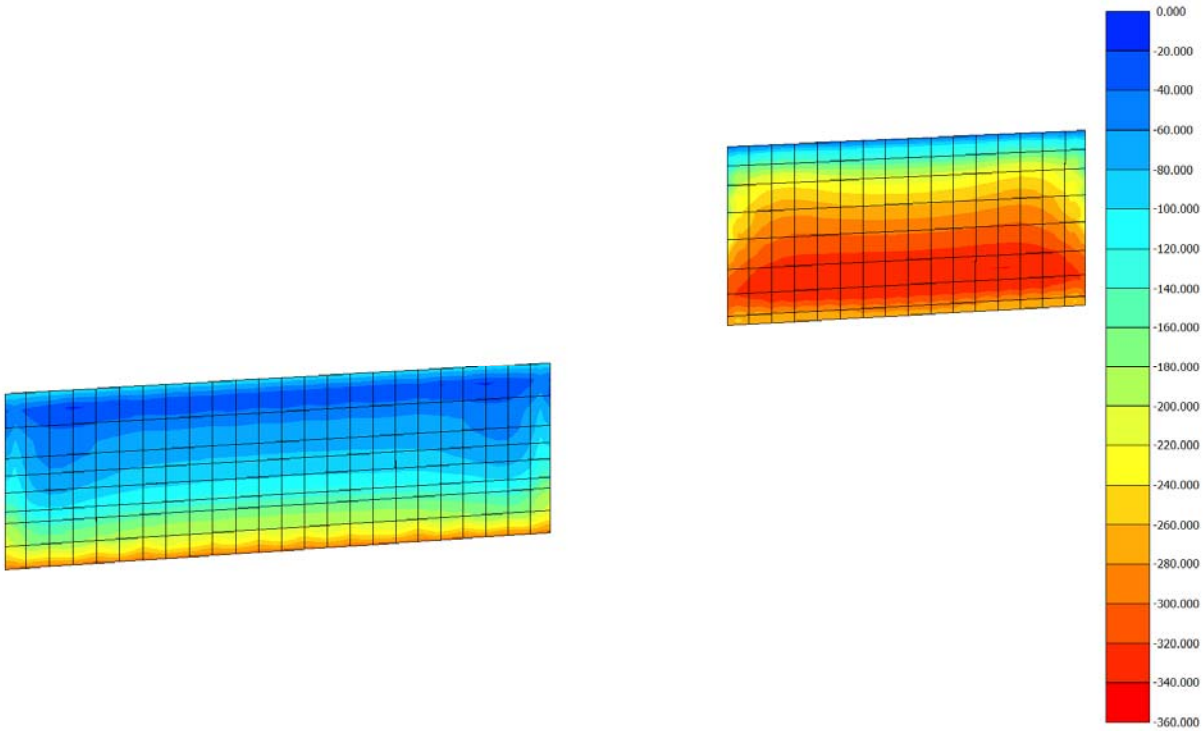

Figure 48. ULS loading condition: contours of σ_N (in kPa) acting on the soil-wall interfaces element of the transversal diaphragm walls

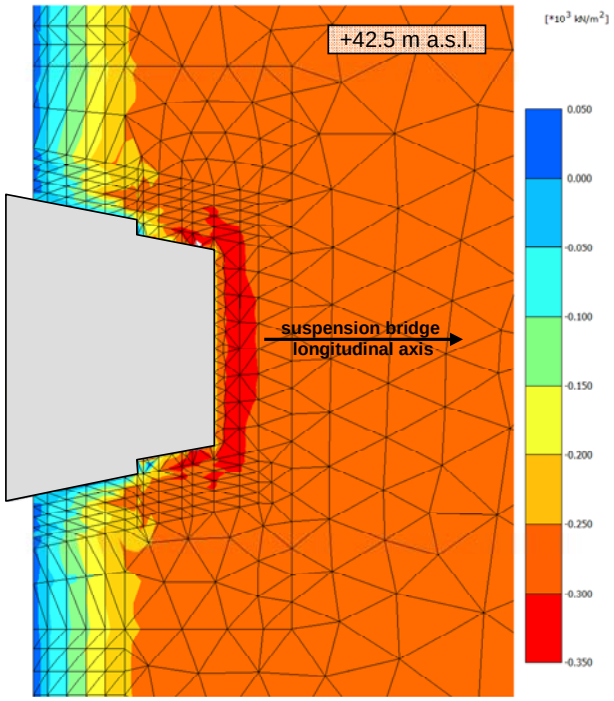

(a)

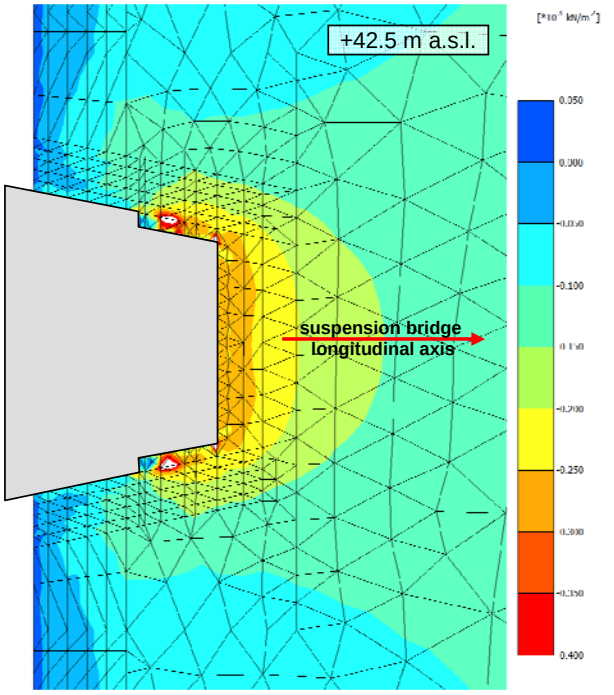

(b)

Figure 49. ULS loading condition: contours of (a) vertical effective stress σ_{YY} and (b) horizontal effective stress σ_{XX} on a horizontal plane at Y = 42.5 m s.l.m

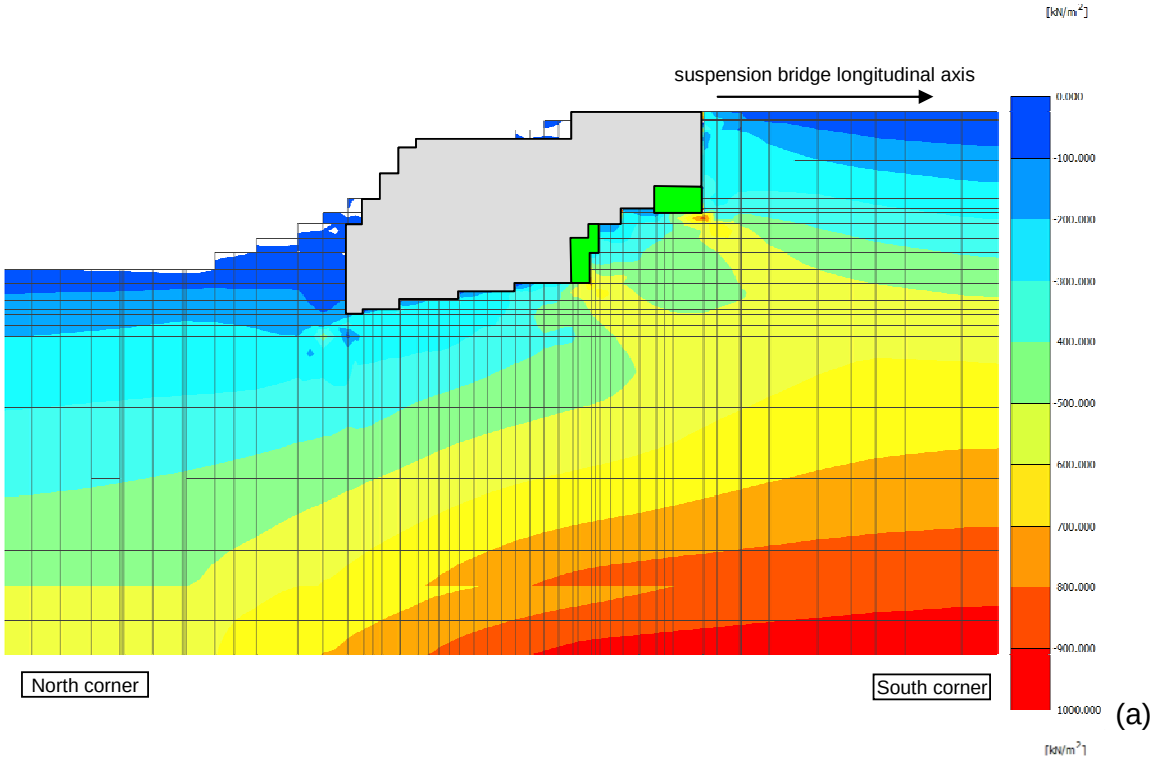

(a)

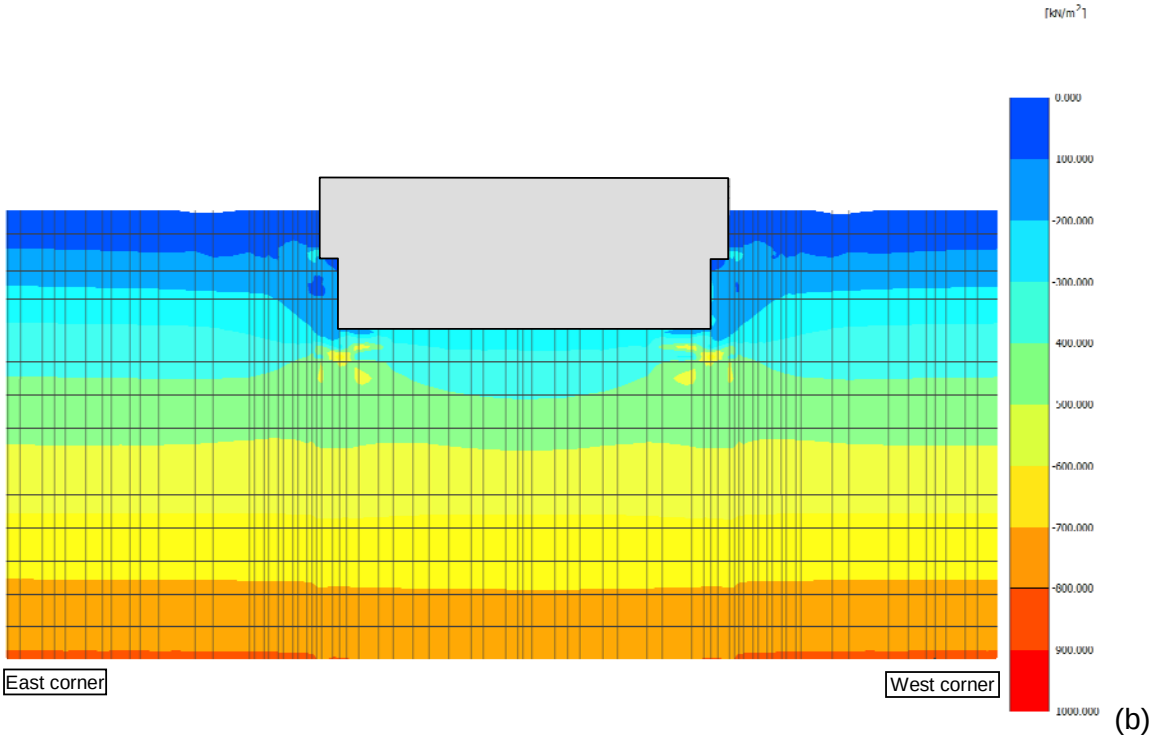

(b)

Figure 50. ULS loading condition: contours of horizontal effective stress (a) σ_{XX} in a longitudinal section at Z = 225 m and (b) σ_{ZZ} in a transversal section at X = 172 m

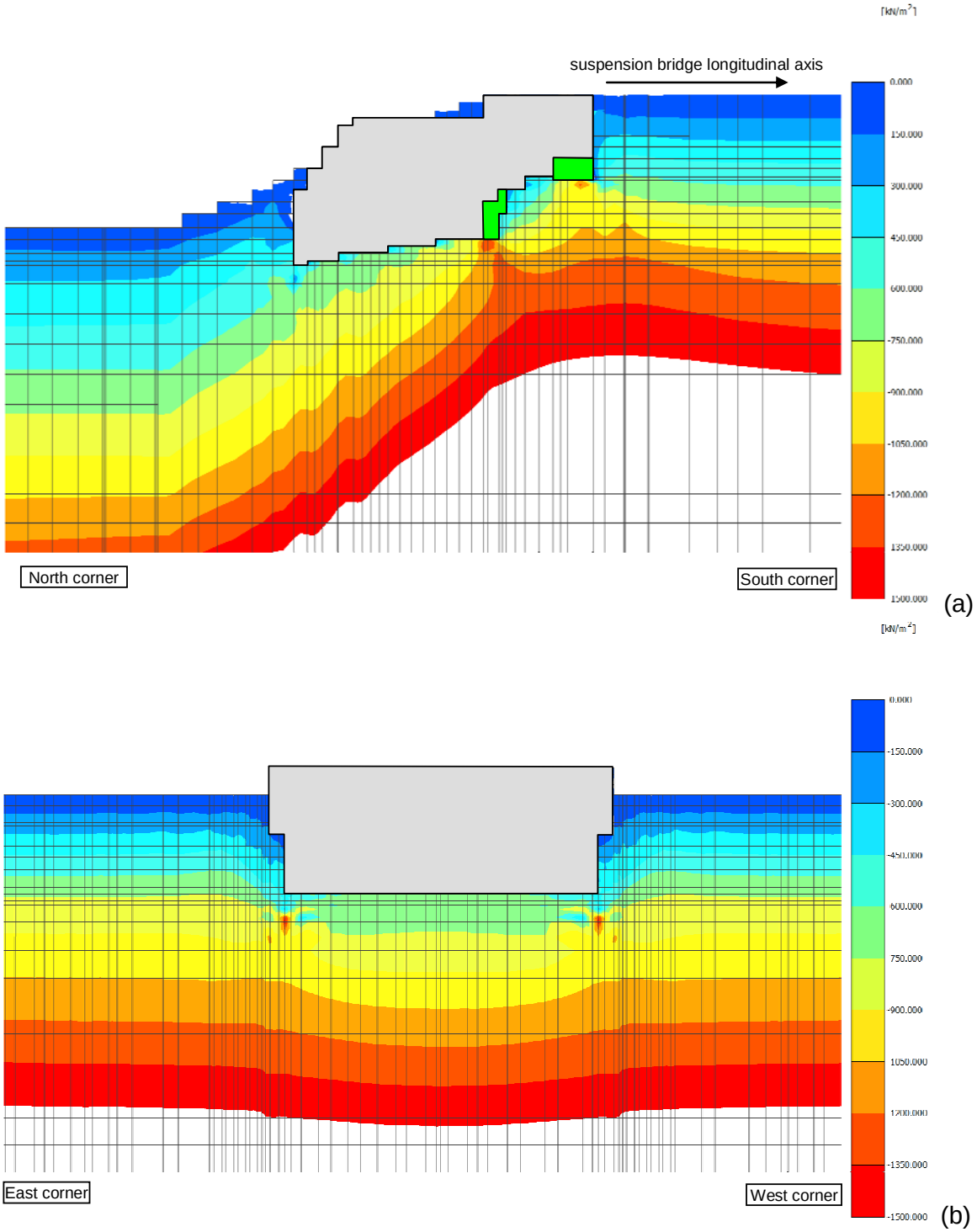

Figure 51. ULS loading condition: contours of vertical effective stress σ_{YY} (a) in a longitudinal section at Z = 225 m and (b) in a transversal section at X = 172 m

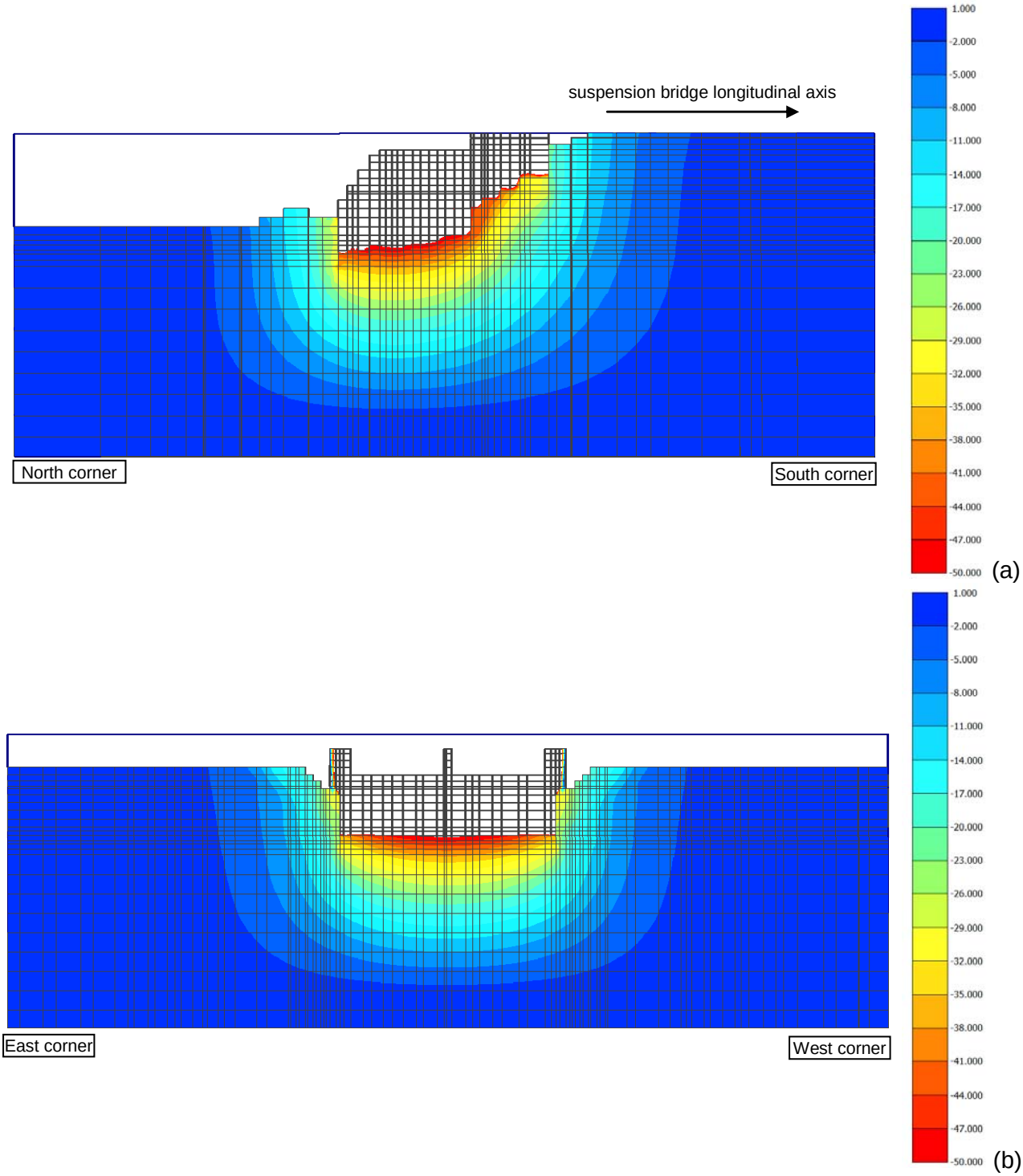

Figure 52. End of block construction: contours of vertical displacement (Y direction; in mm) (a) in a longitudinal section at Z = 225 m and (b) in a transversal section at X = 172 m

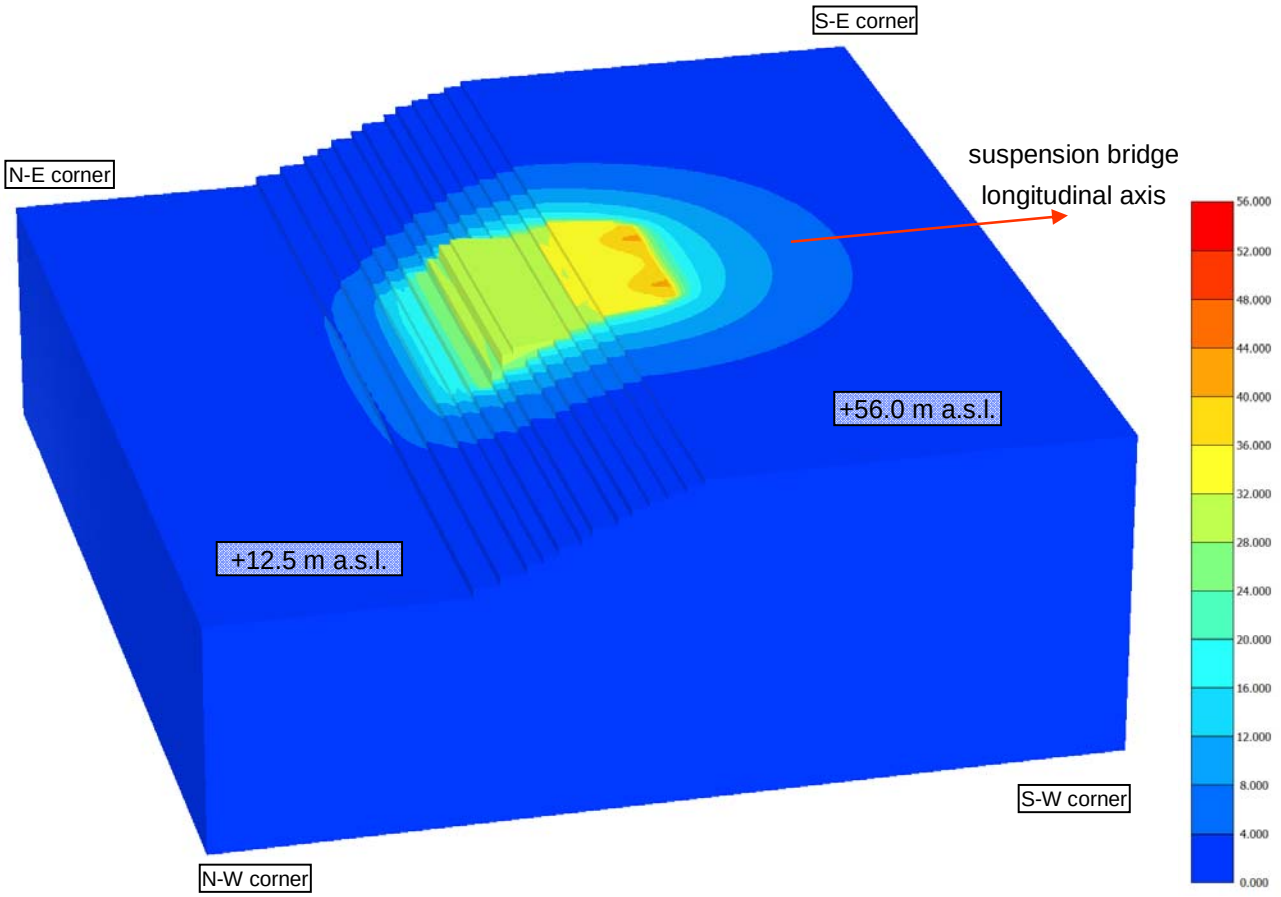

Figure 53. SILS loading condition: contours of total displacement (in mm) in a perspective view of the 3D FE model

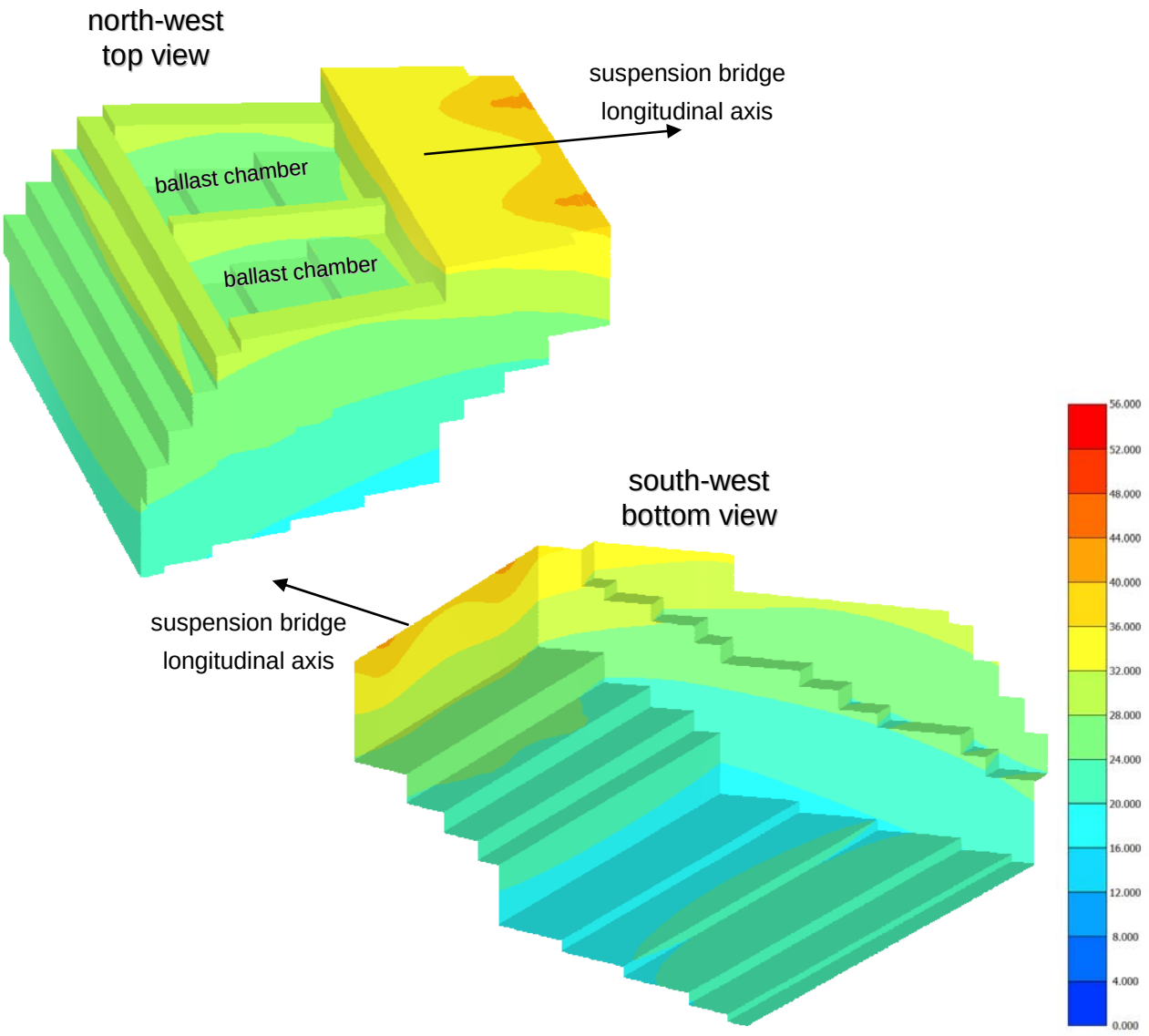

Figure 54. SILS loading condition: contours of total displacement in a perspective view of the Sicily anchor block

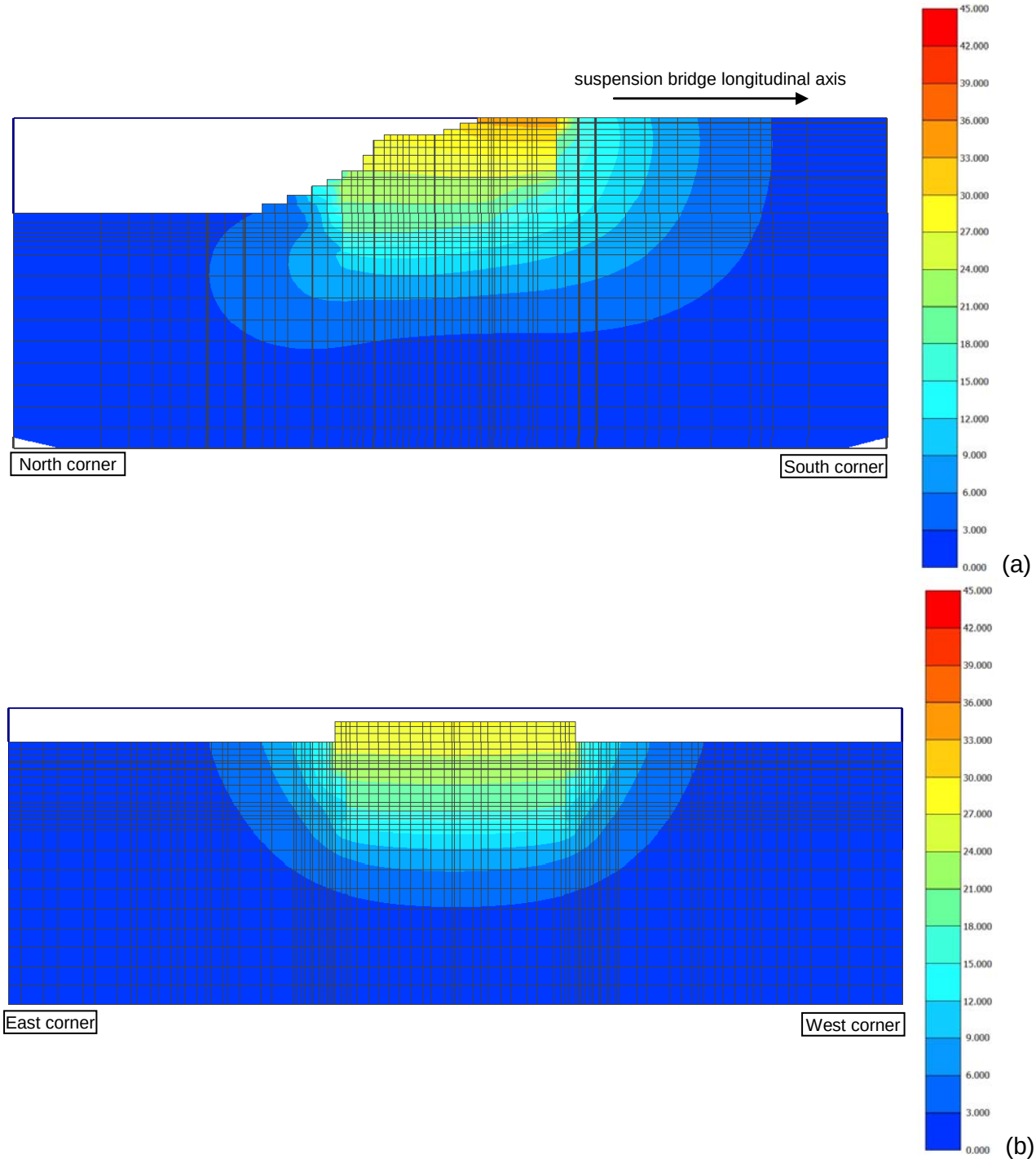

Figure 55. SILS loading condition: contours of longitudinal horizontal displacement (X direction; in mm) (a) in a longitudinal section at Z = 225 m and (b) in a cross section at X = 172 m

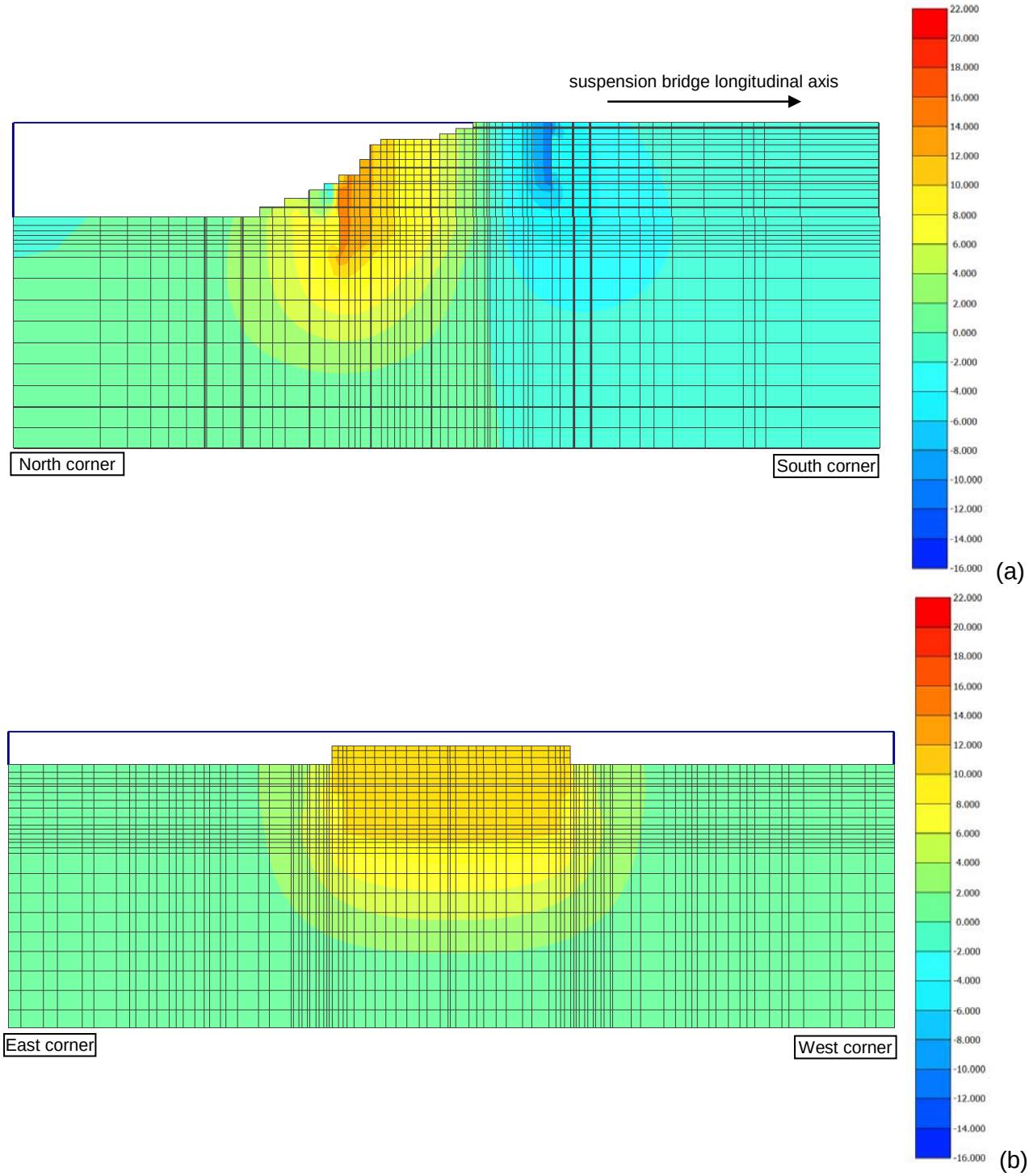

Figure 56. SILS loading conditions: contours of vertical displacement (Y direction; in mm) (a) in a longitudinal section at Z = 225 m and (b) in a cross section at X = 172 m

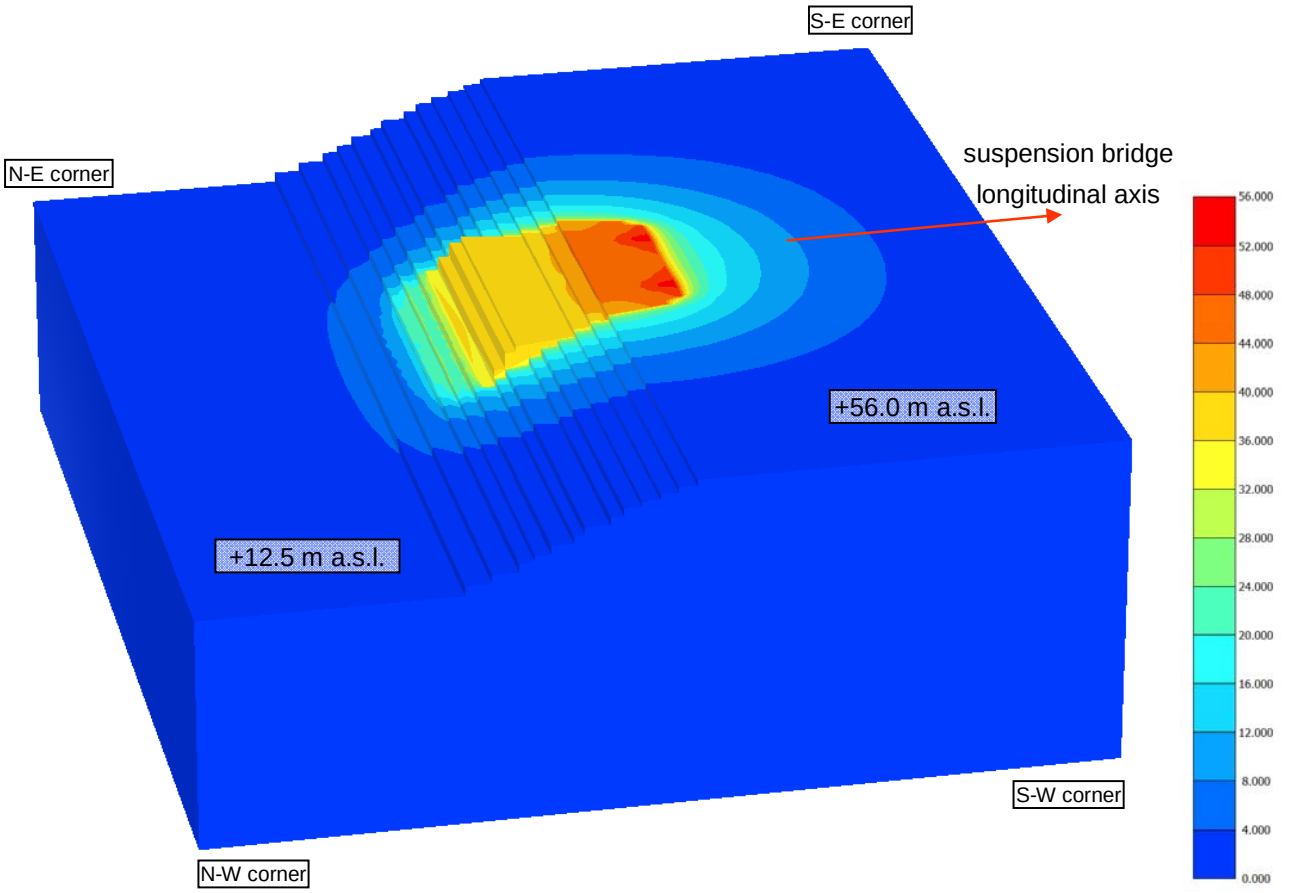

Figure 57. ULS loading conditions: contours of total displacement (in mm) in a perspective view of the 3D FE model

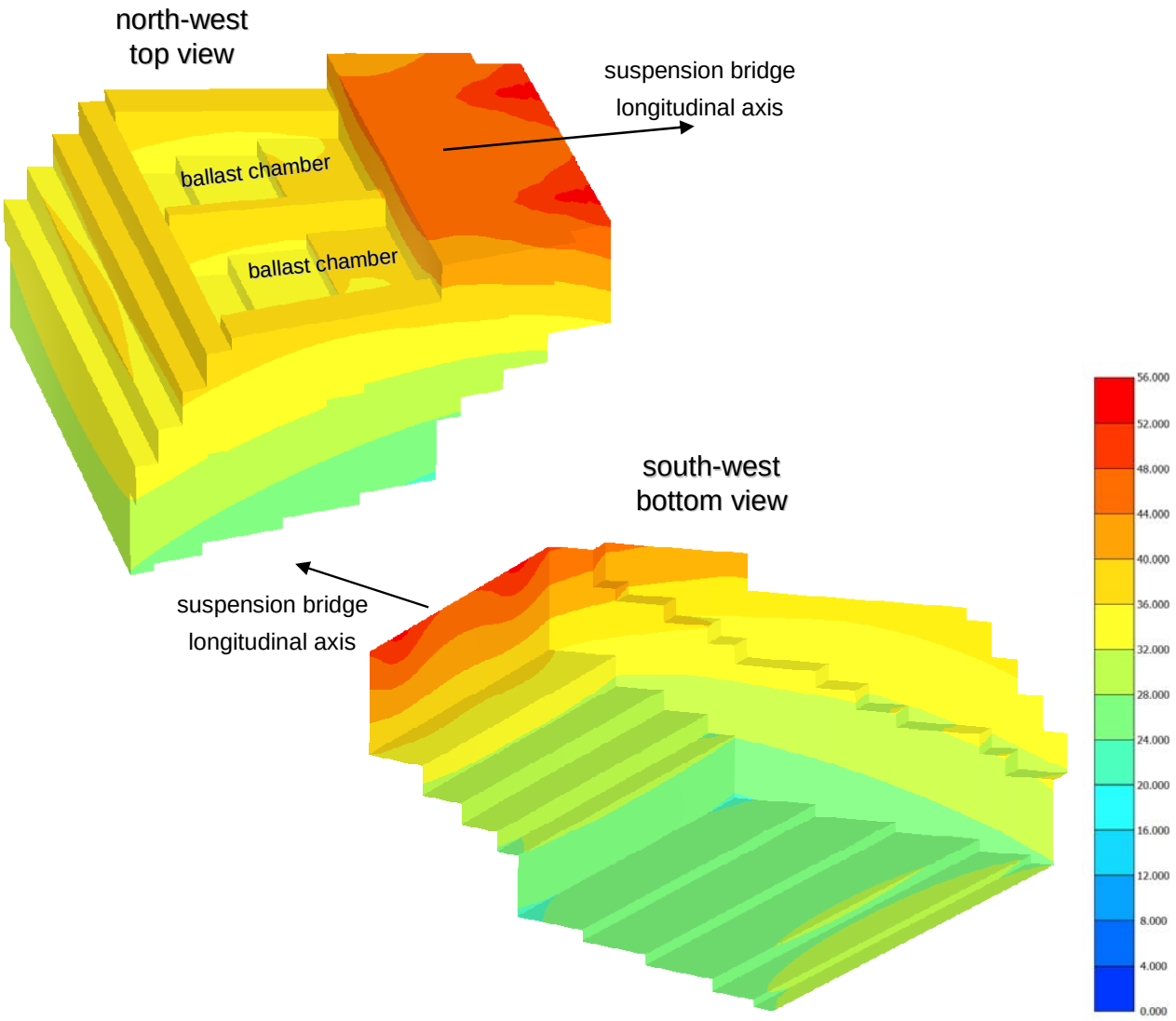

Figure 58. ULS loading conditions: contours of total displacement in a perspective view of the Sicily anchor block

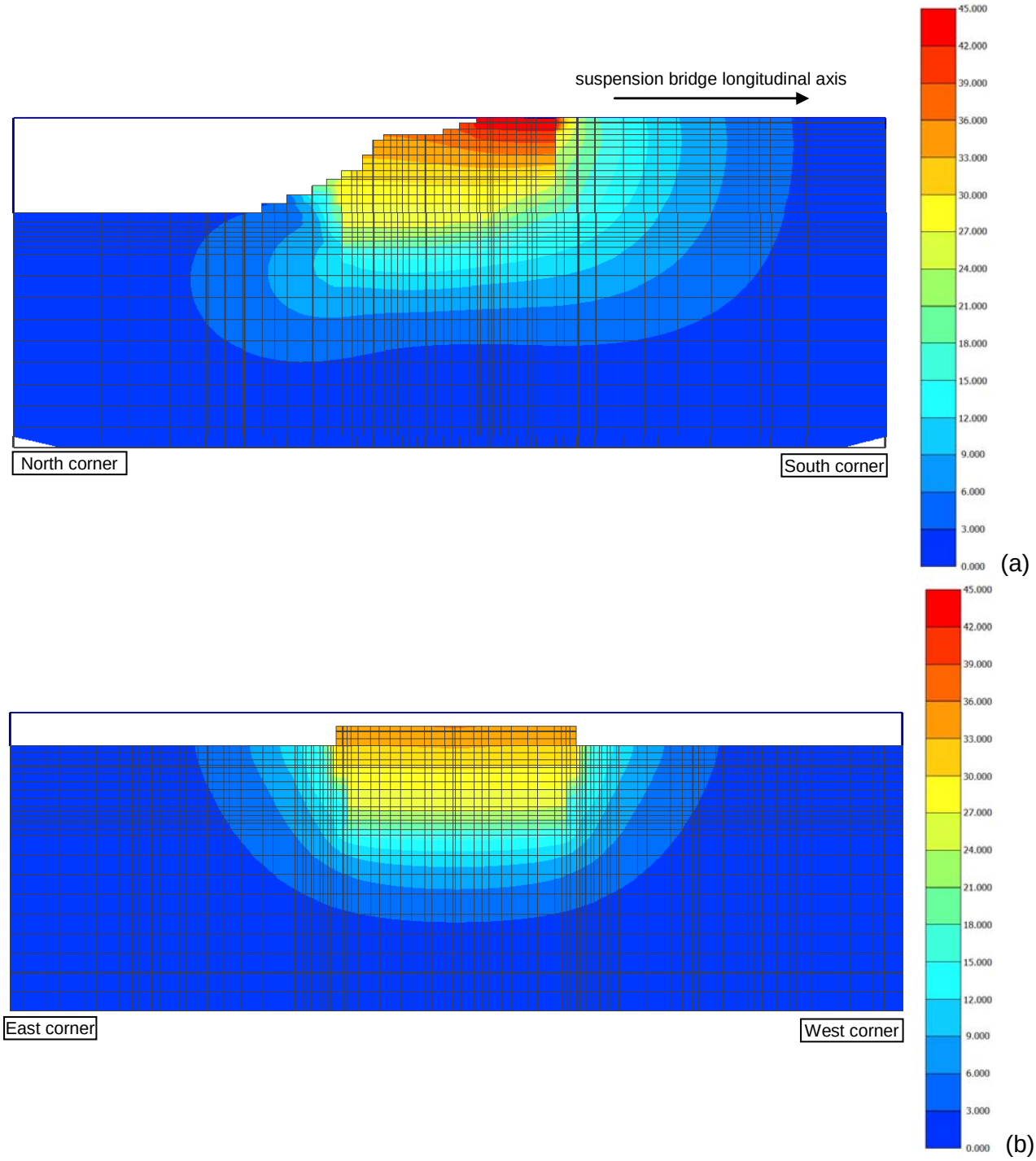

Figure 59. ULS loading conditions: contours of longitudinal horizontal displacement (X direction; in mm) (a) in a longitudinal section at Z = 225 m and (b) in a cross section at X = 172 m

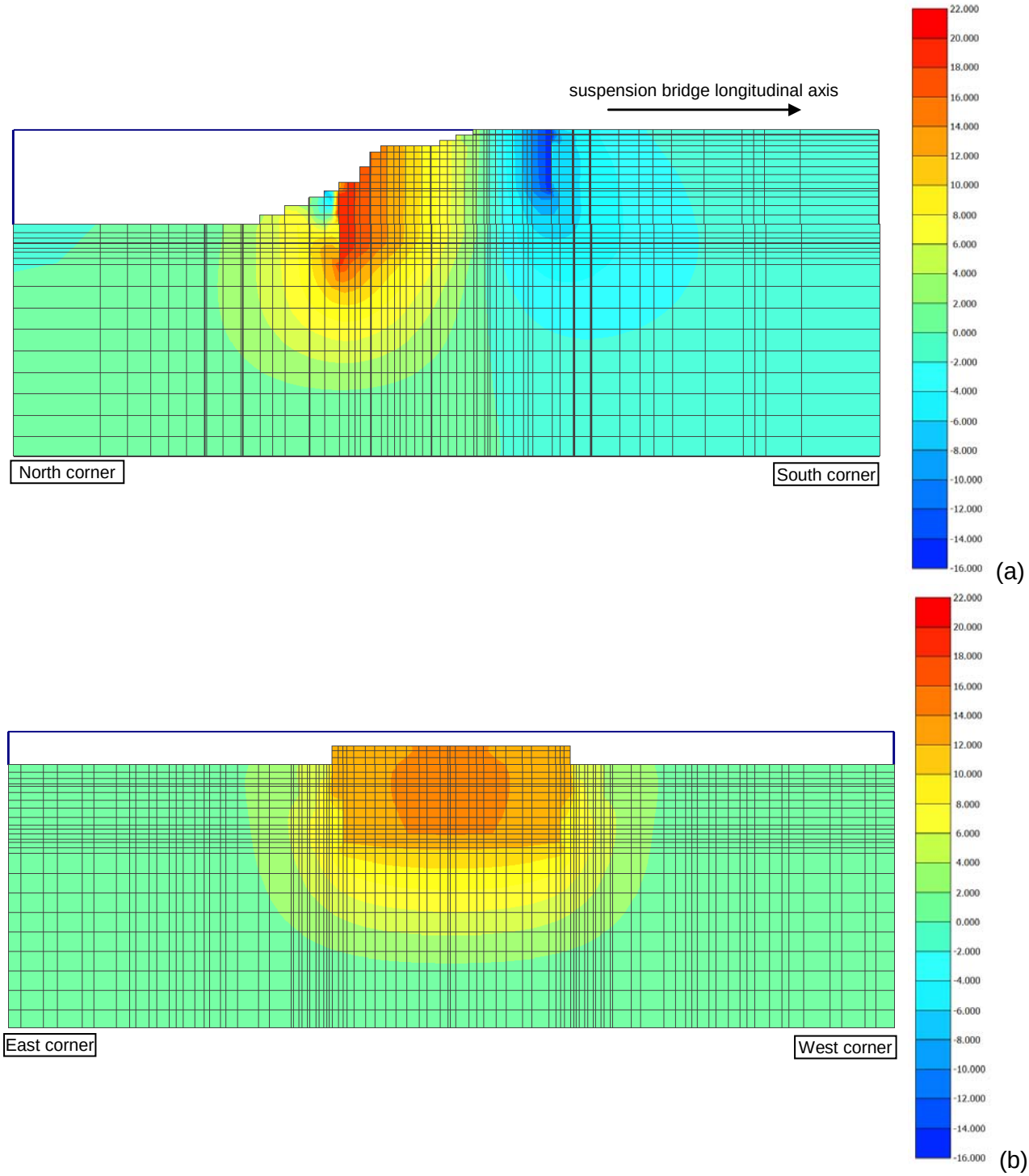

Figure 60. ULS loading conditions: contours of vertical displacement (Y direction; in mm) (a) in a longitudinal section at Z = 225 m and (b) in a cross section at X = 172 m

APPENDIX A – Updated cable forces obtained from global IBDAS model version 3.3b

The forces transmitted by the main cables to the Sicilia Anchor Block have been re-evaluated using the global IBDAS model version 3.3b. The worst load combinations were selected for each limit state (SILS, SLS2 and ULS) for both static and seismic conditions, using 6 different criteria. Table A.1 resumes the values obtained for static loading conditions, while Table A.2 refers to seismic loading conditions.

Low differences are observed between values of the cable forces computed in the tender design and those recently provided by the global IBDAS model version 3.3b. Considering the maximum values of cable forces given by the different criteria for each load case, the ratio of the tender design cable forces to those provided by IBDAS model are in the range 1.06 to 0.90 (Table A.3); the higher ratio refers to the ULS load combination, while the lower is obtained for the SILS load combination.

For the Ultimate Limit State (ULS) cable forces provided by the tender design, referred to in the 3D FE analyses, are 5.8% higher than the corresponding IBDAS values, this resulting in a conservative estimate of the behaviour of the Sicilia Anchor Block. Performance of the anchor block under SILS and SLS2 load cases are also discussed in § 4.

Table A.1 – Static Loading Conditions – updated global IBDAS model version 3.3b

Criteria	Load case	F_{long} (MN)	F_{vert} (MN)	F (MN)
min u_{vert}	ULS	2184	605	2266
max u_{vert}		**3575**	**1081**	**3735**
min u_{hor}		2184	605	2266
max u_{hor}		3575	1081	3735
min R_{transv}		2184	605	2266
max R_{transv}		3575	1081	3735
min u_{vert}	SILS	2479	710	2578
max u_{vert}		3245	945	3380
min u_{hor}		2479	710	2578
max u_{hor}		3245	945	3380
min R_{transv}		2479	710	2578
max R_{transv}		3245	945	3380
min u_{vert}	SLS2	2188	607	2271
max u_{vert}		3215	958	3355
min u_{hor}		2188	607	2271
max u_{hor}		3215	958	3355
min R_{transv}		2188	607	2271
max R_{transv}		3215	958	3355

Table A.2 – Seismic Loading Conditions – updated global IBDAS model version 3.3b

Criteria	Load case	F_{long} (MN)	F_{vert} (MN)	F (MN)
min u_{vert}	ULS	2071	553	2143
max u_{vert}		3488	1064	3647
min u_{hor}		2199	629	2287
max u_{hor}		3360	988	3502
min R_{transv}		2173	623	2260
max R_{transv}		3386	994	3529
min u_{vert}	SILS	2357	653	2446
max u_{vert}		**3341**	**992**	**3485**
min u_{hor}		2498	737	2605
max u_{hor}		3199	909	3326
min R_{transv}		2469	730	2575
max R_{transv}		3228	916	3355
min u_{vert}	SLS2	2143	585	2221
max u_{vert}		**3244**	**974**	**3387**
min u_{hor}		2201	620	2287
max u_{hor}		3185	939	3321
min R_{transv}		2189	617	2275
max R_{transv}		3197	942	3333

Table A.3: Cable forces in the Sicilia Anchor Block: tender design and IBDAS values (model version 3.3b)

	Tender Design	Static IBDAS	Seismic IBDAS	
Load case	F (MN)	F (MN)	F (MN)	F_{TD}/F_{IBDAS}
ULS	3964	3735	3647	1.06
SILS	3146	3380	3485	0.90
SLS2	3250	3355	3387	0.96

APPENDIX B – Updated cable forces obtained from global IBDAS model version 3.3f

The forces transmitted by the main cables to the Sicilia Anchor Block have been further re-evaluated using the global IBDAS model version 3.3f. The worst load combinations were selected for each limit state (SILS, SLS2 and ULS) for both static and seismic conditions, using 6 different criteria. Table B.1 resumes the values obtained for static loading conditions, while Table B.2 refers to seismic loading conditions.

Low differences are observed between values of the cable forces computed in the tender design and those recently provided by the global IBDAS model version 3.3f. Considering the maximum values of cable forces given by the different criteria for each load case, the ratio of the tender design cable forces to those provided by IBDAS model are in the range 1.08 to 0.93 (Table B.3); the higher ratio refers to the ULS load combination, while the lower is obtained for the SILS load combination.

For the Ultimate Limit State (ULS) cable forces provided by the tender design, referred to in the 3D FE analyses, are 8% higher than the corresponding IBDAS values, this resulting in a conservative estimate of the behaviour of the Sicilia Anchor Block. Performance of the anchor block under SILS and SLS2 load cases are also discussed in § 4.

Table B.1 – Static Loading Conditions – updated global IBDAS model version 3.3f

Criteria	Load case	F_{long} (MN)	F_{vert} (MN)	F (MN)
min u_{vert}	ULS	2176	596	2256
max u_{vert}		**3525**	**1057**	**3680**
min u_{hor}		2176	597	2256
max u_{hor}		3525	1057	3680
min R_{transv}		2176	597	2256
max R_{transv}		3525	1057	3680
min u_{vert}	SILS	2439	690	2535
max u_{vert}		3205	924	3336
min u_{hor}		2439	690	2535
max u_{hor}		3205	924	3336
min R_{transv}		2439	691	2535
max R_{transv}		3205	924	3336
min u_{vert}	SLS2	2181	598	2261
max u_{vert}		3175	937	3311
min u_{hor}		2181	598	2261
max u_{hor}		3175	937	3311
min R_{transv}		2181	598	2261
max R_{transv}		3175	937	3311

Table B.2 – Seismic Loading Conditions – updated global IBDAS model version 3.3f

Criteria	Load case	F_{long} (MN)	F_{vert} (MN)	F (MN)
min u_{vert}	ULS	2105	554	2177
max u_{vert}		3397	1030	3550
min u_{hor}		2138	587	2217
max u_{hor}		3364	997	3509
min R_{transv}		2250	638	2339
max R_{transv}		3252	946	3387
min u_{vert}	SILS	2363	645	2449
max u_{vert}		**3255**	**960**	**3394**
min u_{hor}		2399	681	2494
max u_{hor}		3218	924	3348
min R_{transv}		2523	737	2629
max R_{transv}		3094	868	3214
min u_{vert}	SLS2	2154	581	2231
max u_{vert}		**3185**	**949**	**3323**
min u_{hor}		2169	596	2250
max u_{hor}		3170	934	3304
min R_{transv}		2220	619	2305
max R_{transv}		3117	910	3249

Table B.3: Cable forces in the Sicilia Anchor Block: tender design and IBDAS values (model version 3.3f)

	Tender Design	Static IBDAS	Seismic IBDAS	
Load case	F (MN)	F (MN)	F (MN)	F_{TD}/F_{IBDAS}
ULS	3964	3680	3550	1.08
SILS	3146	3336	3394	0.93
SLS2	3250	3311	3323	0.98

REFERENCES

Bustamante M., Doix B. (1985). *Une méthode pour le calcul des tirants et des micropiux injectés*. Bull. Liaison Lab. Ponts et Chaussées, 140, pp 75-95.

Mansur C. I., Kauffman R. I.(1962). *Dewatering*, Cap.3 in Foundation Engineering. McGraw Hill, N.Y.

Mesri. (1989) *Personal communication*.

Rowe P.W. (1962). *The stress – dilatancy relation for static equilibrium of an assembly of particles in contact*. Proceedings Royal Society, London, Ser. A 269, 500 – 527.

Tanaka Y., Kudo Y., Yoshida Y. & Ikemi M. (1987). *A study on the mechanical properties of sandy gravel – dynamic properties of reconstituted samples*. Central Research Institute of Electric Power Industry, Report U87019.